THE EXCITED STATES OF ^{160}Dy

by

HORMOZ AZODI

B.Sc. Washington State University 1971

A THESIS SUBMITTED IN PARTIAL FULFILLMENT OF

THE REQUIREMENTS FOR THE DEGREE OF

MASTER OF SCIENCE

in the Department

of

PHYSICS

We accept this thesis as conforming to the

required standard

THE UNIVERSITY OF BRITISH COLUMBIA

July, 1974

In presenting this thesis in partial fulfilment of the requirements for an advanced degree at the University of British Columbia, I agree that the Library shall make it freely available for reference and study. I further agree that permission for extensive copying of this thesis for scholarly purposes may be granted by the Head of my Department or by his representatives. It is understood that copying or publication of this thesis for financial gain shall not be allowed without my written permission.

Department of Physics

The University of British Columbia
Vancouver 8, Canada

Date July 15th, 1974

Abstract

The gamma-rays and the conversion electrons emitted following the beta decay of $^{160}Tb \rightarrow {}^{160}Dy$ have been studied using Ge(Li) and Si(Li) detectors. The measured energies and intensities of these transitions, together with the results of gamma-gamma coincidence measurements, have allowed us to construct the decay scheme of ^{160}Dy. Four new transitions , namely 97.7, 111.8, 148.5 and 320.5 kev, are placed in the decay scheme on the basis of energy fit and coincidence results. The angular momentum and the parity of the excited states of this nucleus have been deduced as confirmations of previous assignments. The energies and the electromagnetic properties of these states are compared to the predictions of the theory of a rigid asymmetric rotor.

Table of Contents

List of Tables

Acknowledgements

I wish to express my gratitude to Dr. K.C. Mann for guidance and support throughout the course of this work.

I also thank the University of British Columbia Nuclear Orientation Group for making some of their equipment available to me.

This project was supported by Grants-in-Aid of Research to Dr. K.C. Mann from the National Research Council of Canada.

CHAPTER I

INTRODUCTION

All nuclei consist of "protons" and "neutrons", having charges of +e and zero respectively. Protons and neutrons are considered to form the two charge states of a "nucleon", the constituent of all nuclear matter. The complete description of a nucleus is a quantum-mechanical many-body problem, which because of its complexity leads to no specific solutions. To simplify this problem many models have been proposed, each successful to some degree in describing the behavior of certain nuclei.

The earliest and the best known model is the "shell model", which assumes each nucleon to exist in an average central potential due to all other nucleons, as a consequence of which each nucleon will be moving in a definite shell. The "magic numbers" (2,8,20,50,82,126), shown by experiments to be associated with high stability, were explained as the number of protons Z or neutrons N which fill the shells in this model. The shell model predicts successfully the energy, spin and parity of the low-lying energy levels of those odd A nuclei, $A = Z+N$, whose Z and N are close to the magic numbers.

The predictions of the shell model become inadequate as Z or N begin to deviate appreciably from the magic numbers. In this case the motion of the nucleus as a whole, for low energy excitations, becomes predominant over the individual nucleonic motion. Also some nuclear properties such as fission cannot be explained from the point of view of the motion of a single nucleon; rather it has to be explained by the dynamics of the nucleus as a whole.

The "collective model" proposed by Bohr[1] views the nucleus as a rotating and vibrating drop of nuclear matter, like a liquid drop. The equilibrium shape of the nucleus can be spherical or deformed (ellipsoidal), the deformation

occurringwhen there are a considerable number of nucleons outside a closed shell, as for example in the rare earth ($150 \leq A \leq 194$) or actinide ($A \geq 226$) regions. The equilibrium shape of the nucleus and the assumptions regarding the nature of the nuclear matter determine the type of the resulting level structure.

The collective model of even-even deformed nuclei has been developed extensively in two basic ways. Bohr and Faessler[1,2,3] have studied the deformed nucleus as a symmetric ellipsoid, allowing for symmetry preserving vibrations (β-vibrations) and asymmetric vibrations (γ-vibrations). The rotational levels built on the ground state configuration, and those with one β or γ quantum of vibrations are referred to as the ground state, β and γ bands. Band mixing was introduced by Lipas[4] within the context of the symmetric rotor model. Davydov and co-workers[5,6,7] have viewed the deformed nucleus as an asymmetric rotor (a triaxial ellipsoid) and later allowed for surface vibrations. The asymmetric rotor model and the symmetric model with band mixing have been successful to the same degree in explaining the even parity states and their electromagnetic properties in deformed nuclei.

The odd parity states in these nuclei have been studied as rotations and vibrations of an octupole shaped nucleus. J.P. Davidson's theory of odd parity states[8] results in a diagonal inertial tensor and a band structure similar to that of the even parity states, if an assumption regarding the nuclear surface is made (See chapter II, page 12). M.G. Davidson[9] has noted that without this assumption, the inertial tensor will not be diagonal, resulting in a more complicated energy level structure.

To test the validity of these theories, numerous experiments have been carried out on deformed nuclei. The decay $^{160}Tb \rightarrow ^{160}Dy$, both deformed nuclei of the rare earth region, has been studied extensively in previous investigations.

The β^- [11], the conversion electron[11,12] and the gamma spectra[13-17] resulting from the population and depopulation of the excited states of ^{160}Dy have been studied. Experiments on gamma-gamma coincidence[13,14] and directional correlation[18,19] have also been performed. Although the decay scheme of ^{160}Dy, and the spin and parity assignments of the energy levels seem well established, discrepancies exist as to the existence, placement and the intensity of some transitions.

The ^{160}Tb sample used in this investigation was obtained from New England Nuclear Inc. and prepared with an impurity of less than 1% of other activities. The gamma, K-conversion electron and gamma-gamma coincidence spectra were analyzed and are reported in chapters III, IV and V respectively. The energy levels and their electromagnetic properties obtained from these data, presented in chapter VI, are compared to the predictions of the asymmetric rotor model and the theory of odd parity states as proposed by M.G. Davidson.

CHAPTER II

COLLECTIVE MODEL OF EVEN-EVEN DEFORMED NUCLEI

The first step in the development of the collective model is the expansion of the nuclear surface R in the laboratory reference frame L and a body-fixed frame B in terms of spherical harmonics as

$$R^{L}(\theta,\phi) = R_{o}[1 + \sum_{\substack{\lambda,\mu \\ \lambda>1}} a_{\lambda\mu}\, Y_{\lambda\mu}(\theta,\phi)] \tag{1a}$$

$$R^{B}(\theta',\phi') = R_{o}[1 + \sum_{\substack{\lambda,\mu \\ \lambda>1}} a'_{\lambda\mu}\, Y_{\lambda\mu}(\theta',\phi')] \tag{1b}$$

In the above expansions the $\lambda=0$ terms have been set equal to unity since the nuclear volume is to be constant. The $\lambda=1$ terms have been neglected as they correspond to the trivial translation of the centre of mass[9].

Since the nuclear surface is to be real, we require that

$$a_{\lambda-\mu} = (-1)^{\mu}\, a^{*}_{\lambda\mu} \qquad \text{and} \qquad a'_{\lambda-\mu} = (-1)^{\mu}\, a'^{*}_{\lambda\mu}$$

The expansion coefficients $a_{\lambda\mu}$ and $a'_{\lambda\mu}$ are related by

$$a'_{\lambda\mu} = \sum_{\nu} a_{\lambda\nu}\, D^{\lambda}_{\nu\mu}(\theta_i) \tag{2}$$

since

$$Y_{\lambda\mu}(\theta',\phi') = \sum_{\nu} Y_{\lambda\nu}(\theta,\phi)\, D^{*\lambda}_{\nu\mu}(\theta_i)$$

$D^{\lambda}_{\nu\mu}(\theta_i)$'s form a unitary rotation matrix connecting the reference

frames L and B through the three Eulerian angles $\theta_i = (\theta_1,\theta_2,\theta_3)$.

It can be shown that these $a_{\lambda\mu}$'s are the time dependent generalized coordinates of this model[9], and for small oscillations, the kinetic and the potential energies are given by

$$V^L = \frac{1}{2}\sum_{\lambda\mu} c_\lambda |a_{\lambda\mu}|^2 \tag{3a}$$

$$T^L = \frac{1}{2}\sum_{\lambda\mu} B_\lambda |\dot{a}_{\lambda\mu}|^2 \tag{3b}$$

where B_λ is a mass parameter and c_λ a restoring force constant. c_λ has contributions from surface tension and coulomb repulsion, the two forces which are assumed to be responsible for the surface oscillations[27].

From here on we shall restrict ourselves to the quadrupole (λ=2) case which describes the even parity states. The octupole (λ=3) case for odd parity states is discussed in section 3.

Dropping the λ=2 subscript, equation 1 is replaced by

$$R^L(\theta,\phi) = R_o[1 + \sum_{\mu=-2}^{2} a_\mu Y_{2\mu}(\theta,\phi)] \tag{4a}$$

$$R^B(\theta',\phi') = R_o[1 + \sum_{\mu=-2}^{2} a'_\mu Y_{2\mu}(\theta',\phi')] \tag{4b}$$

If the body fixed frame is chosen so that its axes (1,2,3) are along the three principle axes of the deformed body, it can be shown that $a'_{\pm1}=0$[21]. We can define

$$a'_o = \beta\mathrm{Cos}\gamma \qquad \text{and} \qquad a'_{\pm2} = \frac{\beta}{\sqrt{2}}\mathrm{Sin}\gamma \tag{5}$$

where β and γ are new variables determining the shape of the ellipsoid. β is the magnitude of deformation of the nucleus and γ its deviation from axial symmetry, with the nucleus being symmetric about the 3 axes when $\gamma=0$.

Using equations (2) and (5) and the time derivatives of $D^{\lambda}_{\mu\nu}$ (see ref.9, p.18) in equations (3a) and (3b) we obtain for kinetic and potential energies

$$V^L = \frac{1}{2} c\beta^2 \tag{6a}$$

$$T^L = \frac{B}{2}(\dot{\beta}^2 + \beta^2\dot{\gamma}^2) + \frac{1}{2}\sum_k I_k \omega_k^2 \tag{6b}$$

$$I_k = 4B\beta^2 \, \mathrm{Sin}^2(\gamma - \tfrac{2\pi}{3} k) \tag{6c}$$

where I_k's and ω_k's are the moments of inertia and components of angular velocity respectively about the three axes (1,2,3) of the body-fixed reference frame.

The first term in T^L is the vibrational energy and the second the rotational energy.

It can be shown that the Hamiltonian for this system is given by[9]

$$\hat{H} = \hat{T}_{vib} + \hat{T}_{rot} + \frac{1}{2} c\beta^2 \tag{7}$$

$$\hat{T}_{vib} = -\frac{\hbar^2}{2B}\left[\frac{1}{\beta^4}\frac{\partial}{\partial\beta}\beta^4\frac{\partial}{\partial\beta} + \frac{1}{\beta^2\mathrm{Sin}^2(3\gamma)}\frac{\partial}{\partial\gamma}\mathrm{Sin}(3\gamma)\frac{\partial}{\partial\gamma}\right] \tag{7a}$$

$$\hat{T}_{rot} = \frac{\hbar^2}{2}\sum_k \frac{\hat{J}_k^2}{4B\beta^2\mathrm{Sin}^2(\gamma - \frac{2\pi}{3} k)} \tag{7b}$$

where $\hat{J}_k$'s are the components of total angular momentum on the three body-fixed axes (1,2,3), having the commutation relations

$$[\hat{J}_1,\hat{J}_2] = -i\,\hat{J}_3 \qquad \text{cyclically.}$$

The Schrodinger equation is given by

$$(\hat{T}_{vib}+\hat{T}_{rot}+\frac{1}{2}\,c\beta^2)\;\Psi_J(\beta,\gamma,\theta_i) = E_J(\beta,\gamma)\;\Psi_J(\beta,\gamma,\theta_i).$$

2. The Asymmetric Rigid Rotor Model

If we assume the nucleus to be a rigid triaxial ellipsoid, i.e. β and γ are both non-zero constants, the Hamiltonian for the $\lambda=2$ case describing the even parity states of the nucleus is given by

$$\hat{H} = \frac{1}{2}\hbar^2 \sum_k \frac{\hat{J}_k^2}{4B\beta^2 \mathrm{Sin}^2(\gamma - \frac{2\pi}{3}k)} \qquad (2.1)$$

The Schrodinger equation has the form

$$(\hat{H}-\epsilon_J)\;\Psi_{JM}(\theta_i) = 0 \qquad (2.2)$$

where M is the projection of the total angular momentum J on the ż axis of the laboratory frame.

To solve (2.2) one needs to choose a set of basis vectors, the most convenient of which is the set of rotation matrices $D^J_{MK}(\theta_i)$, which are the eigen vectors of a symmetric rotor[9], having the following properties

$$\hat{J}\;D^J_{MK}(\theta_i) = J(J+1)\;D^J_{MK}(\theta_i)$$

$$\hat{J}_3 D^J_{MK}(\theta_i) = K\;D^J_{MK}(\theta_i)$$

$$\hat{J}_z D^J_{MK}(\theta_i) = M\;D^J_{MK}(\theta_i)$$

We can expand the eigen vectors Ψ_{JM} as

$$\Psi_{JM}(\theta_i) = \sum_{K=-J}^{J} A_K\;D^J_{MK}(\theta_i)$$

The only restriction on the choice of the body-fixed system is that its axes must coincide with the principal axes of the rotor. There are 24 ways of assigning such a right-handed coordinate system and Ψ_{JM} should be invariant under rotations from one such system to another. For even nuclei, which experiments show to have K equal to an even integer, this leads to the requirement (for even parity levels) that

$$A_{-K} = (-1)^J A_K.$$

The properly normalized Ψ_{JM} satisfying the above conditions is given by

$$\Psi_{JM} = \sum_{\substack{K=0 \\ K=\text{even}}}^{J} A_K \left(\frac{2J+1}{16\pi^2(1+\delta_{K0})}\right)^{\frac{1}{2}} (D^J_{MK} + (-1)^J D^J_{M-K}) \qquad (2.3)$$

Schrodinger's equation (2.2) can be solved using the Hamiltonian (2.1) and the wave functions (2.3). In solving this equation, a set of N linear equations in A_K's will result, where

$$N = \frac{1}{2}(J+2) \text{ for } J = \text{even} \quad \& \quad N = \frac{1}{2}(J-1) \text{ for } J = \text{odd}.$$

By requiring the N equations to be solvable, one obtains a polynomial of degree N in ϵ_J, the roots of which are the energy eigenvalues. The N coefficients of equation (2.3) are then obtained for each ϵ^N_J, by solving the remaining N-1 equations and normalizing Ψ^N_{JM} to unity.

The energy eigen values ϵ^N_J for J = 2,3,4 and 5 are given in table II-1.

The only state function which corresponds to a definite value of K is the J=3 state with K=2, since the summation in equation (2.3) is over K=0 and K=2 with the K=0 term cancelling out. The other state functions are mixtures of K = 0,2,4 ... etc. states. However it can be shown that for $\gamma<15°$ only one

TABLE II-1

ENERGY EIGEN VALUES OF AN ASYMMETRIC ROTOR

$$\varepsilon_2^1 = \left(\frac{\hbar^2}{4B\beta^2}\right) \frac{9}{\mathrm{Sin}^2(3\gamma)} (1-\Gamma)$$

$$\varepsilon_2^2 = \left(\frac{\hbar^2}{4B\beta^2}\right) \frac{9}{\mathrm{Sin}^2(3\gamma)} (1+\Gamma)$$

$$\varepsilon_3 = \left(\frac{\hbar^2}{4B\beta^2}\right) \frac{18}{\mathrm{Sin}^2(3\gamma)} \qquad \Gamma = \left(1 - \frac{8}{9}\,\mathrm{Sin}\,(3\gamma)\right)^{\frac{1}{2}}$$

$$\varepsilon_5^1 = \left(\frac{\hbar^2}{4B\beta^2}\right) \frac{9}{\mathrm{Sin}^2(3\gamma)} (5-3\Gamma)$$

$$\varepsilon_5^2 = \left(\frac{\hbar^2}{4B\beta^2}\right) \frac{9}{\mathrm{Sin}^2(3\gamma)} (5+3\Gamma)$$

The energies of the J=4 states, in units of $\frac{\hbar^2}{4B\beta^2}$, are the solutions of the cubic equation

$$\varepsilon^3 - \frac{90}{\mathrm{Sin}^2(3\gamma)}\varepsilon^2 + \frac{48[27+26\mathrm{Sin}^2(3\gamma)]}{\mathrm{Sin}^4(3\gamma)}\varepsilon - \frac{640[27+7\mathrm{Sin}^2(3\gamma)]}{\mathrm{Sin}^4(3\gamma)} = 0$$

of the coefficients A_K of equation (2.3) differs appreciably from zero and to a high degree of accuracy the wave functions can be approximated by only one value of K. For example, of the two states with J=2, one corresponds almost exactly to K=0 and the other to K=2; of the three states with J=4, one corresponds to each value of K = 0,2 and 4.

With K now a good quantum number, the energy levels can be divided into bands of definite K. The band with K=0, having the spin sequence J = 0,2,4,6... etc. is called the "ground state rotational band". The K=2 band with J = 2,3,4... etc. is called the "γ-vibrational band", because in the symmetric rotor model this band is attributed to vibrations of the γ degree of freedom. Bands of higher K, for example K = 4,6... etc., with J = K, K+1,... exist at higher excitation energies.

The β-vibrational band, K=0 and J= 0,2,4..., observed in some deformed nuclei at low excitation energies, can be accounted for in this model[7] in the same manner as in the symmetric rotor model, by allowing vibrations in the β degree of freedom.

3. Theory of Odd Parity States

As mentioned earlier the octupole terms in the expansion of the nuclear surface describe the odd parity states. The coefficients in the expansion

$$R^B(\theta',\phi') = R_o[1 + \sum_{\mu=-3}^{3} a'_\mu Y_{3\mu}(\theta',\phi')] \qquad (3.1)$$

can be defined a

$$a'_o = \zeta \, \mathrm{Cos}\eta \, \mathrm{Cos}\omega \qquad a'_{\pm1} = \pm\zeta \frac{\mathrm{Cos}\alpha}{\sqrt{2}} \mathrm{Sin}\omega$$

$$a'_{\pm2} = \zeta \frac{\mathrm{Sin}\eta}{\sqrt{2}} \mathrm{Cos}\omega \qquad a'_{\pm3} = \pm\zeta \frac{\mathrm{Sin}\alpha}{\sqrt{2}} \mathrm{Sin}\omega$$

It can be shown that the Hamiltonian for a rotating rigid octupole shaped nucleus is given by[10)]

$$\hat{H} = \frac{\hbar^2}{2}\frac{1}{\mathcal{I}}\left(I_{33}\hat{J}_1^2 + \frac{\mathcal{I}}{I_{22}}\hat{J}_2^2 + I_{11}\hat{J}_3^2 - I_{13}(\hat{J}_1\hat{J}_3+\hat{J}_3\hat{J}_1)\right) \qquad (3.2)$$

$$\mathcal{I} = I_{11}I_{33} - I_{13}^2$$

The components of the inertial tensor, I_{ij}, are equal to

$$I_{11} = B_3\zeta^2[\mathrm{Sin}^2\omega(1.5+\mathrm{Cos}^2\alpha+\sqrt{15}\ \mathrm{Cos}\alpha\mathrm{Sin}\alpha) + \mathrm{Cos}^2\omega(4+2\mathrm{Cos}^2\eta+2\sqrt{15}\ \mathrm{Sin}\eta\mathrm{Cos}\eta)]$$

$$I_{22} = B_3\zeta^2[\mathrm{Sin}^2\omega(1.5+7\mathrm{Cos}^2\alpha-\sqrt{15}\ \mathrm{Cos}\alpha\mathrm{Sin}\alpha) + \mathrm{Cos}^2\omega(4+2\mathrm{Cos}^2\eta-2\sqrt{15}\ \mathrm{Sin}\eta\mathrm{Cos}\eta)]$$

$$I_{33} = B_3\zeta^2[\mathrm{Sin}^2\omega(8\mathrm{Sin}^2\alpha+1) + 4\mathrm{Cos}^2\omega\mathrm{Sin}^2\eta]$$

$$I_{13} = I_{31} = B_3\zeta^2[\mathrm{Sin}\eta(5\sqrt{6}\ \mathrm{Sin}\alpha+3\sqrt{10}\ \mathrm{Cos}\alpha) + 2\sqrt{6}\ \mathrm{Cos}\eta\mathrm{Cos}\alpha]\ \frac{1}{4}\ \mathrm{Sin}2\omega$$

$$I_{32} = I_{23} = 0$$

$$I_{21} = I_{12} = 0 \qquad (3.3)$$

In the body-fixed system, chosen to diagonalize the quadrupole inertial tensor, the octupole inertial tensor is not diagonal. Since $I_{13} = I_{31}$ are the only non-zero off-diagonal elements, only the 2 axis coincides with a principal axis of the rotor. Using this rotational symmetry in the expansion of the wave function Ψ_{JM} in terms of $D^J_{MK}(\theta_i)$, it can be shown that[10)]

$$\Psi_{JM} = \left(\frac{2J+1}{8\pi^2}\right)^{\frac{1}{2}} \sum_{K=0}^{J} \frac{A_K}{\sqrt{2}}\left(D^{J*}_{MK} - (-1)^{J-K}\ D^{J*}_{M-K}\right) \qquad (3.4)$$

with the normalizing condition

$$\sum_{K=0}^{J}(1+\delta_{K0})\ A_K^2 = 1$$

The assumption $a'_{\pm1}=a'_{\pm3}=0$ in the theory of odd parity states proposed by J.P. Davidson[8] is equivalent to setting $\omega=0$. This diagonalizes the inertial tensor, resulting in more stringent symmetry conditions, which leads to the requirement that K is even.

The Hamiltonian of equation (3.2), when operating on D^J_{MK}, changes K by $\Delta K=0, \pm1, \pm2$, thus allowing for even and odd values of K simultaneously. Schrodinger's equation will result in N states of angular momentum J, where

$$N = J + \frac{1-(-1)^J}{2}$$

If ϵ^N_J is the energy of the N^{th} state of angular momentum J, then neglecting the $\frac{\hbar^2}{2}$ constant

$$\begin{aligned}
\epsilon^1_1 &= \left(\frac{1}{I_{22}} + \frac{1}{2\mathcal{I}}\,(I_{11}+I_{33}) - I'\right)\\
\epsilon^2_1 &= \left(\frac{1}{I_{22}} + \frac{1}{2\mathcal{I}}\,(I_{11}+I_{33}) - I'\right)\\
\epsilon^1_2 &= \left(\frac{1}{I_{22}} + \frac{5}{2\mathcal{I}}\,(I_{11}+I_{33}) - 3I'\right)\\
\epsilon^2_2 &= \left(\frac{1}{I_{22}} + \frac{5}{2\mathcal{I}}\,(I_{11}+I_{33}) + 3I'\right)
\end{aligned} \qquad (3.5)$$

where $I' = \frac{1}{2\mathcal{I}}\left((I_{11}-I_{33})^2 + 4I^2_{13}\right)$

No analytic forms can be obtained for the energies of the J=3 and J=4 states, since each involves the solution of a set of 4 linear equations in 4 A_K's. These eigen values are to be obtained by diagonalizing the determinants of these equations, using computer programs, for a given set of I_{11}, I_{22}, I_{33} and I_{13}.

As in the theory of the even parity states, the nucleus can be softened

to allow for surface vibrations[10]. These vibrations, which are associated with the ζ degree of freedom, are analogous to the β vibrations of the theory of the even parity states. Introduction of these vibrations results in rotational level structures, built on states with one or more quanta of ζ vibrations.

4. Reduced E2 Branching Ratios

The probability per unit time for an electric 2^{λ}-pole transition between states of J_i and J_f is given by[9]

$$T(\lambda) = \frac{8\pi(\lambda+1)}{\hbar\lambda[(2\lambda+1)!!]^2} \left(\frac{E_\gamma}{\hbar c}\right)^{2\lambda+1} B(E\lambda;\ J_i \to J_f) \qquad (4.1)$$

where $E\gamma$ is the energy of the emitted photon of angular momentum λ, and $B(E\lambda,\ J_i \to J_f)$ is an energy independent matrix element, called the reduced $E\lambda$ transition probability, defined as

$$B(E\lambda,\ J_i \to J_f) = \frac{1}{2J_i+1} \sum_{M_i, M_f} \sum_{\mu} |\langle J_f M_f | Q^L_{\lambda\mu} | J_i M_i \rangle|^2 \qquad (4.2)$$

where $Q^L_{\lambda\mu}$ is the appropriate electric multiple operator defined in the laboratory reference frame. $Q^L_{\lambda\mu}$ is related to the same operator in the body-fixed system, $Q^B_{\lambda\nu}$, by

$$Q^L_{\lambda\nu} = \sum_{\nu} Q^B_{\lambda} D^{\lambda *}_{\mu\nu}$$

It can be shown that for electric quadrupole transitions, $Q^B_{\lambda\nu}$, is given by[5]

$$Q^B_{2\nu} = \frac{3ze}{\sqrt{5r}} R_o^2 a'_\nu \qquad (4.4)$$

where a_ν's are defined by equation (5). The operator $Q^L_{2\mu}$, which is to be used in equation (4.2), is obtained by substituting (4.4) into (4.3), and is equal to

$$Q^L_{2\mu} = Q_o[\mathrm{Cos}\gamma D^{2*}_{\mu o} + \frac{\mathrm{Sin}\gamma}{\sqrt{2}}(D^{2*}_{\mu -2} + D^{2*}_{\mu 2})] \tag{4.5}$$

$$Q_o = \frac{3ze}{\sqrt{5\pi}} R_o^2 \beta$$

The reduced transition probabilities, B(E2; JN→J'N'), for a transition from the N^{th} state of angular momentum J to the N^{th} state of J', can be calculated using the $Q^L_{2\mu}$ of (4.5) and the state functions of (2.3) in equation (4.2). The exact forms of these reduced transition probabilities are given in references 5 and 6. However it can be shown that for $\gamma<15^\circ$, with K being approximately a good quantum number, these expressions simplify to

$$\begin{aligned}
B(E2;\ JK\to J'K) &= (Q_o^2/16\pi)5\mathrm{Cos}^2\gamma(2J0K|J'K)^2 \\
B(E2;\ JK\to J'K-2) &= (Q_o^2/16\pi)\tfrac{5}{2}(1+\delta_{K2})\mathrm{Sin}^2\gamma(2J-2K|J'K-2)^2 \\
B(E2;\ JK\to J'K+2) &= (Q_o^2/16\pi)\tfrac{5}{2}(1+\delta_{K0})\mathrm{Sin}^2\gamma(2J+2K|J'K+2)
\end{aligned} \tag{4.6}$$

where $(\lambda JK_f - K_i K_i | J'K_f)$ are the Clebsch-Gordon coefficients.

CHAPTER III

GAMMA-RAY SINGLES SPECTROSCOPY

The energies and the intensities of the gamma-rays emitted following the β^- decay of ^{160}Tb were measured with two Lithium drifted Germanium (Ge(Li)) crystals. The first detector used was a 45 cc coaxial detector with a resolution of 5.7 kev at 1332 kev, and the second a 35 cc coaxial with a resolution of 2.9 kev at 1332 kev. Although the results of measurements with the two detectors agreed well for fairly intense transitions, the smaller detector, because of its superior resolution, facilitated the identification of weak transitions and the measurement of their energies and intensities to a greater accuracy. The spectra and the results presented in this thesis are those obtained with the 35 cc detector.

In order to provide a test for identification of sum peaks, three spectra were taken at D=15, 7.5 and 0 cm, where D is the distance from the source to the crystal chamber wall, with the detector's front surface 2 cm inside the chamber.

The analyzing circuit employed consisted of a TENNELEC 135 M preamplifier, a TENNELEC 203 BLR amplifier with built-in baseline restorer and a 4096 Multi-Channel Analyzer (MCA).

1. PEAK FITTING

A limiting factor in the accuracy of energy and intensity measurements of a gamma-ray is the uncertainty in estimating the position of the peak and its area. Such estimates can be obtained with ease with good accuracy, without recourse to analytic functions, for peaks well defined above background with no other peaks in their immediate vicinity. This is not the case

in general; peaks can overlap, fall on a Compton edge and so on - which then requires the fitting of the peak or peaks, with some appropriate function using a computer fitting program.

The function and the fitting method used in this work have been described in greater detail elsewhere[26]. In short, the shape of a peak may be approximated by a distorted Gaussian function, superimposed upon a step function. The function used in the fitting routine was

$$y(x) = P_1 + P_2x + S + E_1 + E_2 \qquad (3.1)$$

where

$$S = P_3\left(\frac{\pi}{2} - \text{Arctan}\ (2.0(x-P_5))\right)$$

$$E_1 = P_4 \exp\ -\frac{(x-P_5)^2}{2P_6^2}$$

$$E_2 = P_7 \exp\ -\frac{(x-P_8)^2}{2P_9^2}$$

In this function, P_1 through P_9 are the fitting parameters, P_1+P_2x providing a linear background and S the step function. E_1 is the main Gaussian of height P_4, position P_5, and standard deviation P_6; E_2 is the satellite Gaussian which accounts for the distortion in the pure Gaussian shape.

Each spectrum was fitted in two steps in order to reduce the number of parameters, thereby facilitating the fitting procedure in the case of overlapping peaks. First a number of well defined peaks were fitted over the whole of the energy range, relations P_7/P_4, P_9/P_6 and P_5-P_8 were obtained as functions of energy, thus reducing the number of parameters to six. Figure III-1 shows the above mentioned functions obtained for the spectrum at D=7.5 cm. As the

Figure III-1
Parameters of the Peak Fitting Program

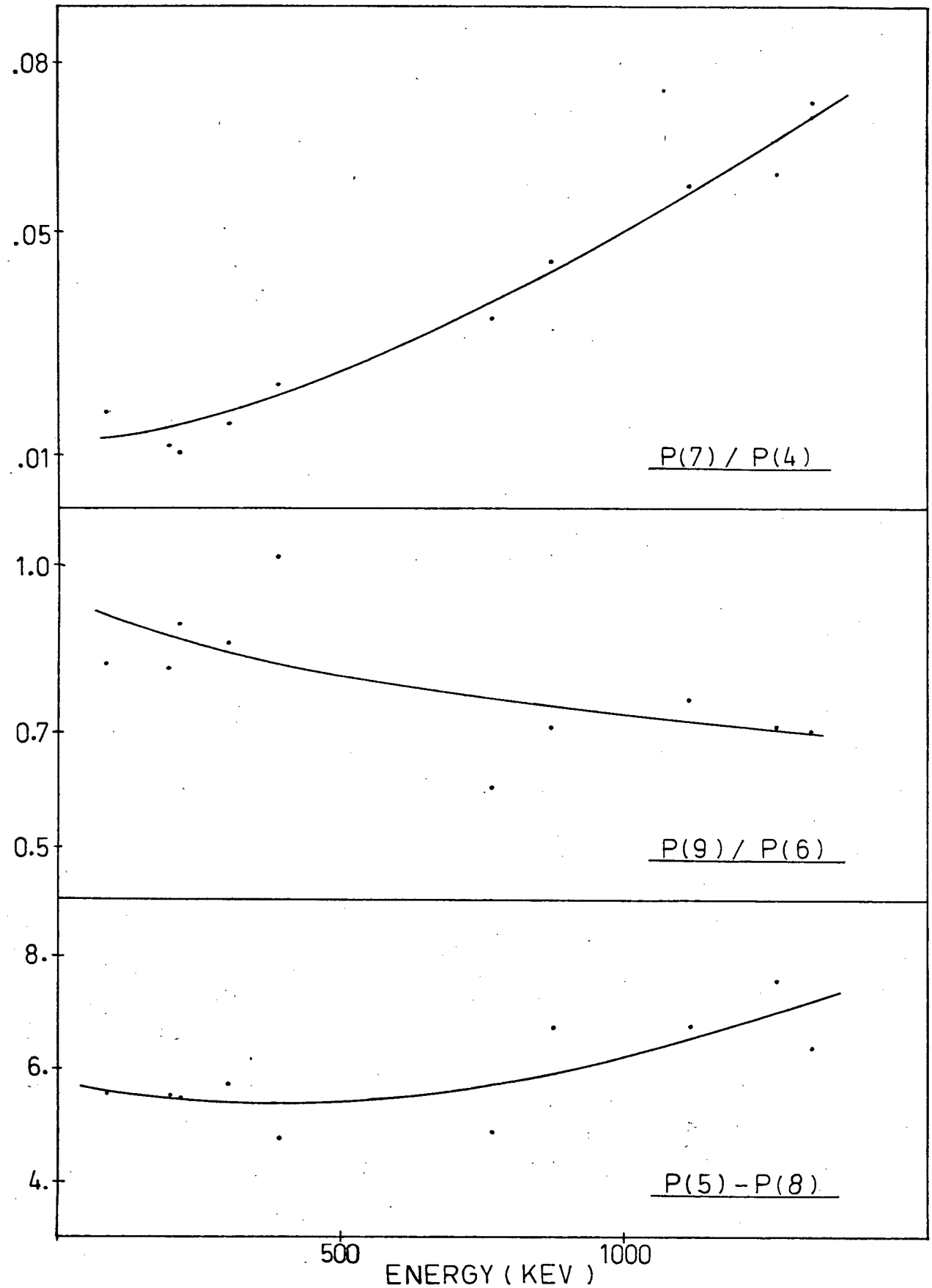

second step these functions were employed in the original function, equation (3.1), to fit all the peaks in the spectrum.

The position of a peak was taken to be the position of the centroid of the main Gaussian, and its area as the sum of the areas of the main and the satellite Gaussians. The errors in position and areas used were those returned by the RLQF (Restricted-Least-Square Fit) subroutine of the UBC Computer Centre Library.

2. ENERGY CALIBRATION

The energy calibration of the gamma spectra was done in two steps. First a spectrum was taken of the ^{160}Tb source and a set of standard sources listed in Table III-1. The peaks of the standard sources and all the intense peaks of ^{160}Tb, listed in Table III-2, were fitted using the previously mentioned fitting program and their positions found. A function of the form

$$\text{ENERGY} = a+b(\text{CHANN.NO.}) + c(\text{CHANN. NO.})^2$$

was least-square-fitted to the positions and the energies of the standard peaks. The energies of the intense peaks of ^{160}Tb, the secondary standards, were found from the above function. Figure III-2 shows the plot of the energies of the standard peaks against their position and the fitted function with

$$a = -74.0\pm.2\ , \qquad b = .4254\pm.0001\ , \qquad c = -.228\times10^{-6}.$$

As the second step in the energy calibration, the energies of the secondary standard peaks of ^{160}Tb were used in each subsequent spectrum to obtain the energies of all other gamma-ray peaks.

TABLE III-1

STANDARD SOURCES FOR ENERGY CALIBRATION

SOURCE	ENERGY (kev)
^{57}Co	121.97±.03
	136.33±.03
^{22}Na	511.006±.002
	1274.55±.04
^{137}Cs	661.64±.08
^{54}Mn	834.81±.03
^{60}Co	1173.23±.04
	1332.49±.05

TABLE III-2

SECONDARY ENERGY STANDARDS OF ^{160}Dy

ENERGY (kev)
86.8
196.9
215.5
298.4
879.3
1178.2
1272.0

Figure III-2
Energy Calibration

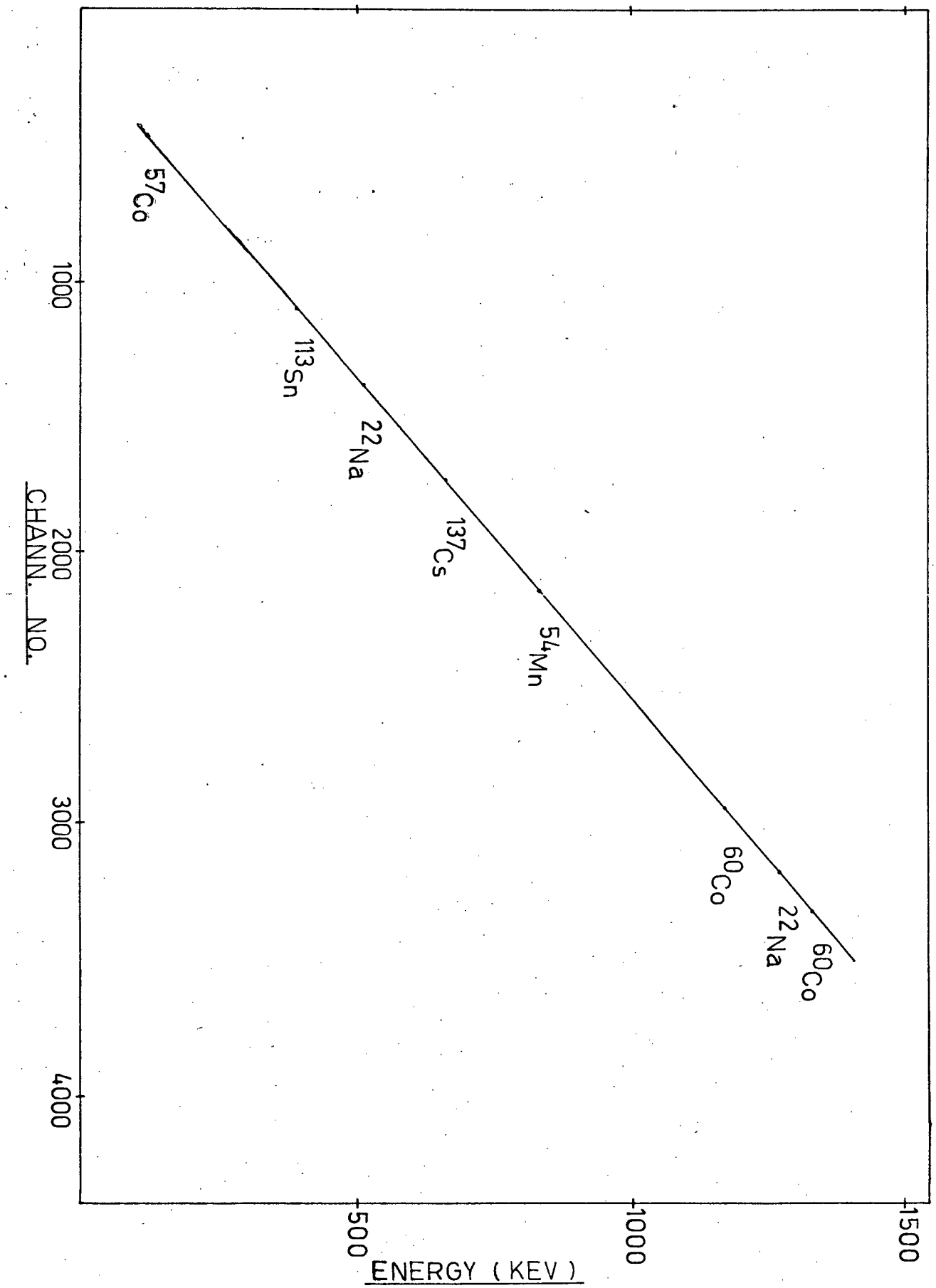

3. EFFICIENCY CALIBRATION

The total efficiency of a detector, defined as the ratio of the measured gamma-ray intensity I to the total intensity I_o, is given by

$$\frac{I}{I_o} = \frac{\Omega}{4\pi} \varepsilon(E)$$

where Ω is the solid angle subtended by the detector and ε is the intrinsic efficiency of the detector, a function primarily of gamma-ray energy E.

The efficiency of a GE(Li) detector, I/I_o, has a maximum in the vicinity of 100 kev. For higher gamma-ray energies (E>100 kev), the function $\frac{I}{I_o}$ decreases slowly with increasing energy, while for E<100 kev the efficiency drops sharply. This drop in efficiency is due to absorption effects in the detector window which is the insensitive layer at the front face of the detector[28].

To obtain the efficiency of the GE(Li) detector below this maximum, we have used as secondary standards some of the intense transitions in ^{160}Dy decay in a manner to be discussed later. Table III.3 lists the standard sources available for the efficiency calibration of the 35 cc GE(Li) detector. These sources, encapsulated in aluminum disks, were obtained from the International Atomic Energy Agency, Vienna.

In order to obtain the relative intensities of the transitions below 100 kev, i.e. the 86.8, 93.9 and 97.7 kev gamma-rays, a previously calibrated 3 mm Lithium drifted Silicon (Si(Li)) detector was used to obtain the ratio of the intensity of the 86.8 kev transition to that of the 298.3 kev transition of ^{160}Tb. Figure III-3 shows the inverse efficiency function, $\frac{I_o}{I}$, of the Si(Li) detector for gamma-rays. The relevant portion of the ^{160}Tb gamma spectrum obtained with this Si(Li) detector is shown in Figure III-4.

TABLE III-3

EFFICIENCY CALIBRATION STANDARDS

Source	Transition energy (kev)	Half-Life	Strength (μ curies) at Jan.1, 1970	Relative Intensity (%)
^{57}Co	122	271.6±.5 days	11.43±.7%	85.0±1.7
	136			11.4±1.3
^{113}Sn	393	115.0±.5 days	4.22×10^5 gamma/sec.	
^{22}Na	511	2.602±.005 years	9.16±1.0%	181.1±.2
	1275			99.95±.02
^{137}Cs	662	30.5±.3 years	10.35±1.8%	85.1±.4
^{54}Mn	835	312.6±.3 days	10.96±.7%	100.0
^{60}Co	1173	5.28±.01 years	10.57±.6%	99.87±.05
	1332			99.999±.001

Figure III-3

Gamma-Ray Efficiency of Si(Li) Detector

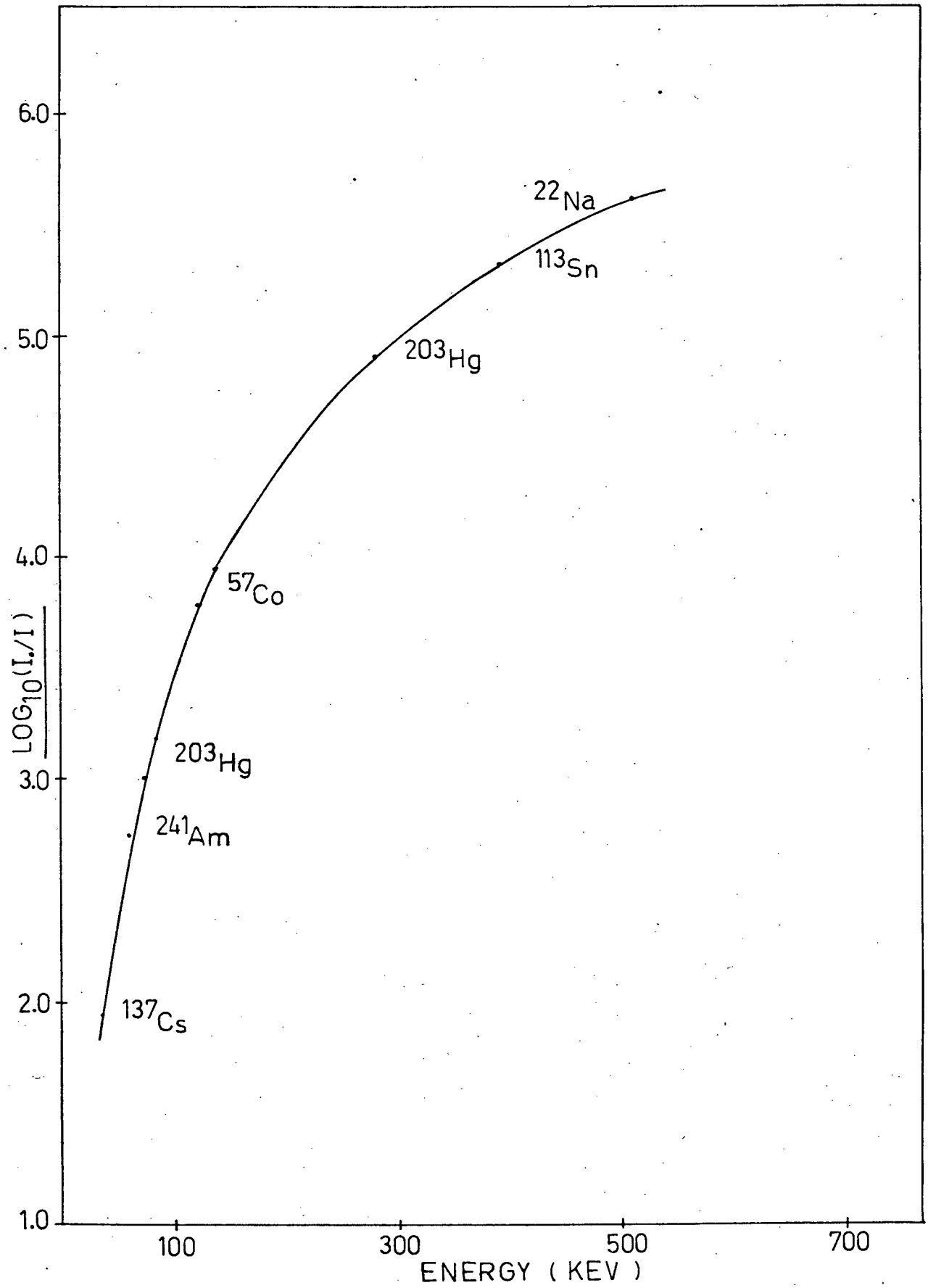

Figure III-4

^{160}Dy Gamma Spectrum With Si(Li) Detector

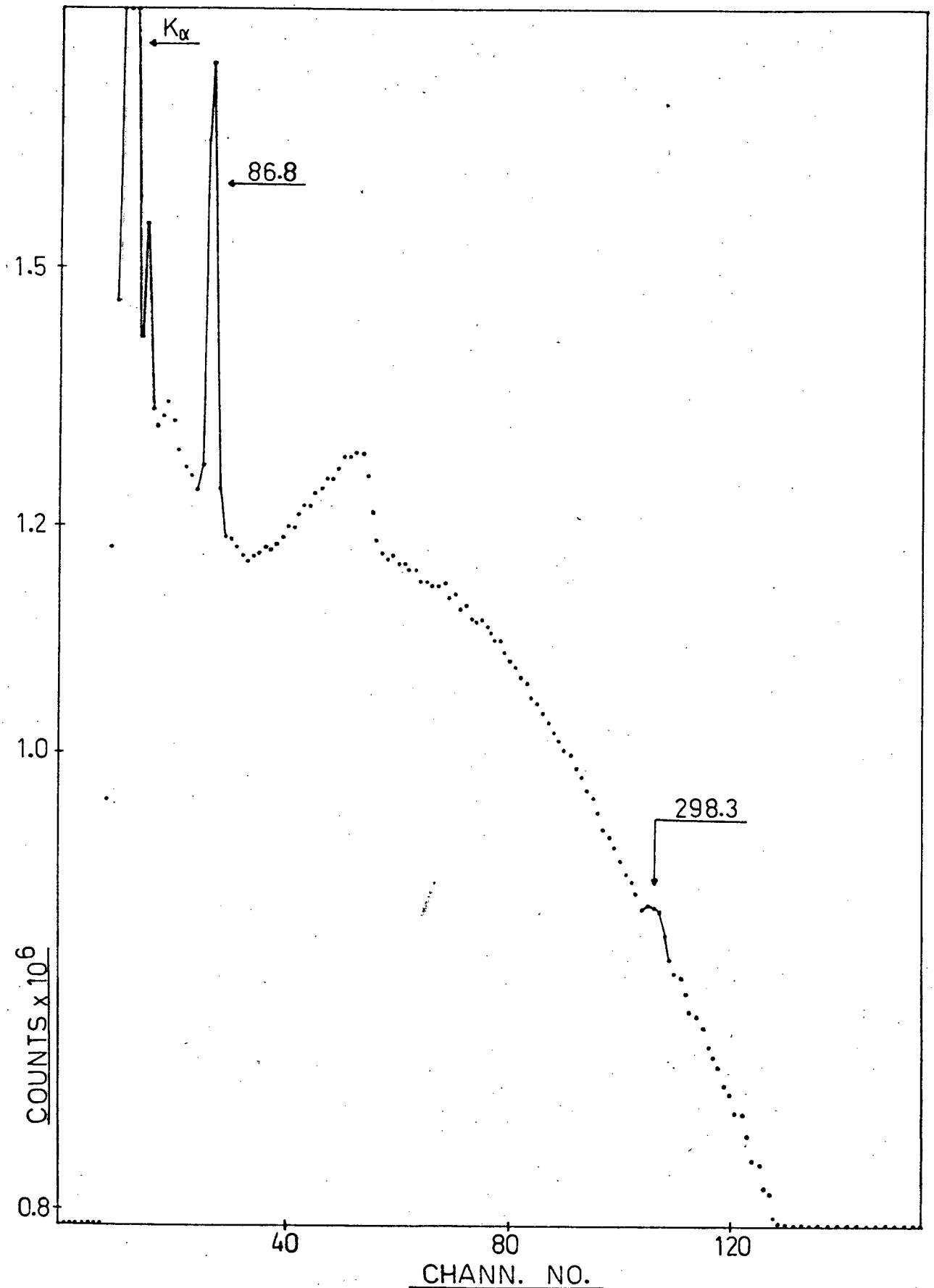

A 1 mm thick aluminum absorber was placed between the source and the detector to eliminate the low energy electrons. The result of the measurement was

$$\frac{I_o(298.3)}{I_o(86.8)} = 1.93 \pm .1$$

The efficiency of the GE(Li) detector was obtained at E = 86.8 kev, using the measured intensity of the 86.8 kev transition, I(86.8), and its total intensity, $I_o(86.8)$, obtained from $I_o(298.3)$ using the above ratio. The total intensities of the 93.9 and the 97.7 kev transitions were obtained from their measured intensities, by taking the efficiency of the detector at these energies to be approximately equal to the efficiency at 86.8 kev.

The uncertainty in the efficiency of the GE(Li) detector at each calibration energy is due to the following factors:

i) The uncertainty in calculating I_o due to the errors in data used; i.e. half lives, initial source strength and systematics of decay schemes (see table III-3);

ii) The error associated with the calculation of the area under each peak, because of background estimation and random counting error;

iii) The error from the analyzer dead time correction. Once the MCA has received a pulse for analysis, its input is blocked to all other pulses until the original pulse has been analyzed. A fraction of all pulses are lost due to this dead time, the time that the MCA input is blocked, and this fraction is the same for all channels since the pulses arrive at the MCA at random[26]. This correction factor was measured by analyzing on the same spectrum the signals from the source and the pulses from a pulser, generating 60 pulses per second. The pulses, fed into the preamplifier stage, are random with respect to the true signals from the source, so they have the same probability

of being blocked as other signals. Then the correction factor is given by the ratio of the number of pulser signals generated to the number detected, the error arising from the uncertainty in calculating the area of the pulser peak.

The inverse efficiency function, $\frac{I_o}{I}$, of the 35 cc GE(Li) detector for gamma-ray energies in the range 100-1400 kev is shown in Figure III-5; also shown by the error bars at each calibration energy are the errors in $\frac{I_o}{I}$ calculated from the above factors. The curve shown is the function

$$\frac{I_o}{I} = a + b(E-120) + c(E-120)^2 + d(E-120)^3$$

which was least square-fitted to the data. E is the energy in kev, and

$a = 485 \pm 30$ $\qquad$ $c = 1.65 \times 10^{-3}$

$b = 3.346 \pm .03$ $\qquad$ $d = -\ 0.8 \times 10^{-6}$

The above calibration function was obtained with the source at D=15 cm. The efficiency of the detector was also calibrated for D=0 cm, and it was found that the efficiency calibration functions at these two distances differed, within the error limits, by a constant factor, which is the change in the solid angle. Since we are interested only in the relative gamma-ray intensities, the calibration function for D=15 cm was used for all three spectra with D = 15, 7.5 and 0 cm.

4. ^{160}Tb GAMMA SPECTRA

As mentioned earlier, three gamma spectra were taken at D = 15, 7.5 and 0 cm. Figure III-6 (a through h) shows the spectrum taken at D = 7.5 cm. The positions and the area of the peaks were found using the fitting routine described earlier, and the energies and intensities found using the calibration functions. Table III-4 lists the average energies of all the

Figure III-5
Efficiency of Ge(Li) Detector

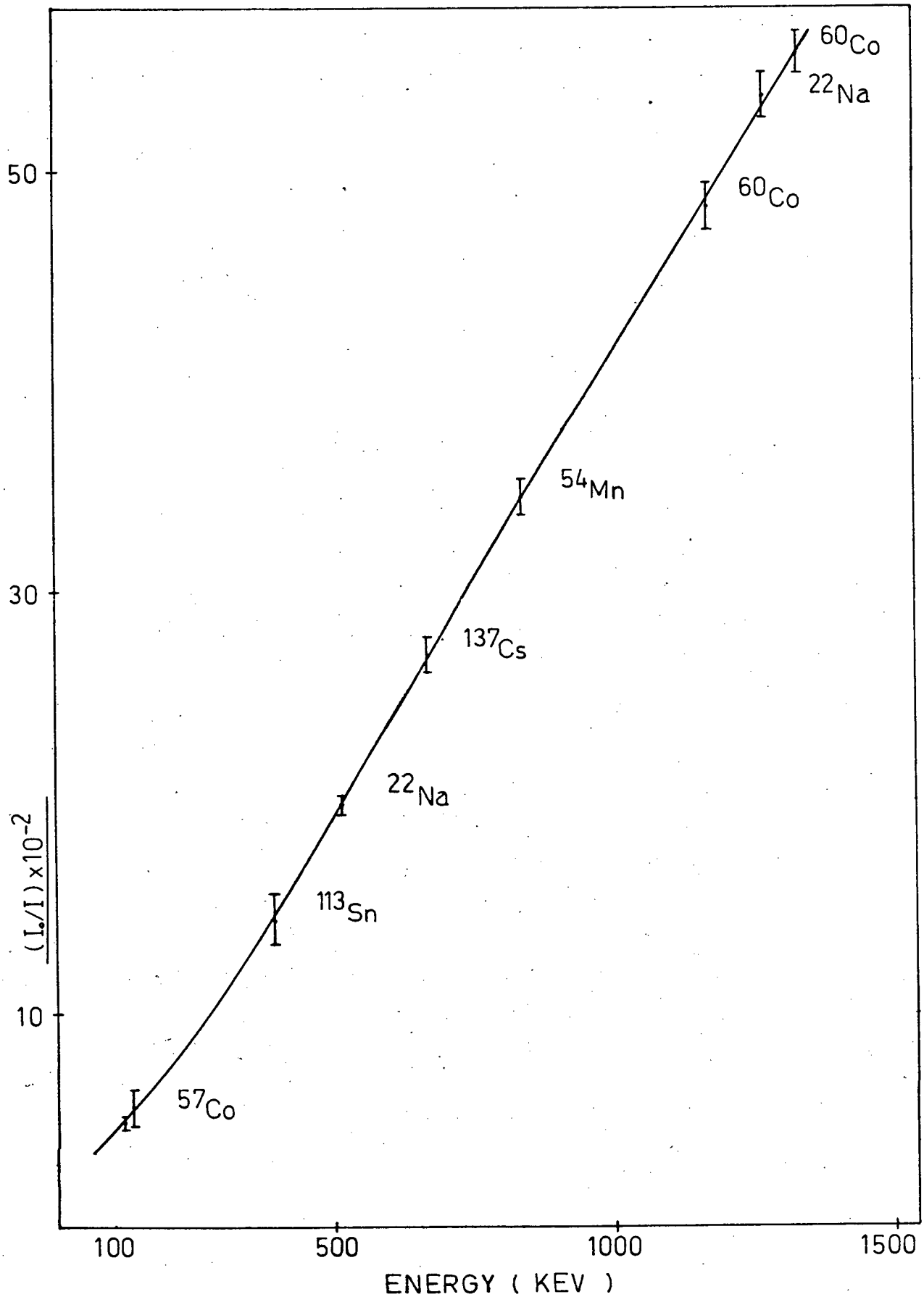

Figure III-6 (a)

^{160}Dy Gamma Spectrum With Ge(Li)

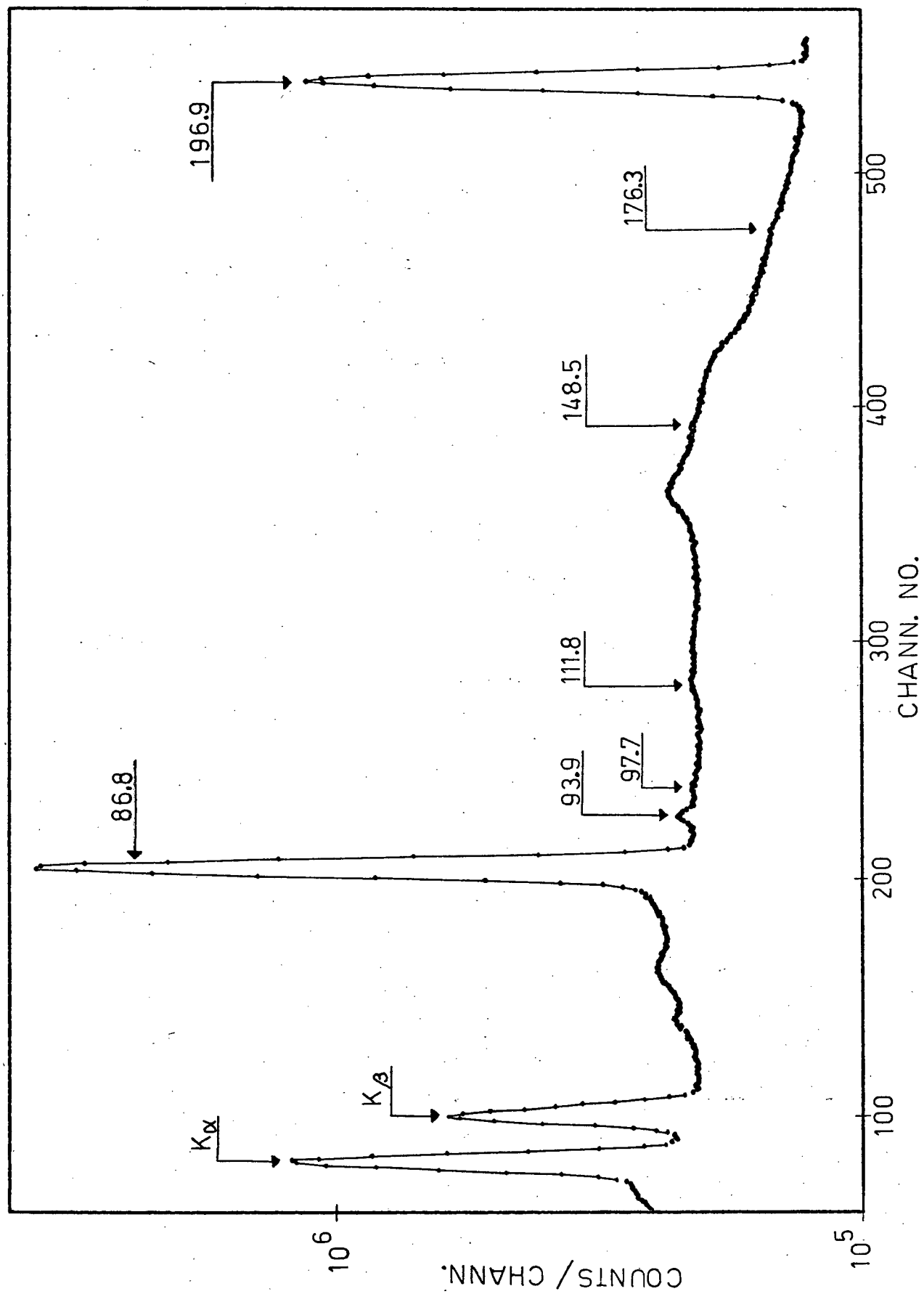

Figure III-6 (b)

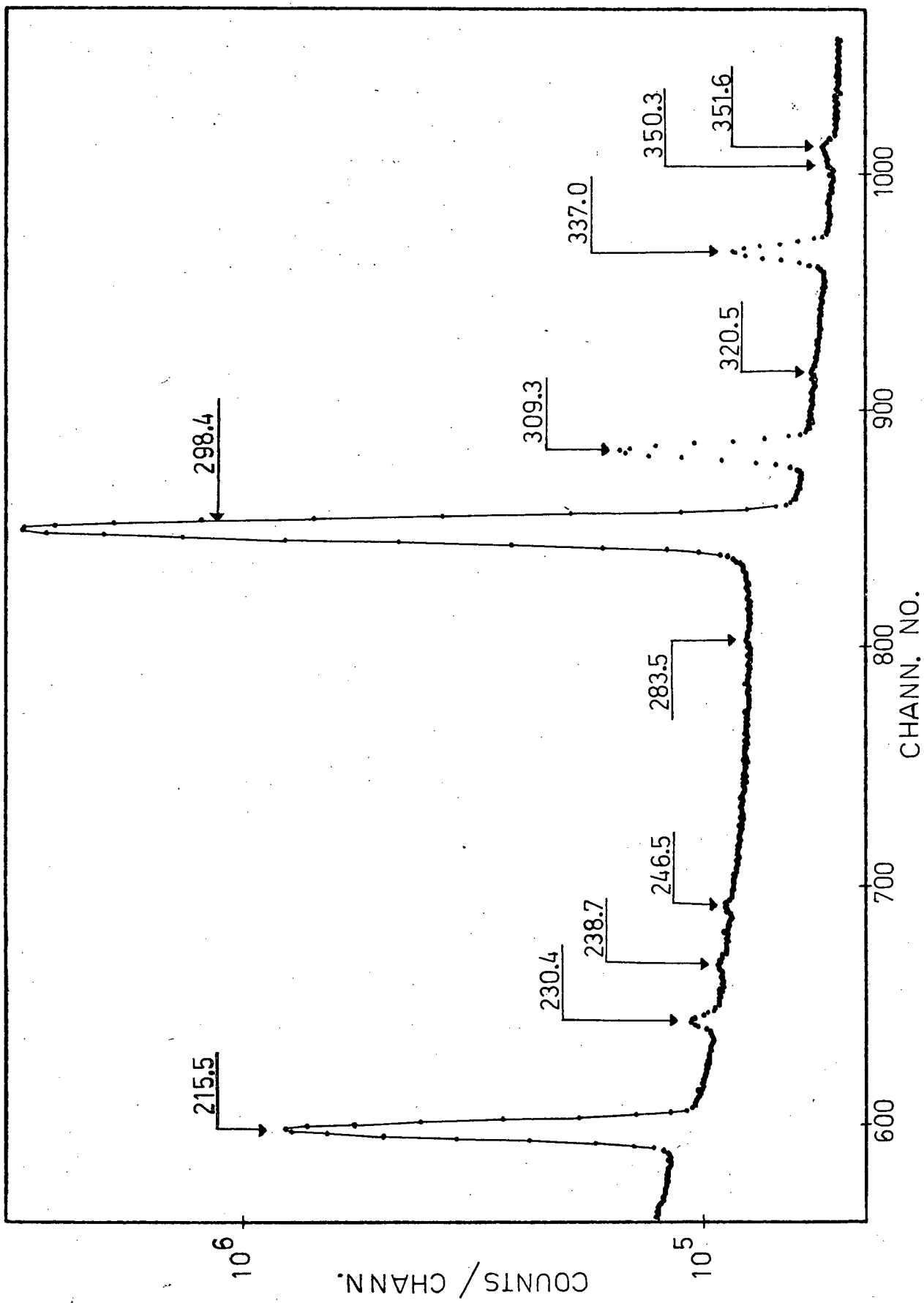

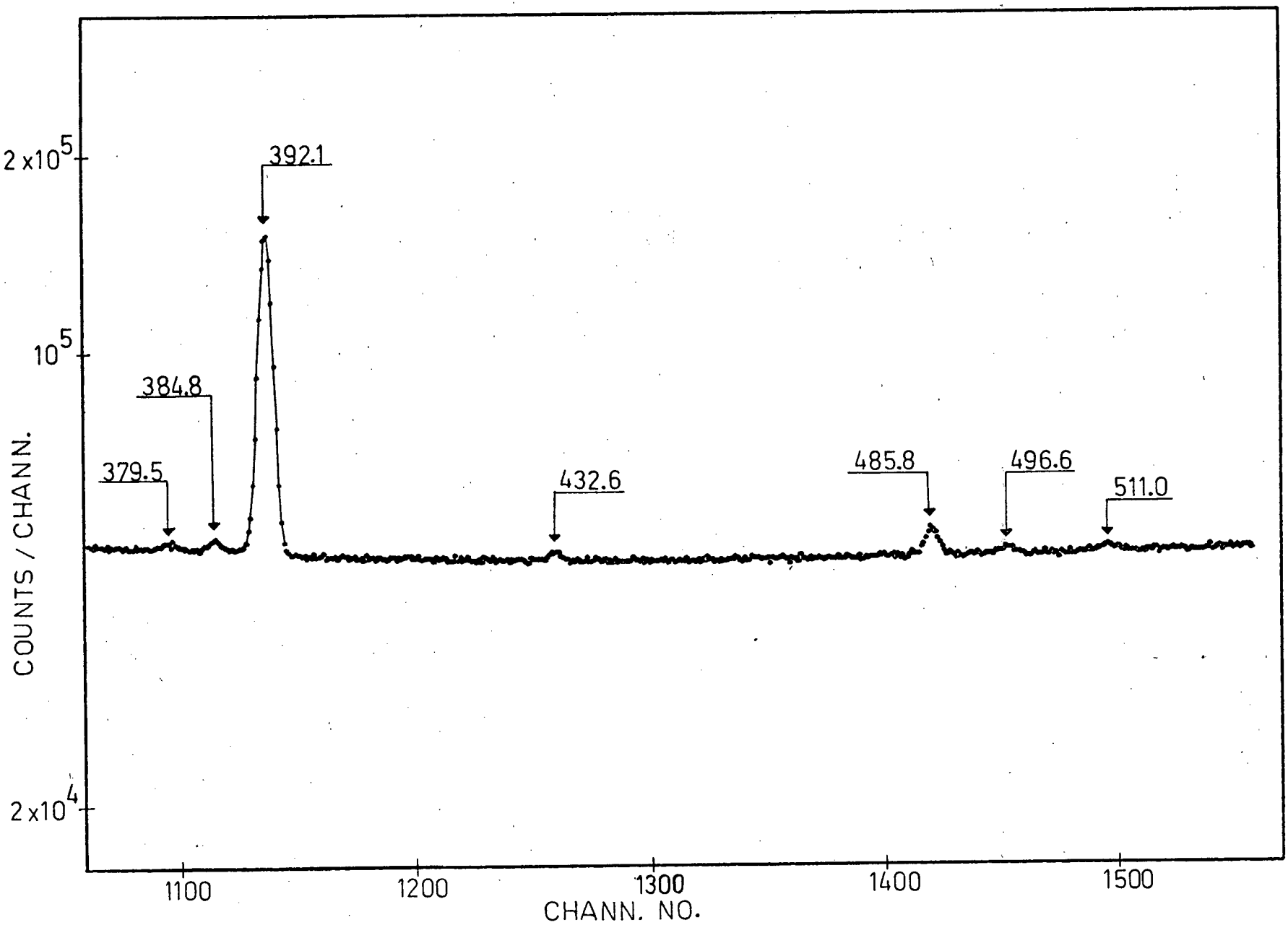

Figure III-6 (c)

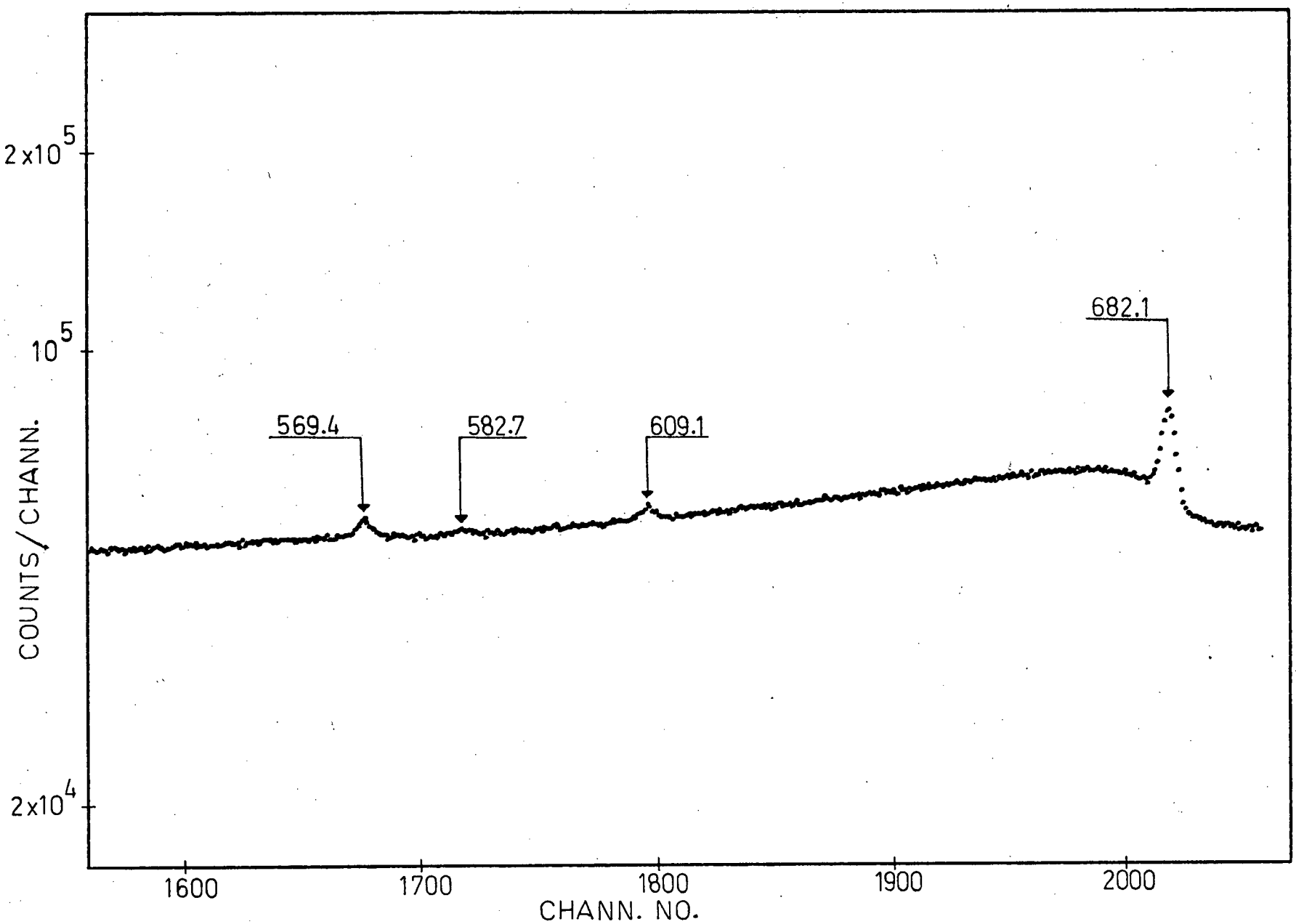

Figure III-6 (d)

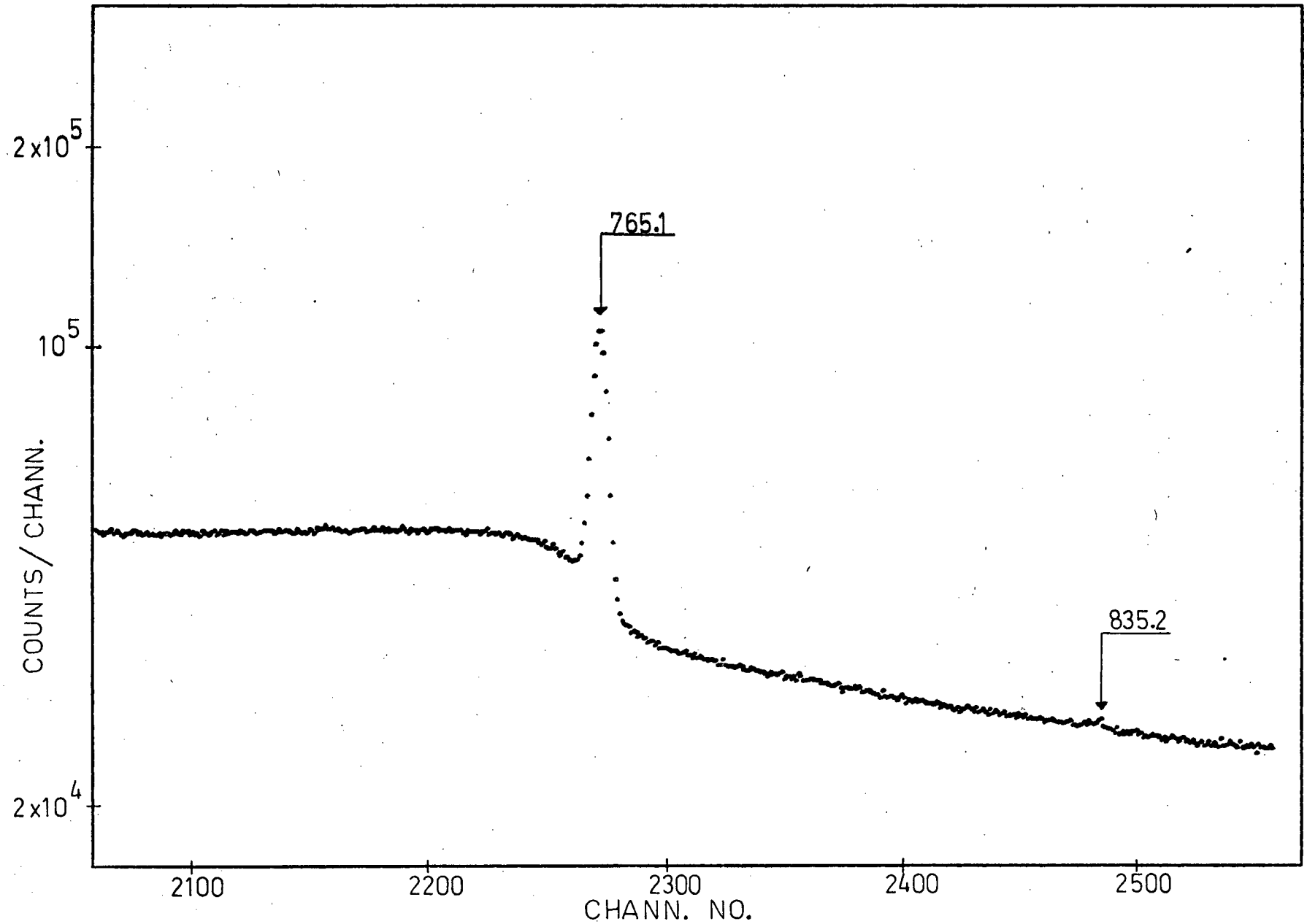

Figure III-6 (e)

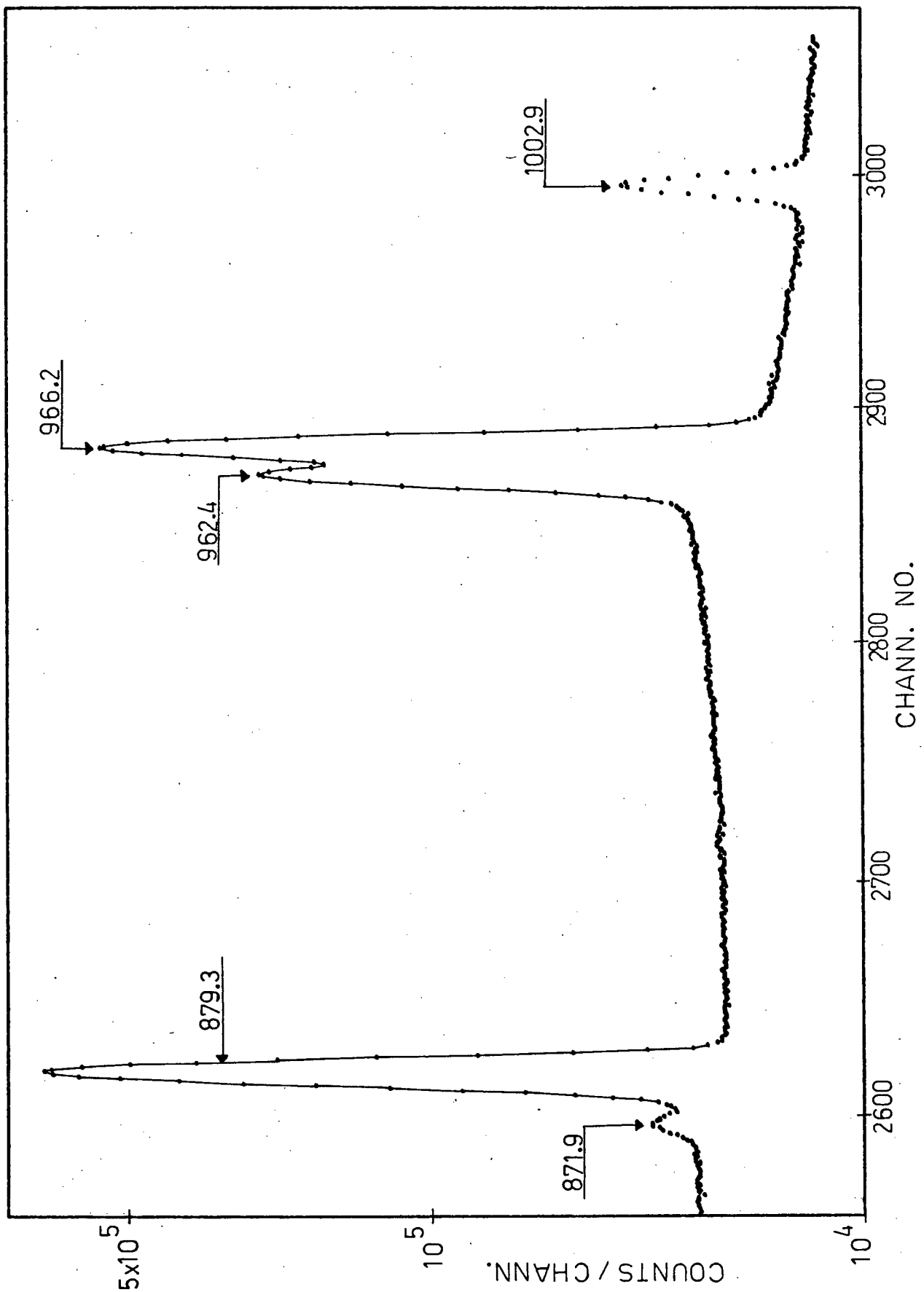
1002.9
966.2
962.4
879.3
871.9
5x10^5
10^5
10^4
COUNTS / CHANN.
2600
2700
2800
2900
3000
CHANN. NO.

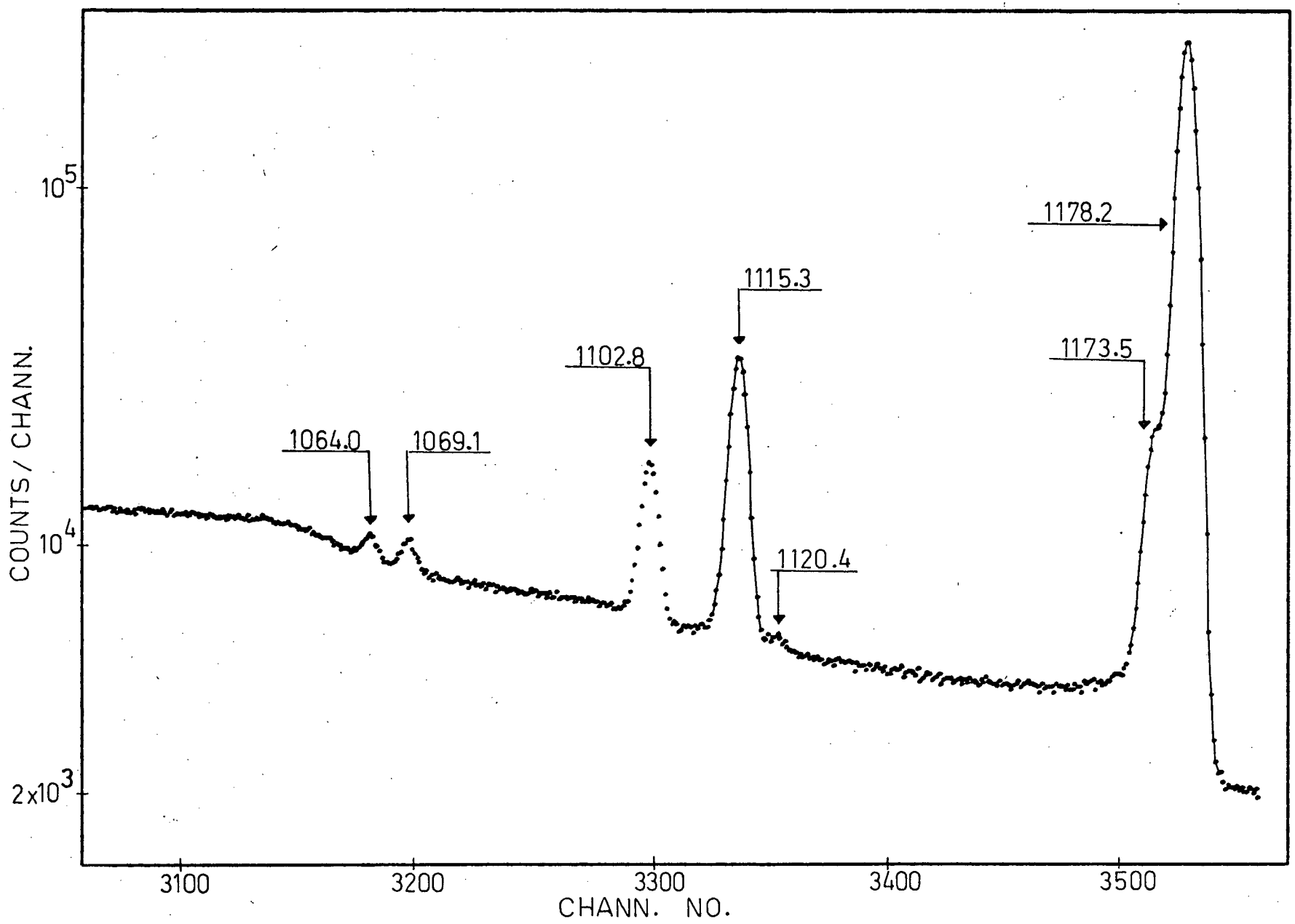

Figure III-6 (g)

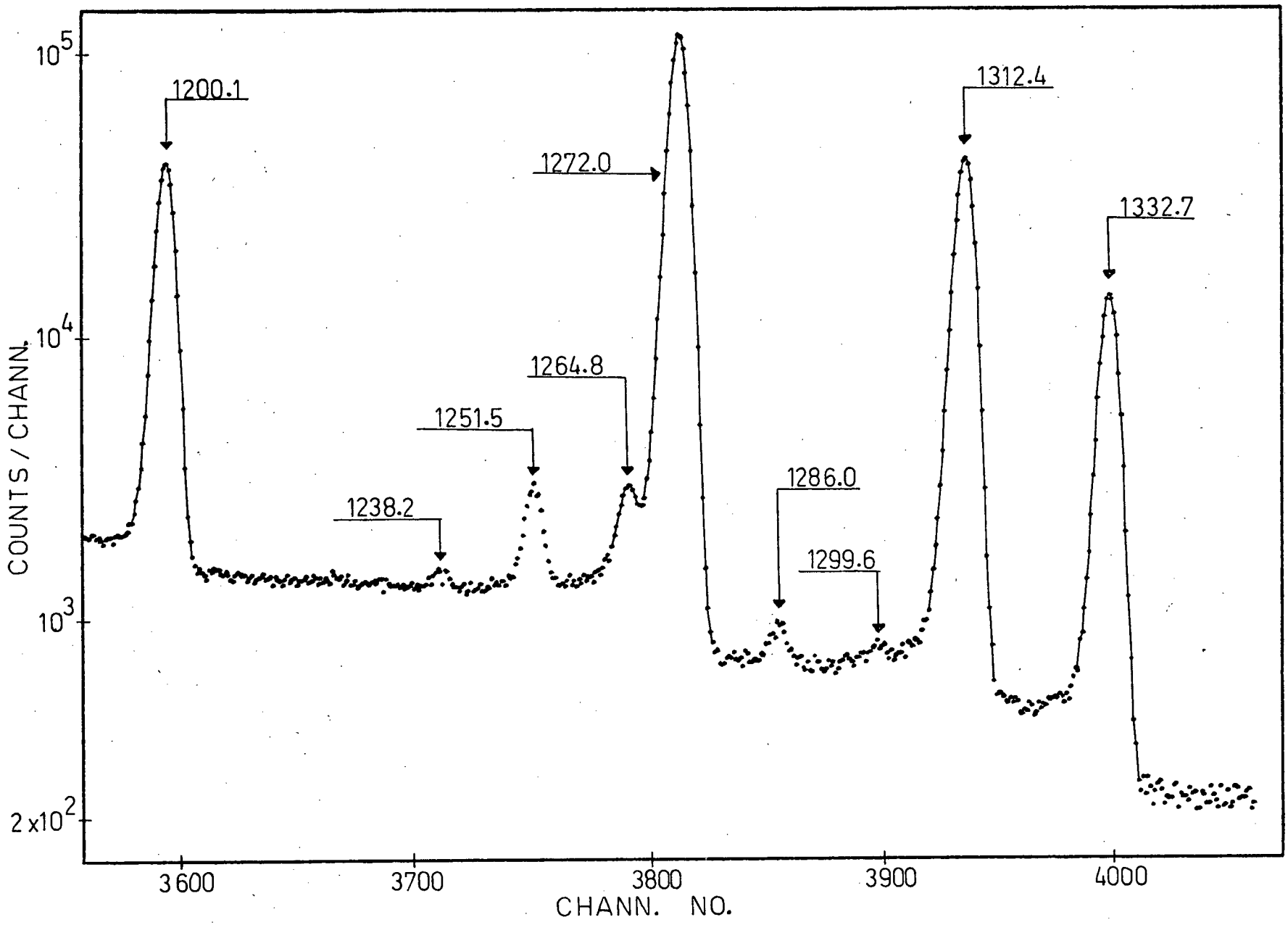

Figure III-6 (4)

TABLE III-4

PEAKS OBSERVED IN γ-SPECTRA

ENERGY (kev)	INTENSITY						COMMENT
	D = 15 cm		D = 7.5 cm		D = 0 cm		
86.8	15.2	(.8)	15.5	(1.4)	15.1	(1.4)	
93.9	.07	(.02)	.06		.10	(.03)	
97.7	.007	(.003)	.01	(.001)	.07	(.01)	+S.C.
111.8			.027	(.01)			
132.4					.005	(.002)	S
148.5	.01	(.005)	.006	(.003)			
173.1					.007	(.003)	R.S.
176.3	.006		.007				
196.9	6.25	(.35)	6.45	(.35)	6.26	(.33)	
215.5	4.70	(.30)	4.90	(.30)	4.78	(.30)	
230.4	.09	(.01)	.094	(.01)	.077	(.008)	
238.7	.066	(.016)	.017	(.004)			B
241.7	.02	(.01)	.003	(.005)			B
242.5					.06	(.003)	S
246.5	.007	(.005)	.022	(.005)			
249.3			.014	(.004)	.080	(.004)	S
261.3					.058	(.013)	S
268.1					.046	(.018)	S
283.5	.004		.013	(.004)	.29	(.02)	S
298.4	29.5	(1.5)	30.0	(1.6)	29.2	(1.7)	
309.3	.96	(.09)	.97	(.10)	.72	(.20)	
320.5	.008		.008	(.004)	.005	(.002)	
337.0	.39	(.03)	.38	(.02)	.35	(.03)	
344.0			.009	(.006)	.15	(.02)	
349.3	.024	(.003)	.014	(.008)			
350.3					.071	(.003)	S
351.6	.10	(.01)	.036	(.01)	.016	(.003)	B
379.5			.02	(.008)	.04	(.008)	
384.8			.024	(.006)	.71	(.03)	S
392.1	1.44	(.08)	1.44	(.08)	1.37	(.07)	

TABLE III-4 (continued)

ENERGY (kev)	INTENSITY						COMMENT
	D = 15 cm		D = 7.5 cm		D = 0 cm		
412.3					.16	(.02)	S
432.5	.025	(.01)	.02	(.006)	.019	(.01)	
478.6					.029	(.007)	S
485.8	.081	(.016)	.077	(.013)	.083	(.014)	
494.8					.067	(.011)	S
496.6	.082	(.014)	.027	(.009)			B
505.6					.030	(.009)	S
569.4	.20	(.02)	.062	(.008)			B
582.7	.071	(.017)	.034	(.02)			B
596.6					.024	(.01)	R.S.
609.1	.16	(.01)	.057	(.01)			B
682.1	.58	(.03)	.58	(.025)	.47	(.03)	
765.1	2.12	(.07)	2.09	(.07)	1.67	(.06)	
835.2	.073	(.022)	.025	(.012)			B
851.8					.095	(.02)	S
871.9	.08	(.02)	.06	(.02)			
879.3	≡30.0		≡30.0		≡30.0		
916.8					.052	(.001)	S
925.0					.214	(.005)	S
931.4					.096	(.014)	S
962.4	10.2	(.45)	10.18	(.41)	10.70	(.41)	
966.2	25.2	(.8)	25.0	(.8)	27.6	(.8)	+S.C.
980.2					.11	(.01)	S
1002.9	1.04	(.04)	1.04	(.03)	.94	(.02)	
1007.9					.082	(.006)	S
1014.0					.041	(.009)	S
1049.4					.39	(.03)	S
1064.0	.22	(.016)	.06	(.01)			B
1069.1	.095	(.015)	.095	(.013)	.128	(.015)	
1089.3					.055	(.015)	S
1102.8	.57	(.02)	.57	(.02)	.50	(.02)	

TABLE III-4 (continued)

ENERGY (kev)	INTENSITY						COMMENT
	D = 15 cm		D = 7.5 cm		D = 0 cm		
1115.3	1.55	(.05)	1.52	(.05)	1.37	(.04)	
1120.4	.105	(.003)	.031	(.001)			B
1173.5	2.24	(.16)	1.0	(.10)	.12	(.03)	B
1178.2	14.85	(.45)	14.82	(.44)	18.00	(.45)	+S.C.
1189.5					.012	(.006)	S
1200.1	2.34	(.08)	2.33	(.08)	2.67	(.08)	S.C.
1224.1					.19	(.01)	S
1230.3					.93	(.01)	S
1238.2	.038	(.008)	.011	(.003)			B
1251.5	.10	(.008)	.10	(.01)	.09	(.006)	
1264.8	.024	(.008)	.07	(.02)	1.90	(.10)	S
1272.0	7.35	(.22)	7.37	(.23)	7.92	(.23)	
1286.0	.011	(.003)	.017	(.003)	.106	(.009)	+S.C.
1299.6	.004		.004	(.002)	.09	(.01)	+S.C.
1312.4	2.78	(.09)	2.78	(.09)	3.18	(.08)	+S.C.
1317.8			.013	(.003)	.106	(.008)	S
1324.1					.046	(.001)	S
1332.7	2.46	(.08)	.90	(.03)	.07	(.01)	B
1359.1			.016	(.004)	.36	(.02)	S

B = Background Peak

S = Sum Peak

R.S. = Random Sum Peak

+S.C. = Plus Sum Contribution

peaks observed in the three spectra and the relative intensities in each spectrum, all normalized to $I_o(879.3) = 30.00$. This normalization is particularly useful as it represents the number of gamma-rays emitted in 100 ^{160}Tb disintegrations[12].

A search for single and double escape peaks of the gamma-rays of energies above 1022 kev revealed no such peaks in our spectra. To identify the gamma-rays due to other possible radioactive sources in the surroundings, the ^{160}Tb source was removed and a spectrum taken. The transition found in the background are identified in Table III-4.

Ludington et al.[14] reported two gamma-rays of energies 237.6 and 242.5 kev; these same transitions were reported by McAdams and Otteson[17] as 237.8 and 243.0 kev respectively. In this work two peaks were observed at energies of 238.7 and 242.0 kev but were identified as the 238.6 kev gamma ray of ^{228}Th and the 241.9 kev transitions from ^{226}Ra. The identification was made on the following basis. Having found these transitions in the background spectrum, their expected areas in the D = 15 and 7.5 cm spectra were calculated using the other background peaks and compared to the observed intensities. The results of this comparison are presented in Table III-5.

5. SUM PEAKS

Sum peaks in general can be divided into two classes; those which are due to the random summing of two transitions and those which are caused by the summing of two coincident gamma-rays.

The rate of random summing, I_{1+2}, of two transitions E_1 and E_2, each of a counting rate I_1 and I_2, in producing a peak at an energy of E_1+E_2 is given by:

$$I_{1+2} = 2\tau I_1 I_2 \qquad (3.3)$$

where τ is the maximum time difference between two pulses in which they may

TABLE III-5

THE 238 AND 242 KEV BACKGROUND TRANSITIONS

Spectrum	Observed Energy	Calculated Intensity from Background Spectrum	Measured Intensity
D=7.5	238.7	$(1.7\pm.2)\times10^{4}$	$(1.5\pm.2)\times10^{4}$
	242.0	$(5.2\pm1.3)\times10^{3}$	$(3.7\pm1.1)\times10^{3}$
D=15	238.8	$(2.05\pm.04)\times10^{4}$	$(2.1\pm.1)\times10^{4}$
	241.6	$(6.2\pm.8)\times10^{3}$	$(5.6\pm1.1)\times10^{3}$

still add together to produce one pulse of energy E_1+E_2. This time difference τ depends only on the analyzing circuit employed and can be found by measuring the rate of summing of an intense gamma-ray with itself. The 596.0 kev peak in the D=0 cm spectrum, caused by the summing of the 298.3 kev transition with itself, was used to calculate τ. The count rates are

$$I_{(298.3)} = (9.2\pm.04) \times 10^3 \text{ sec}^{-1} \qquad I_{(596.0)} = (.43\pm.1) \text{ sec}^{-1}$$

which results in τ = 250 nsec. Using this value of τ, the area of the sum peak of the 86.8 kev transition with itself was calculated to be $(1.3\pm.4)\times10^4$ which agrees reasonably well with the value of $(.9\pm.3)\times10^4$ for the area of the 173.0 kev peak in the D=0 cm spectrum.

The rate of coincidence summing of two cascading transitions, 1 and 2, with transition 1 preceding transition 2, is given by

$$I_{1+2} = I_1 \Omega\varepsilon_2 K_2 \tag{3.4}$$

where $\Omega\varepsilon_2$, as before, is the total efficiency of the detector for transition 2 and K_2 is some constant, dependent on the details of the decay scheme (see Chapter V, page 59).

In general a peak at an energy of E_1+E_2 can represent the gamma-ray corresponding to a true cross-over transition, the pure summing of the coincident gamma-rays E_1 and E_2 with no cross-over transition or the result of a certain combination of these two processes. The area of each peak has to be corrected for the possible contribution from random summing. In most cases this correction was found to be too small and was neglected.

The method used to ascertain the nature of a coincident sum peak is as follows. When the distance between the source and the detector is decreased,

D_1 to D_2, the intensity of a true gamma-ray peak increases by a factor of $(\frac{D_1}{D_2})^2$ (the ratio of the two solid angles). The intensity of a sum peak, random or coincident, increases by $(\frac{D_1}{D_2})^4$, as can be seen from equations (3.3) and (3.4). Since in all spectra the intensities of all peaks are normalized to the same value for the 879.3 kev gamma-ray, i.e. $I_o(879.3) = 30.0$, then the normalized intensities of the true transitions should remain constant when changing the distance D, while the intensity of a sum peak increases by $(\frac{D_1}{D_2})^2$.

If I_1, I_2 and I_{1+2} are the intensities of the peaks at energies E_1, E_2 and E_1+E_2 respectively, then a plot of

$$(\frac{I_1}{I_{1+2}})^{\frac{1}{2}} \qquad \text{or} \qquad (\frac{I_2}{I_{1+2}})^{\frac{1}{2}}$$

against source-to-detector distance determines the nature of the peak at E_1+E_2. If the plot is a straight line with zero slope then the peak at E_1+E_2 is entirely due to a true cross-over transition; a straight line with a positive slope indicates a pure coincidence sum peak. A curve would indicate a mixture of the two, in which case the value of I_{1+2} in the spectrum taken at the largest source to detector distance is taken as the intensity of the true cross-over transition.

The sum peaks and the true transitions with large sum contributions are identified in Table III-4. The pure sum nature of the 283.3, 1264.7 and the 1359.1 kev peaks are evident in the above mentioned plots presented in Figure III-7. Figure III-8 shows the substantial sum contributions to the true gamma-rays of energies 1200 and 1286 kev.

The case of the 97.7 kev peak is of interest since it could conceivably be due to the coincidence summing of the K_α and the K_β x-rays. If this peak

Figure III-7

Identification of Sum Peaks

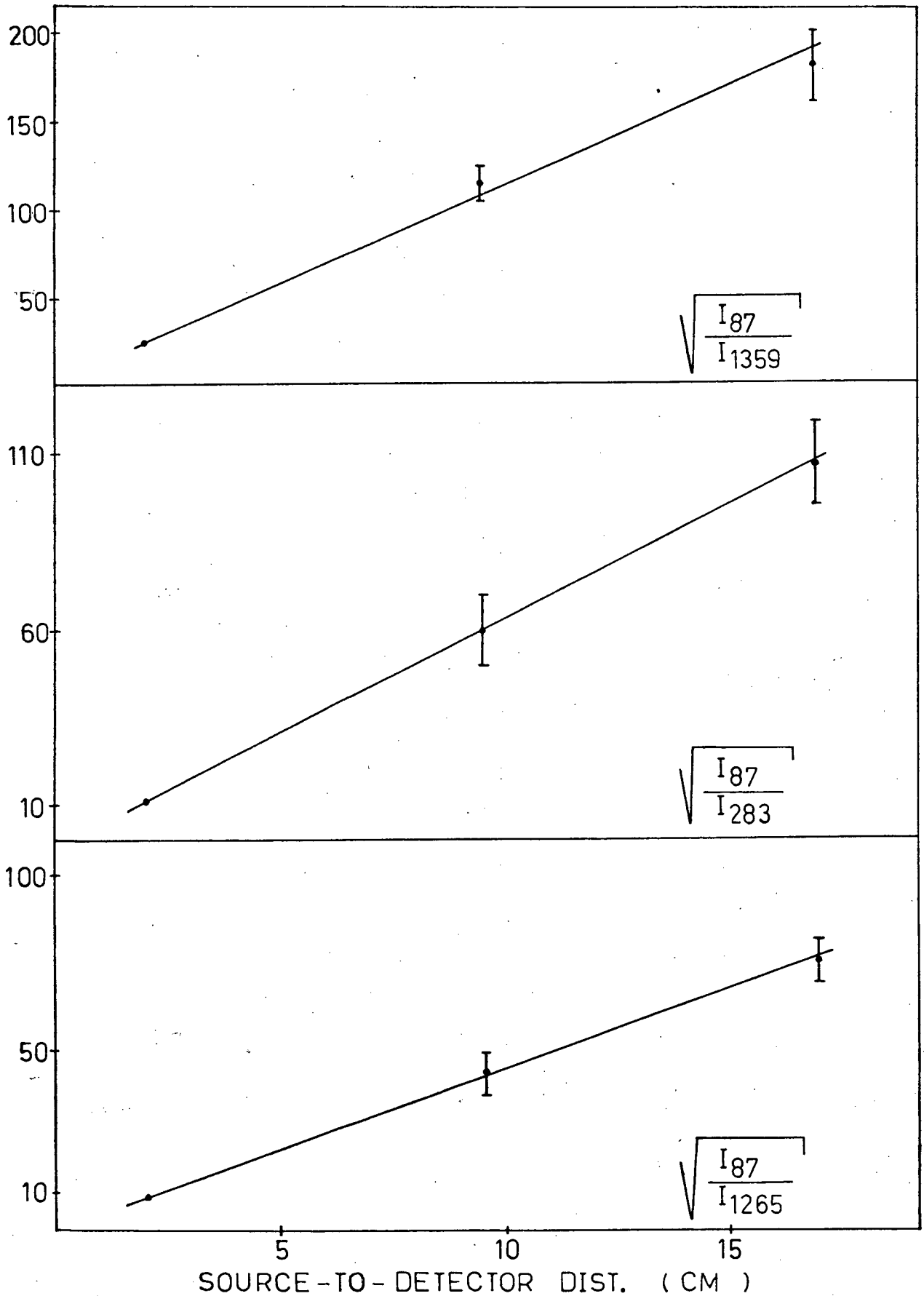

Figure III-8
Identification of Sum Contributions

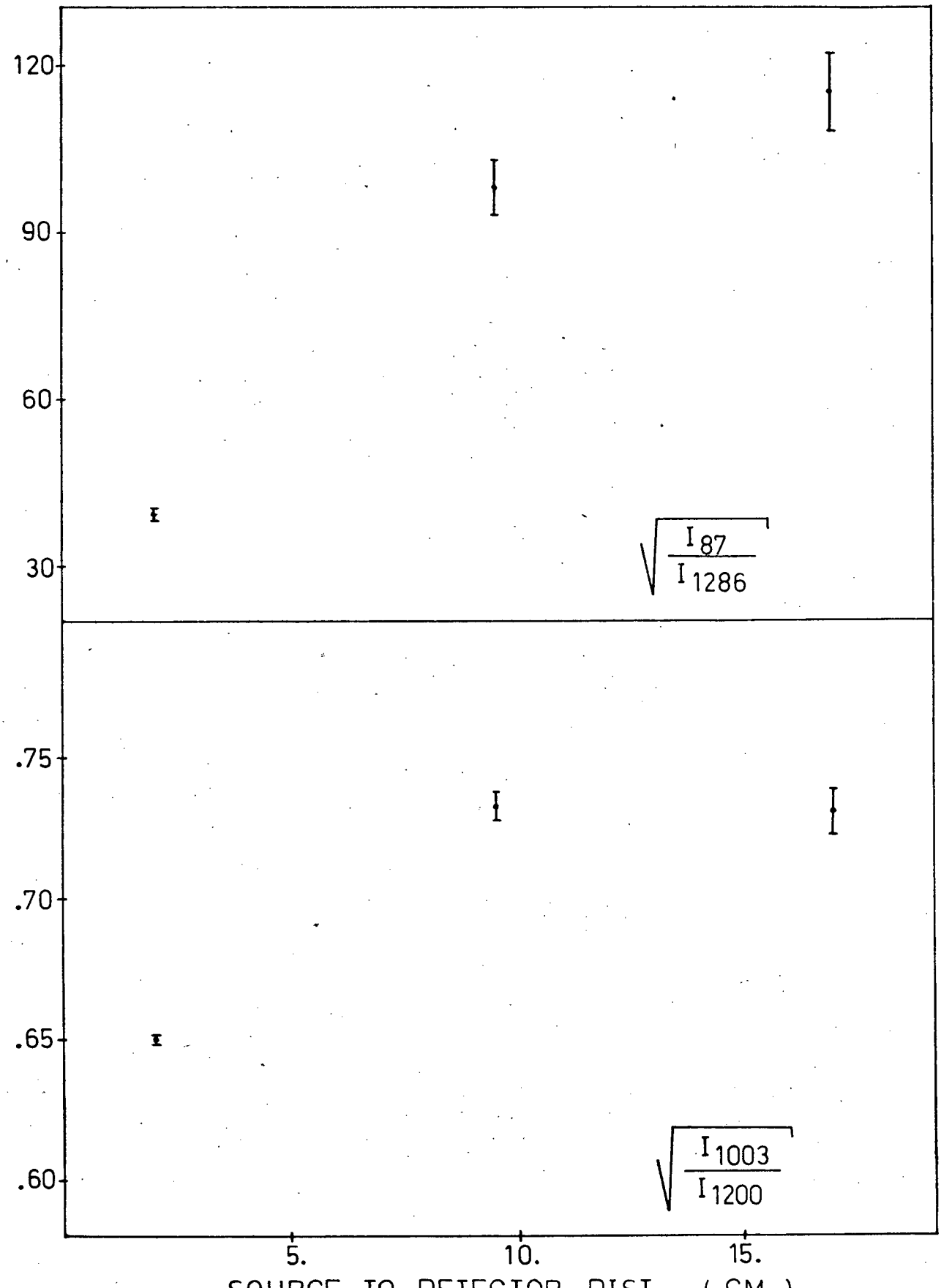

was a pure sum peak then

$$\left(\frac{I_{(97.7)}}{I_{(93.9)}}\right)_{D=0} = \left(\frac{\Omega_{D=0}}{\Omega_{D=7.5}}\right)\left(\frac{I_{(97.7)}}{I_{(93.9)}}\right)_{D=7.5}$$

where the ratio of the solid angles is known to be

$$\frac{\Omega_{D=0}}{\Omega_{D=7.5}} = 22.6$$

But it is observed that

$$\left(\frac{I_{(97.7)}}{I_{(93.9)}}\right)_{D=7.5} = .18 \quad \text{and} \quad \left(\frac{I_{(97.7)}}{I_{(93.9)}}\right)_{D=0} = 1.0$$

which indicates that a part of the 97.7 kev peak is due to a true transition.

Table III-6 lists the energies and the adopted intensities of all the true transitions observed, included for comparison are the results of Gunther et al.[13] and McAdams and Otteson[17].

TABLE III-6

ENERGIES AND INTENSITIES OF THE ^{160}Dy TRANSITIONS

ENERGIES				INTENSITIES			
Present Work		Of Ref.17	Of Ref.13	Present Work		Of Ref.17	Of Ref.13
86.8	(.2)	86.8	86.7	15.3	(.8)	13.0	13.5
93.9	(.2)	93.9	-	.06	(.02)	.054	-
97.7	(.3)	-	-	.008	(.004)	-	-
111.8	(.5)	-	-	.025	(.015)	-	-
148.5	(.3)	-	-	.008	(.004)	-	-
176.3	(.5)	176.4	-	.007	(.003)	-	-
196.9	(.2)	197.0	197.0	6.3	(.3)	5.2	5.3
215.5	(.2)	215.6	215.6	4.8	(.3)	4.0	4.55
230.4	(.2)	230.6	230.7	.09	(.01)	.082	.136
246.5	(.3)	246.4	-	.015	(.005)	.026	-
298.4	(.2)	298.6	298.5	29.7	(.6)	27.3	29.8
309.3	(.2)	309.6	309.6	.96	(.09)	.92	.97
320.5	(.3)	-	320.4	.008	(.004)	-	<.018
337.0	(.2)	337.3	337.1	.38	(.02)	.36	.40
349.3	(.2)	349.7	349.6	.019	(.008)	.018	<.014
379.5	(.3)	379.3	-	.03	(.008)	.017	-
392.1	(.2)	392.5	392.4	1.44	(.08)	1.40	1.52
432.5	(.2)	432.7	432.6	.022	(.006)	.024	.017
485.8	(.2)	485.9	485.7	.08	(.01)	.088	.091
682.1	(.2)	682.3	682.2	.58	(.03)	.617	.665
765.1	(.2)	765.3	765.3	2.10	(.07)	2.16	2.25
871.9	(.3)	872.0	-	.19	(.02)	.207	-
879.3	(.2)	879.4	879.2	≡30.00		≡30.00	≡30.00
962.4	(.2)	962.4	962.1	10.2	(.4)	9.42	10.2
966.2	(.2)	966.2	965.8	25.1	(.8)	24.8	25.9
1002.9	(.2)	1002.9	1002.7	1.04	(.03)	1.02	1.13
1069.1	(.2)	1069.1	-	.095	(.015)	.104	-
1102.8	(.2)	1102.6	1102.2	.57	(.02)	.56	.59
1115.3	(.2)	1115.1	1115.0	1.53	(.05)	1.48	1.58

TABLE III-6 (Continued)

ENERGIES				INTENSITIES			
Present Work		Of Ref.17	Of Ref.13	Present Work		Of Ref.17	Of Ref.13
1178.2	(.2)	1178.0	1177.7	14.8	(.4)	15.0	15.9
1200.1	(.2)	1199.9	1199.8	2.34	(.08)	2.37	2.53
1251.5	(.3)	1251.3	1250.8	.10	(.01)	.104	.12
1272.0	(.2)	1271.9	1271.5	7.4	(.2)	7.48	7.9
1285.4	(.3)	1285.6	-	.014	(.003)	.015	-
1299.6	(.3)	1299.3	1299.2	.004	(.001)	.006	<.045
1312.4	(.2)	1312.1	1311.8	2.78	(.09)	2.87	3.02

CHAPTER IV

K-CONVERSION ELECTRONS

Internal Conversion is the process by which a nucleus in an excited state loses its energy by ejecting an atomic electron from the atom, a process which is always in competition with direct photon emission. The electron shall have a kinetic energy of $E_\gamma - E_B$, where E_B is the binding energy of the atomic electron. This process is due to the direct interaction of the bound electron with the multipole field which would have caused the emission of a gamma-ray of energy E_γ. The electron may be ejected from any of the atomic shells K,L,M,... etc., following which the atom is de-excited by emitting the binding energy as an x-ray or an Auger electron.

The Coefficient of Internal Conversion (ICC) is defined as $\alpha \equiv \frac{W_e}{W_\gamma}$, where W_γ and W_e are the transition probabilities for emission of a photon and of an electron respectively. The ICC can be defined for single shells as α_K, α_L... etc. where

$$\alpha_K = \frac{W_{eK}}{W_\gamma}, \qquad \alpha_L = \frac{W_{eL}}{W_\gamma}, \ \ldots \qquad \text{with } \alpha = \alpha_K + \alpha_L + \ldots$$

W_{eK}, W_{eL}, ... etc. are the probabilities for emission of an electron from the atomic shells K,L,... etc.

Coefficients α_K, α_L,... etc. depend on the atomic number Z, the transition energy E_γ, the parity and the multipole order of the transition, but not on the nuclear wavefunctions for these enter into W_K, W_L... etc. in the same manner as into W_γ, and thus cancel[22]. The theoretical conversion coefficients, which are used in Table IV-2, have been calculated by Sliv and Band[25] for α_K and α_L.

Once the intensity of K-conversion electrons, I_K, and that of the gamma-

rays, I_γ, have been calculated for a given transition, the experimental ICC can be calculated by $\alpha_K = \frac{I_K}{I_\gamma}$. Upon comparing this value to the theoretical predictions, the transition multipolarity can often be deduced.

1. K-CONVERSION ELECTRONS IN COINCIDENCE WITH K-X-RAYS

A single spectrum of the conversion electrons taken with a Si(Li) detector is frequently not very helpful for measuring the intensities of the K-conversion electrons, because the peaks are too weak. This is because such a spectrum contains a very large background due to the β^- transitions and the electrons from the Compton scattered gamma-rays. There is also the possibility that a K-conversion peak may be superimposed on the L- or M- conversion peak of another transition. This background can be reduced by accepting only those events which are in coincidence with the K-x-rays, which are generated and are in coincidence with the K-conversion electrons. Other events, such as some β^-, gamma and L- or M- conversion transitions, may also be in coincidence with the K-x-rays, but the K-conversion peaks are enhanced above all others. Figure IV-1 shows this enhancement of the K-conversion peaks in the coincidence spectrum as compared to the singles electron spectrum. Because of different amplifier gains, the position of peaks in these spectra are different.

The fast coincidence network employed is shown in Figure IV-2; the electronic equipment used were the same as those described in Table V-2. A 2 mm Si(Li) detector was used to gate the K-x-rays, and a 3 mm Si(Li) detector (with constant electron efficiency) was used as the analog detector. Figure IV-3 (a,b) shows the low energy electron spectrum obtained, and the high energy spectrum is shown in Figure IV-4(a,b).

The measured intensities of the K-conversion peaks were normalized to the

Figure IV-1

K-Conversion Peaks

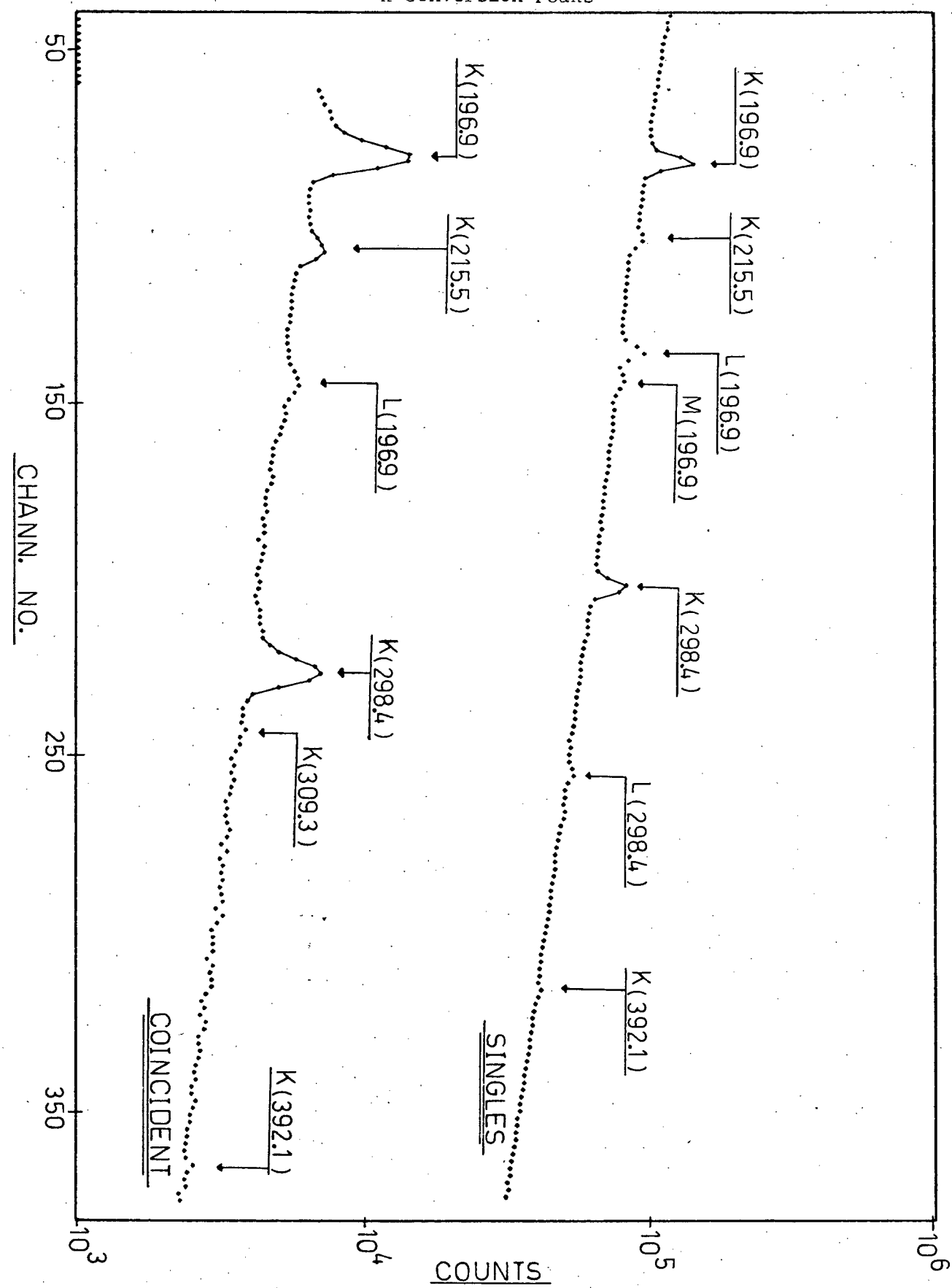

Figure IV-2

K-X-Ray Coincidence Network

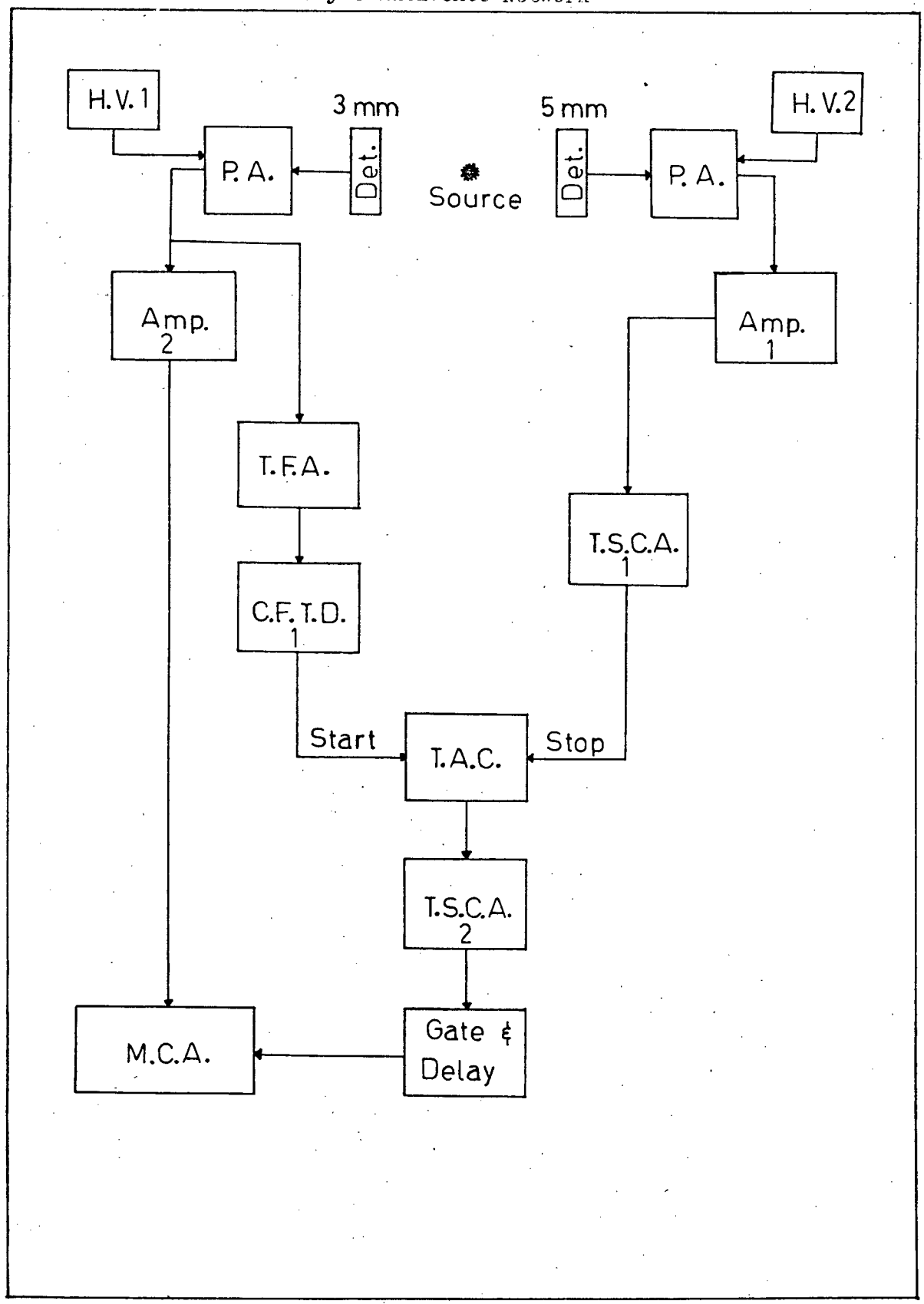

Figure IV-3 (a)

Low Energy K-X-Ray Coincidence Spectrum

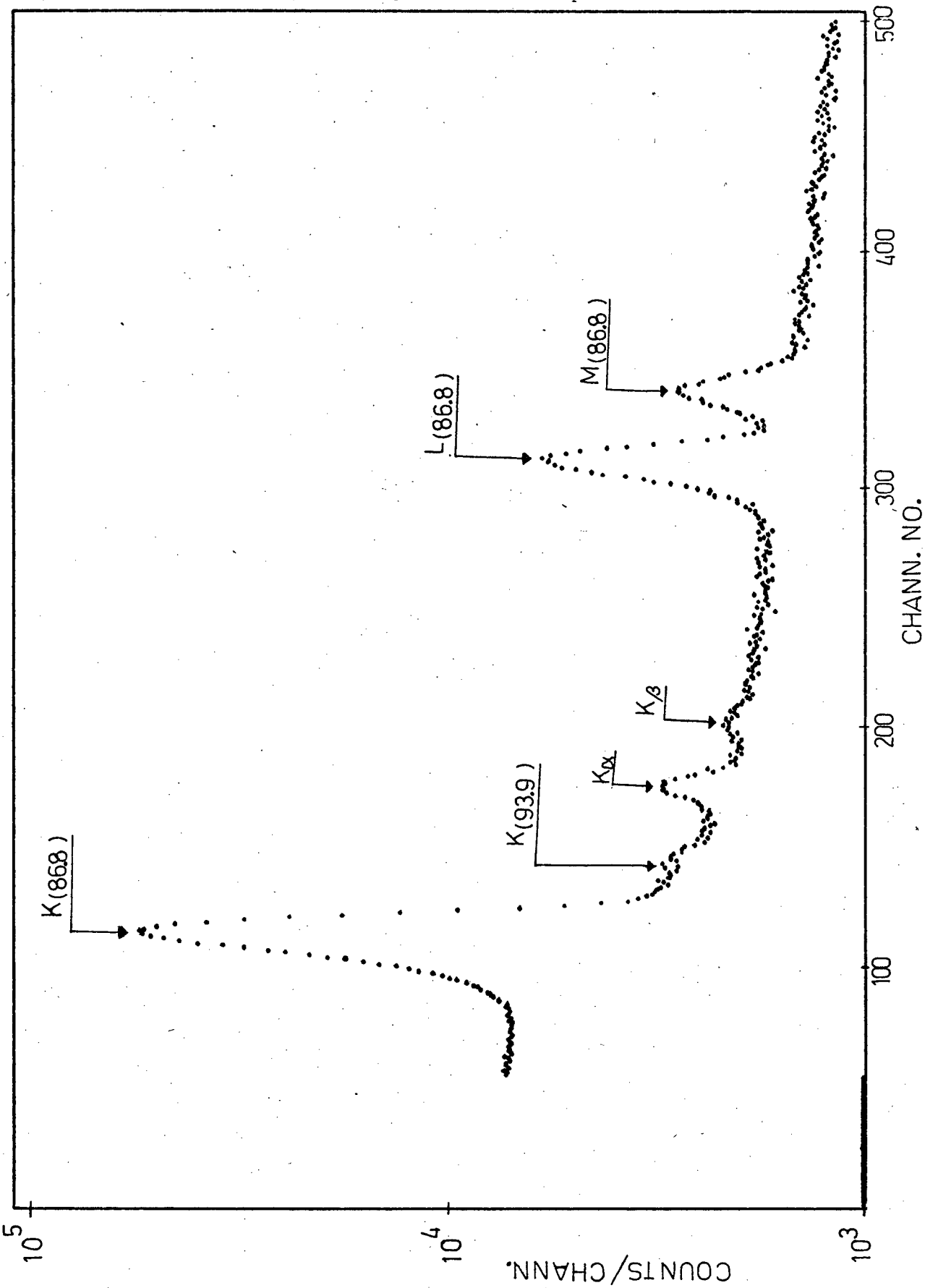

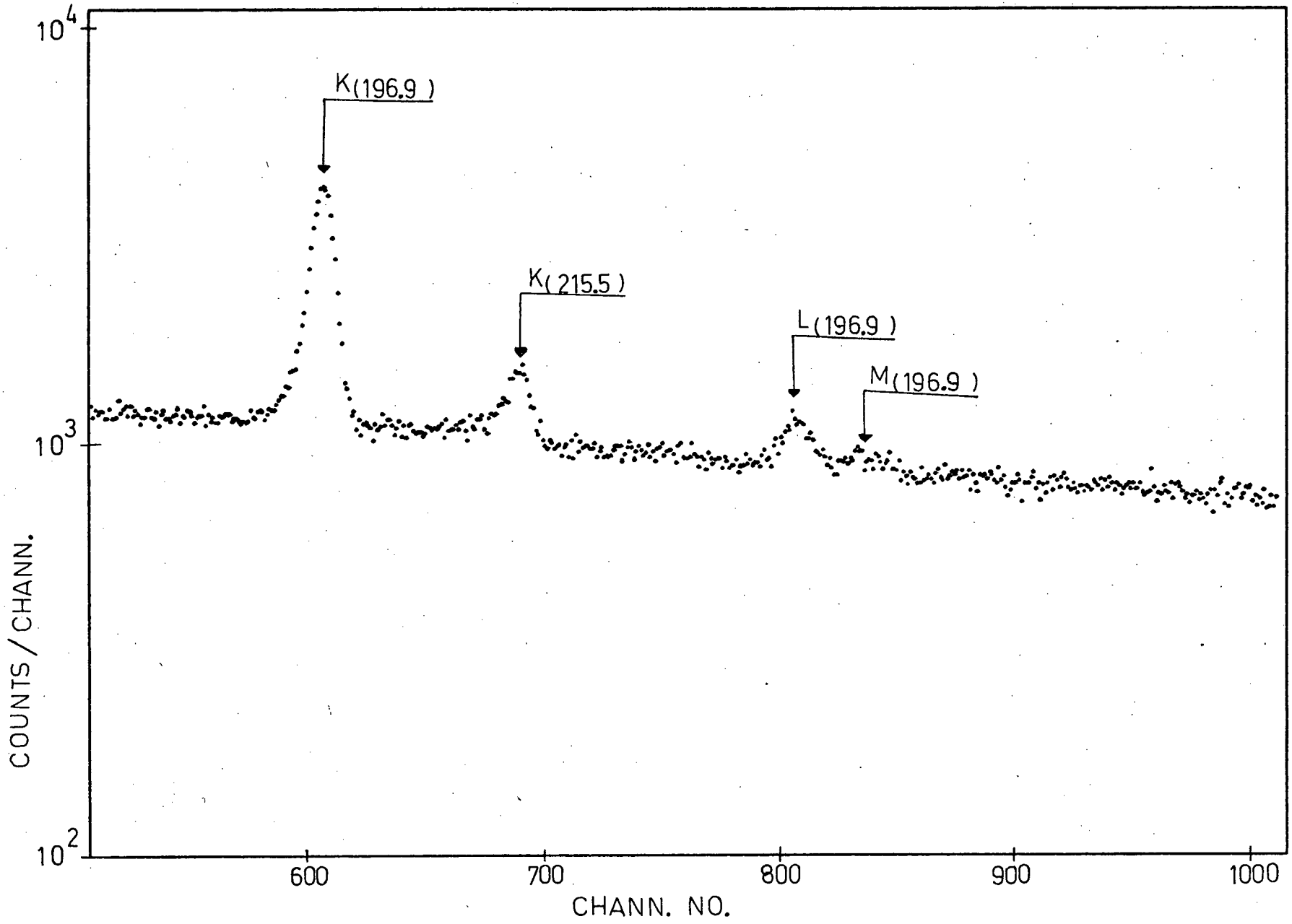
10^4
10^3
10^2
K(196.9)
K(215.5)
L(196.9)
M(196.9)
COUNTS / CHANN.
600
700
800
900
1000
CHANN. NO.

Figure IV-3 (b)

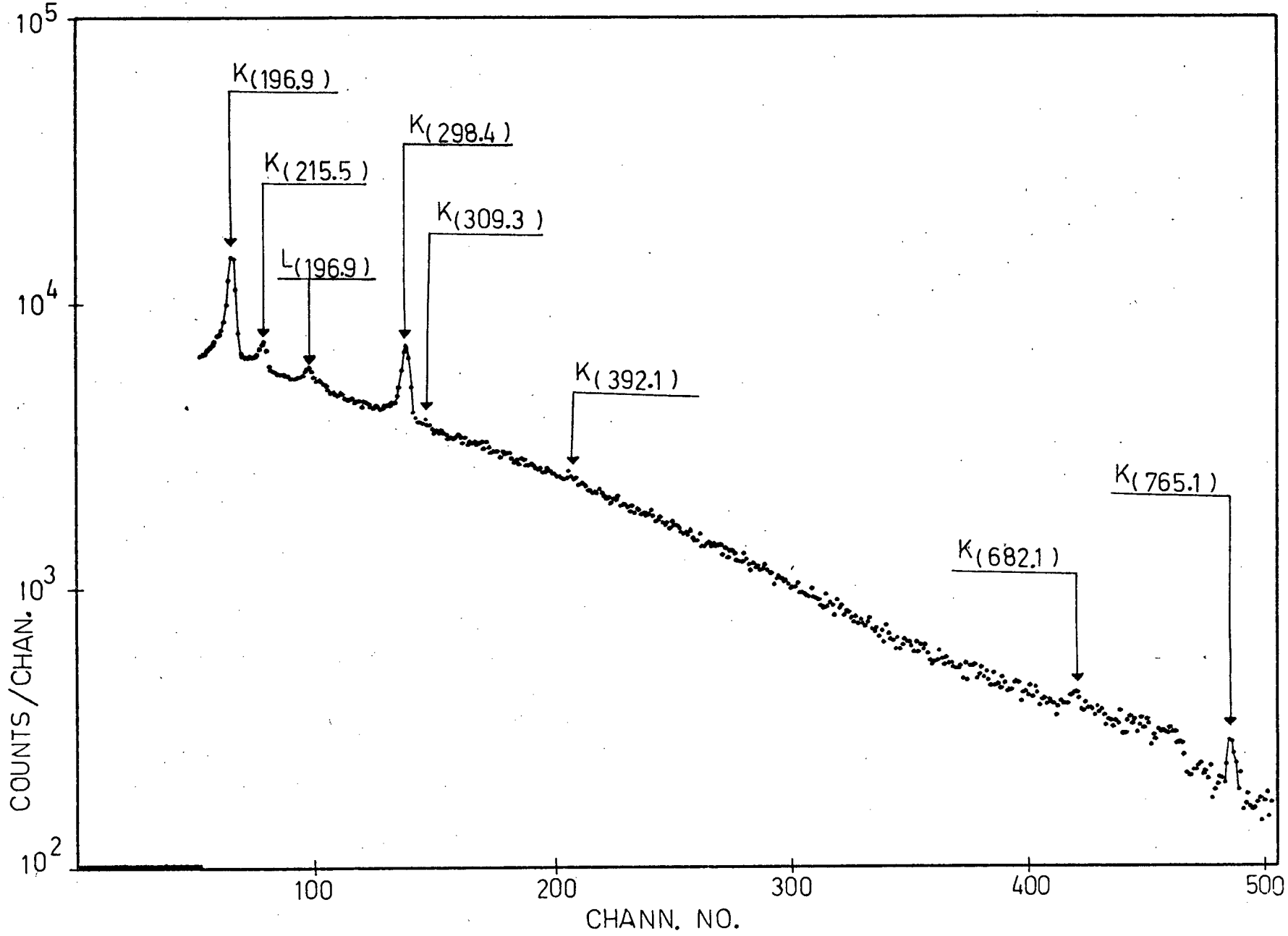

Figure IV-4 (a)
High Energy K-X-Ray Coincidence Spectrum

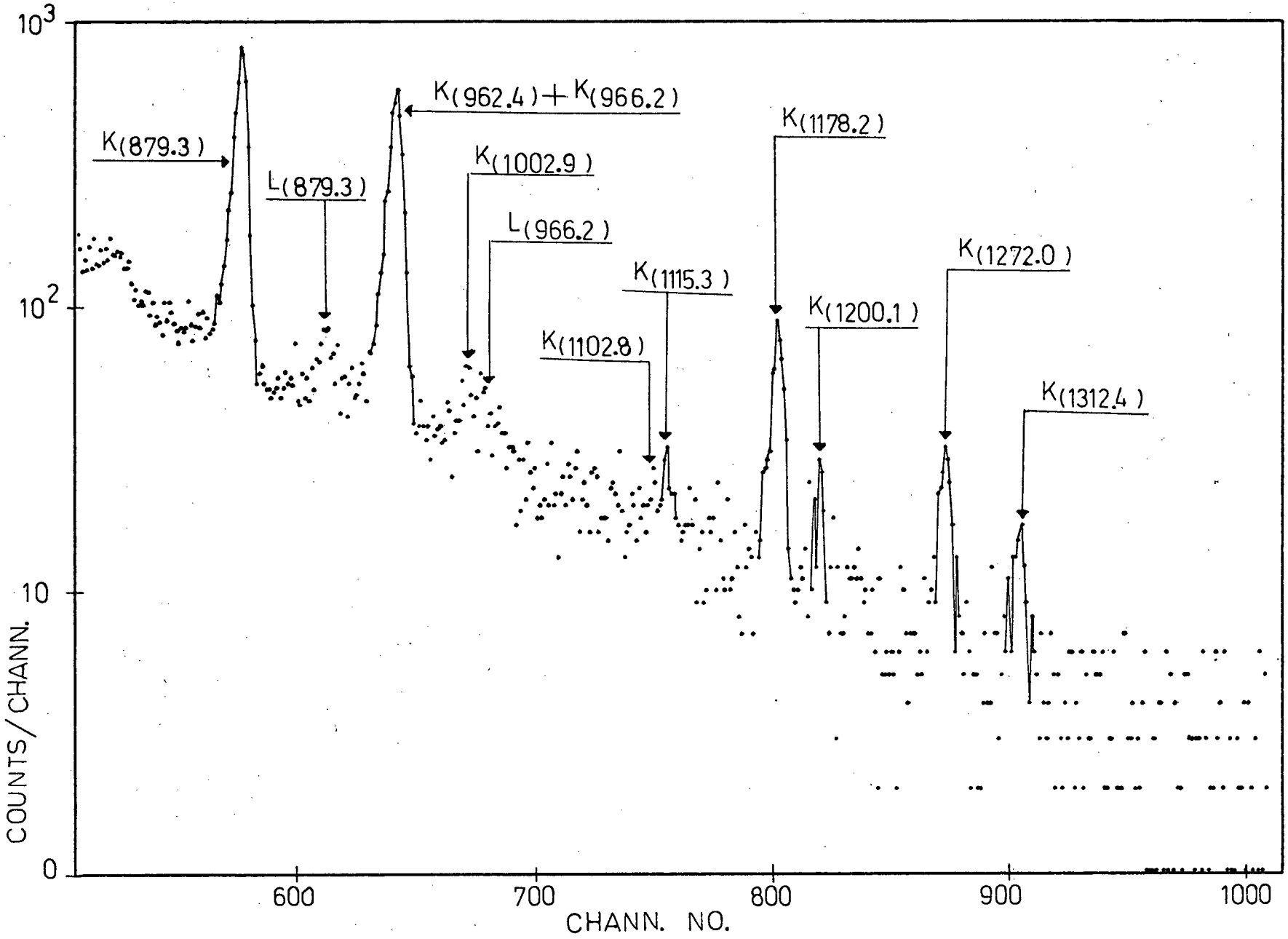
10^3
10^2
10
0
COUNTS / CHANN.
600
700
800
900
1000
CHANN. NO.
K(879.3)
L(879.3)
K(962.4)+K(966.2)
K(1002.9)
L(966.2)
K(1115.3)
K(1102.8)
K(1178.2)
K(1200.1)
K(1272.0)
K(1312.4)

Figure IV-4 (b)

gamma intensities, by assuming the 196.9 transition to be of pure E2 multipolarity. These normalized K-conversion intensities are presented in Table IV-1 along with the data of Ewan et al.[12] for comparison. The ratio $\frac{I_K(962)}{I_K(966)} = .403$ of Ewan et al. was used to separate the K-conversion double peak of the 962-966 transitions with

$$I_K(962) + I_K(966) = .107 \pm .002$$

The normalized K-conversion intensities, along with the gamma intensities were used to calculate the α_K's, and to assign the multipolarities of the transitions. These data and the adopted multipolarities are presented in Table IV-2.

The upper limits placed on the K-conversion intensities of the 379.5, 485.8 and 1251.5 kev transitions, result in an E1 or an E3 assignment for these transitions. The change of parity involved in these transitions excludes the E2 or M1 possibilities. These transitions are most likely E1, since no other E3 transitions are observed and also an E1 assignment being the lowest multipolarity possible, is more likely.

TABLE IV-1

INTENSITY OF K-CONVERSION ELECTRONS†

TRANSITION ENERGY (kev)	K-CONVERSION INTENSITY			
	This Work		Ewan et al.[12]	
86.8	19.9	(2.2)	24	(3)
93.9	.06	(.01)	.08	(.02)
196.9	1.07	(.06)	.88	(.04)
215.5	.16	(.03)	.14	(.007)
230.4	.0039	(.0009)		
298.3	.41	(.03)	.39	(.02)
309.3	.017	(.004)	.012	(.0015)
337.0	<.0045			
379.5	<.003			
392.1	.01	(.002)	.011	(.0015)
485.8	<.003			
682.1	.004	(.001	.005	(.0015)
765.0	.011	(.002)	.0125	(.001)
879.3	.13	(.01)	.103	(.005)
962.4	.031	(.004)	.029	(.002)
966.2	.076	(.004)	.072	(.004)
1002.9	.0015	(.0004)	.0008	(.0002)
1103.0	<.0003			
1115.3	.0012	(.0004)	.0016	(.0001)
1178.2	.013	(.001)	.012	(.006)
1200.1	.0026	(.0006)	.0018	(.0002)
1251.5	<.0003			
1272.0	.006	(.001)	.0049	(.0003)
1312.4	.0024	(.0007)	.0019	(.0001)

†Intensities normalized to events in 100 ^{160}Tb disintegrations.

TABLE IV-2

K-CONVERSION COEFFICIENTS AND TRANSITION MULTIPOLARITIES

TRANSITION ENERGY (kev)	α_K EXPERIMENTAL		α_K THEORETICAL E1	E2	M1	E3	ASSIGNMENT
86.8	1.23	(.3)	.37	1.50	3.00		E2
93.9	1.10	(.2)	.30	1.25	2.37		E2
196.9	≡.166		.043	.166	.30		E2
215.5	.033	(.008)	.033	.12	.23		E1
230.4	.042	(.01)	.028	.10	.19		E1
298.3	.014	(.02)	.014	.05	.097		E1
309.3	.017	(.005)	.013	.043	.087		E1
337.0	<.012	(.001)	.011	.035	.071		E1
379.5	<.1	(.03)	.008	.0255	.050	.078	E1 (E3)
392.1	.007	(.001)	.0077	.024	.046		E1
485.8	<.04	(.01)	.0047	.0106	.025	.039	E1 (E3)
682.1	.007	(.002)	.0023	.0057	.011		E2
765.0	.0052	(.0012)	.0018	.0045	.0087		E2
879.3	.0042	(.0004)	.0014	.0036	.0061		E2
962.4	.003	(.0005)	.0011	.0027	.0049		E2
966.2	.0029	(.0004)	.0011	.0027	.0049		E2
1002.9	.0013	(.0004)	.0010	.0026	.0044		E1
1103.0	<.0006		.0009	.0021	.0035		E1
1115.3	.0008	(.0003)	.00086	.0020	.0034		E1
1178.2	.0009	(.0001)	.0008	.0018	.0030		E1
1200.1	.001	(.0003)	.0008	.0017	.0029		E1
1251.5	<.003	(.001)	.0007	.0016	.0026	.0037	E1 (E3)
1272.0	.0008	(.0002)	.00068	.0016	.0025		E1
1312.4	.0008	(.0003)	.00064	.0015	.0024		E1

CHAPTER V

GAMMA-GAMMA COINCIDENCE SPECTROSCOPY

Information derived from gamma-gamma coincidences is necessary for the proper construction of the decay scheme of the daughter nucleus. Although sum peaks of the singles spectra provide a certain amount of coincidence information for strong transitions, some questions regarding the decay scheme can only be resolved by gamma-gamma coincidence measurements.

A 1005 kev transition reported by Ludington et al.[14] cannot be observed in the singles spectrum, because of its low intensity and its position on the tail of the fairly intense 1003 kev peak. The existence of this transition can only be ascertained by the coincidence method. Such measurements can also provide further information on the placement in the decay scheme of four new transitions, namely 97.7, 111.8, 148.5 and 320.5 kev gamma-rays, observed in the singles spectra. These transitions are expected to be difficult to observe in the coincidence spectra, because of the extremely slow coincidence count rate.

1. COINCIDENCE DATA FROM SUM PEAKS

Some information on gamma coincidences was obtained from the sum peaks of the singles spectra. The existence of a sum peak at an energy of E_1+E_2, established as not being entirely due to random summing (See Chapter III, section 5), implies the coincidence of the two separate transitions, E_1 and E_2.

The intensity of the sum peak of two cascading gamma transitions E_1 and E_2, with gamma-ray 1 preceding gamma-ray 2 in the cascade, is given by

$$I_{1+2} = I_1 \Omega \varepsilon_2 b_2 \frac{1}{1+\alpha_2} \qquad (5.1)$$

where as before $\Omega\varepsilon_2$ is the total efficiency of the detector for gamma-ray 2, and I_1 and I_{1+2} are the measured intensities of the gamma-ray 1 and of the sum peak. b_2 is the fraction of the decays of the intermediate excited states that go by transition 2 and $\frac{1}{1+\alpha_2}$ is the probability that this transition takes place by gamma emission, rather than by internal conversion, where α_2 is the ICC coefficient for this transition ($\frac{b_2}{1+\alpha_2}$ is the constant K_2 of the equation 3.4 of page 41).

For example

$$I_{1+3} = I_1 \Omega\varepsilon_3 \left(\frac{I_{o3}}{I_{o2}+I_{o3}}\right)\left(\frac{1}{1+\alpha_3}\right)$$

$$I_{1+5} = I_1 \Omega\varepsilon_5 \left(\frac{I_{o3}}{I_{o2}+I_{o3}}\right)\left(\frac{I_{o5}}{I_{o4}+I_{o5}}\right)\left(\frac{1}{1+\alpha_5}\right)$$

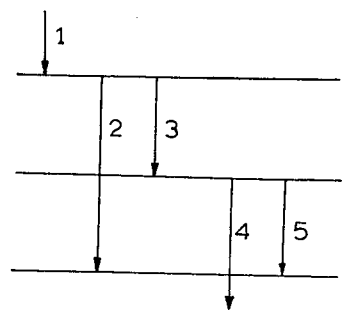

where I_{oi} is the total emitted intensity of transition i. In equation (5.1) we have neglected any angular correlation effects between the directions of emission of transitions 1 and 2. For the purpose of obtaining coincidence information, true sum peaks (in contrast to random sum peaks) and true sum contributions to true cross-over transitions can be divided into two groups.

i. Those which, on the basis of energy fit, are the result of the summing of only one possible pair of two gamma-rays E_1 and E_2. The existence of the sum peak of energy $E = E_1+E_2$ implies the coincidence of these two transitions. Such sum peaks and sum contributions to cross-over transitions are presented in Table V-1 a).

ii. Those sum peaks and sum contributions, which on the basis of energy fit, can have contributions from two or more pairs of gamma-rays. These are shown in Table V-1 b). In such cases, it is not possible to decide which of the two or more pairs are actually in coincidence. Equation 5.1 cannot be used for

TABLE V-1

a) COINCIDENCE DATA FROM UNIQUE SUM PEAKS

SUM PEAK ENERGY	$(E_1) + (E_2)$	SUM PEAK ENERGY	$(E_1) + E_2)$
283.5	(86.8) + (196.9)	966.2	(86.8) + (879.3)
384.8	(86.8) + (298.4)	1049.4	(86.8) + (962.4)
412.4	(196.9) + (215.5)	1089.3	(86.8) + (1002.9)
478.6	(86.8) + (392.1)	1189.5	(86.8) + (1102.8)
494.7	(196.9) + (298.4)	1200.1	(196.9) + (1002.9)
505.6	(196.9) + (309.3)	1286.8	(86.8) + (1200.1)
851.8	(86.8) + (765.1)		

b) COINCIDENCE DATA FROM POSSIBLE MULTIPLE SUMS

SUM PEAK ENERGY	$(E_1) + (E_2)$	SUM PEAK ENERGY	$(E_1) + (E_2)$
980.2	(215.5) + (765.1)	1299.6	(196.9) + (1102.8)
	(298.4) + (682.1)		(337.0) + (962.4)
			(230.4) + (1069.1)
1178.2	(298.4) + (879.3)		
	(215.5) + (962.4)	1312.4	(196.9) + (1115.3)
			(432.5) + (879.3)
1264.8	(86.8) + (1178.2)		(349.3) + (962.4)
	(298.4) + (966.2)		
		1359.1	(86.8) + (1272.0)
1272.0	(392.1) + (879.3)		(392.1) + (966.2)
	(309.3) + (962.4)		

this purpose, since the application of this equation requires detailed knowledge of the decay scheme.

2. EXPERIMENTAL PROCEDURE

The gamma-gamma coincidence spectra were taken using two GE(Li) detectors (45 cc and 30 cc), and the fast-slow coincidence network shown in Figure V-1. Table V-2 specifies the apparatus used.

The fast coincidence is performed on the fast negative outputs of two constant fraction timing discriminators. These outputs are used as the start and the stop pulses for a time-to-amplitude convertor TAC. The output of the TAC contains a peak which represents all the coincident events in the two detectors. Figure V-2 shows the output spectrum of the TAC taken with a ^{60}Co source in coincidence with the 1173 kev transition.

The slow coincidence is performed by coincidence unit on the logic pulses from two timing single channel analyzers TSCA. The TSCA #1 is used to energy gate the desired transition from the 45 cc detector (the gate detector) and the TSCA #2 is set to gate the time peak of the TAC output. The output of the coincidence unit is used to gate the spectrum of the 30 cc detector (the analog detector) at the input of the multi-channel analyzer. The resulting spectrum contains that portion of the spectrum of the analog detector which is in coincidence with the gated transition. This spectrum will also have contributions from the following sources.

In the "on-peak" spectrum, i.e. with the TSCA #1 gating the desired transition, there will also be events which are in coincidence with the background under the gated peak. This can be corrected for by taking an "off-peak" spectrum, where the TSCA #1 is moved to a nearby region of the spectrum, clear of other peaks. In applying this correction, the off-peak

Figure V-1

Gamma-Gamma Coincidence Network

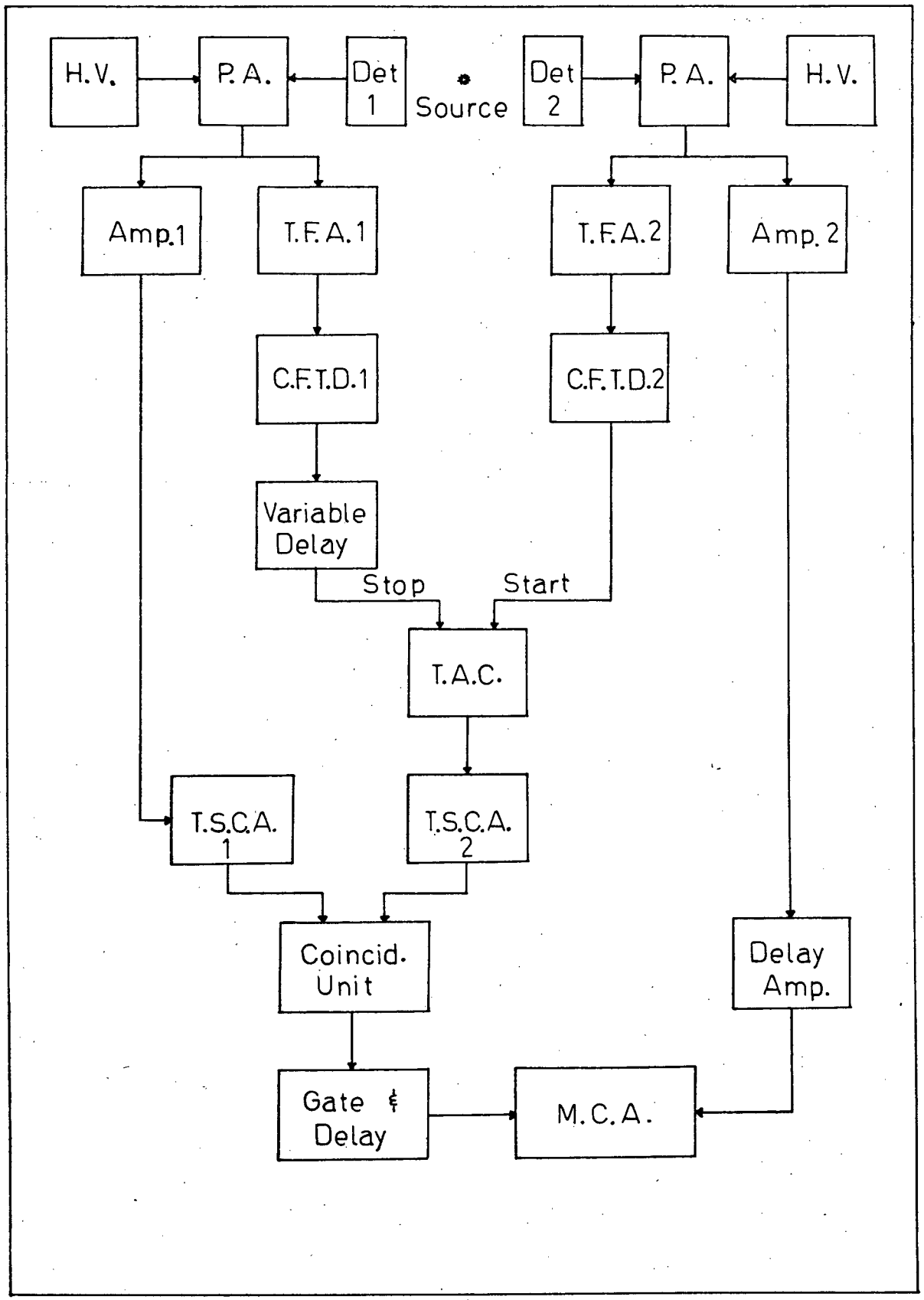

TABLE V-2

SPECIFICATION OF MODULAR UNITS USED FOR COINCIDENCE MEASUREMENTS

Gate detector:	a 45 cc coaxial GE(Li) from Nuclear Diodes
Analog detector:	a 30 cc coaxial GE(Li) from Nuclear Diodes
T.F.A. #1 & 2:	Ortec 454 Timing Filter Amplifiers
C.F.T.D. #1:	Ortec 463 Constant-Fraction Timing Discriminator
C.F.T.D. #2:	Ortec 453 Constant-Fraction Timing Discriminator
Delay:	Coaxial cable
T.A.C.:	Ortec 437A Time-to-Amplitude Converter
T.S.C.A. #1:	Ortec 420A Timing Single Channel Analyzer
T.S.C.A. #2:	C.I. Model 1435 Timing Single Channel Analyzer
Amp. 1:	Tennelec 203 Active Filter Amplifier
Amp. 2:	Tennelec 203 BLR Active Filter Amplifier with Baseline Restorer
Coinc. Unit:	Ortec 418 Universal Coincidence or Nuclear Chicago 27351 Coincidence Unit
Gate & Delay Generator:	Ortec 416
MCA:	Northern Scientific NS-900, 1024 Channels

Figure V-2

Output of TAC for ^{60}Co

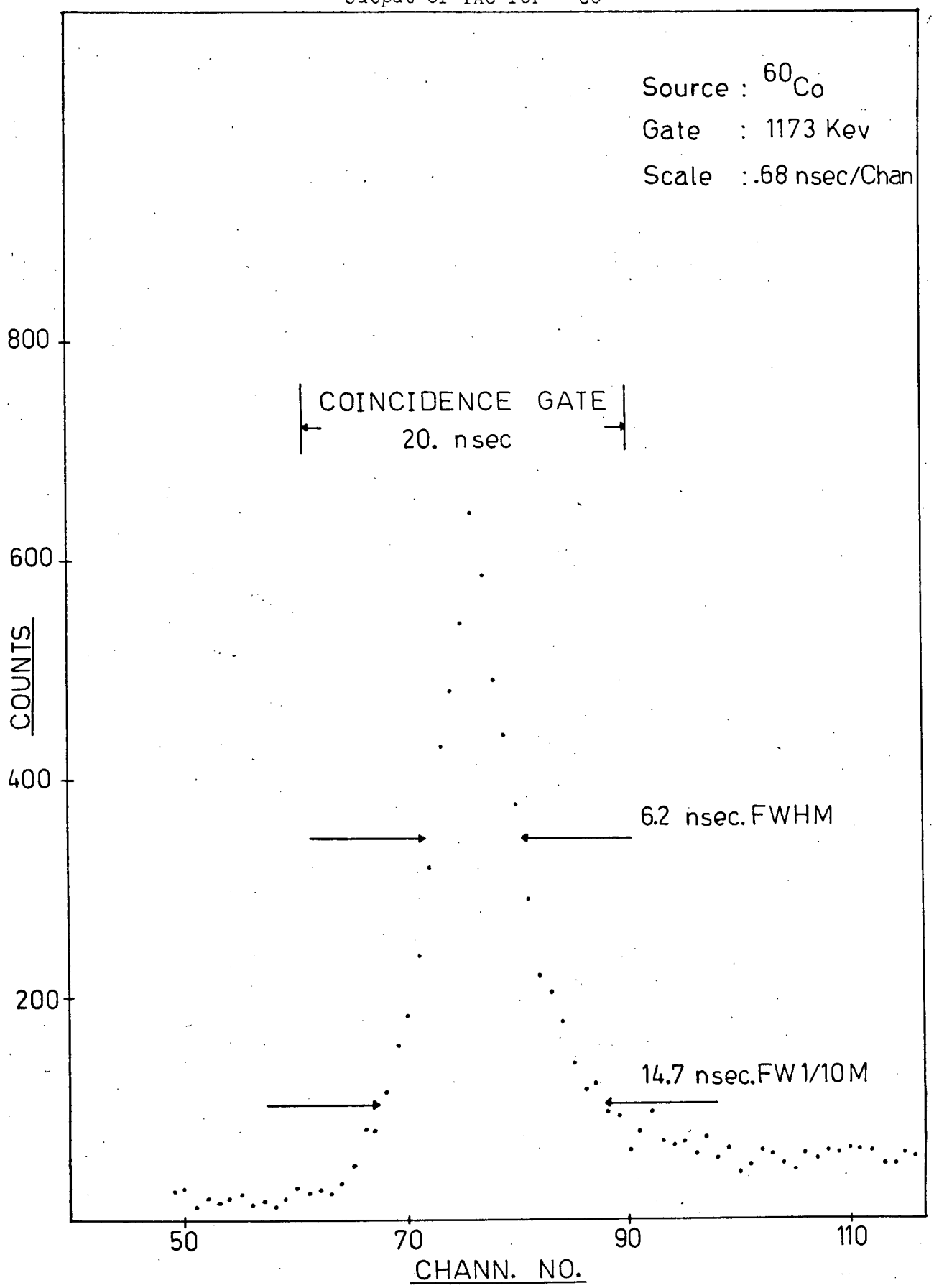

spectrum has to be corrected for any difference between the background intensities in the gates of the two spectra and any measurable decay of the source between the two measurements. An example of on-peak and off-peak spectra of ^{60}Co taken in coincidence with the 1173 kev transition is shown in Figure V-3. The low energy portions of these spectra, below 1 Mev, are omitted.

Chance coincidences are another contribution to the on-peak spectrum. The rate of these random coincidences between a gated transition i and another transition j is given by

$$C_{ij} = I_i I_j \, 2\tau$$

where I_i is the counting rate of transition i in the gate detector and I_j is that of transition j in the analog detector; 2τ is the width of the gate set by TSCA #2 on the time peak (See Figure V-2).

After background corrections have been made with the off-peak spectrum, the following method can be used to correct the on-peak spectrum for chance coincidences. If a spectrum is taken in coincidence with a transition i, then any appearance in this spectrum of transition i must be entirely due to chance coincidences. If C_{ii} is the intensity of this peak, then the chance contribution to any other peak j in the coincidence spectrum is given by

$$C_{ij} = \frac{I_j}{I_j} C_{ii}$$

where, as before, I_i and I_j are the transition rates in the analog detector known from the singles spectra. In this way all peaks in a coincidence spectrum may be corrected for chance coincidences.

Figure V-3

^{60}Co Coincidence Spectrum

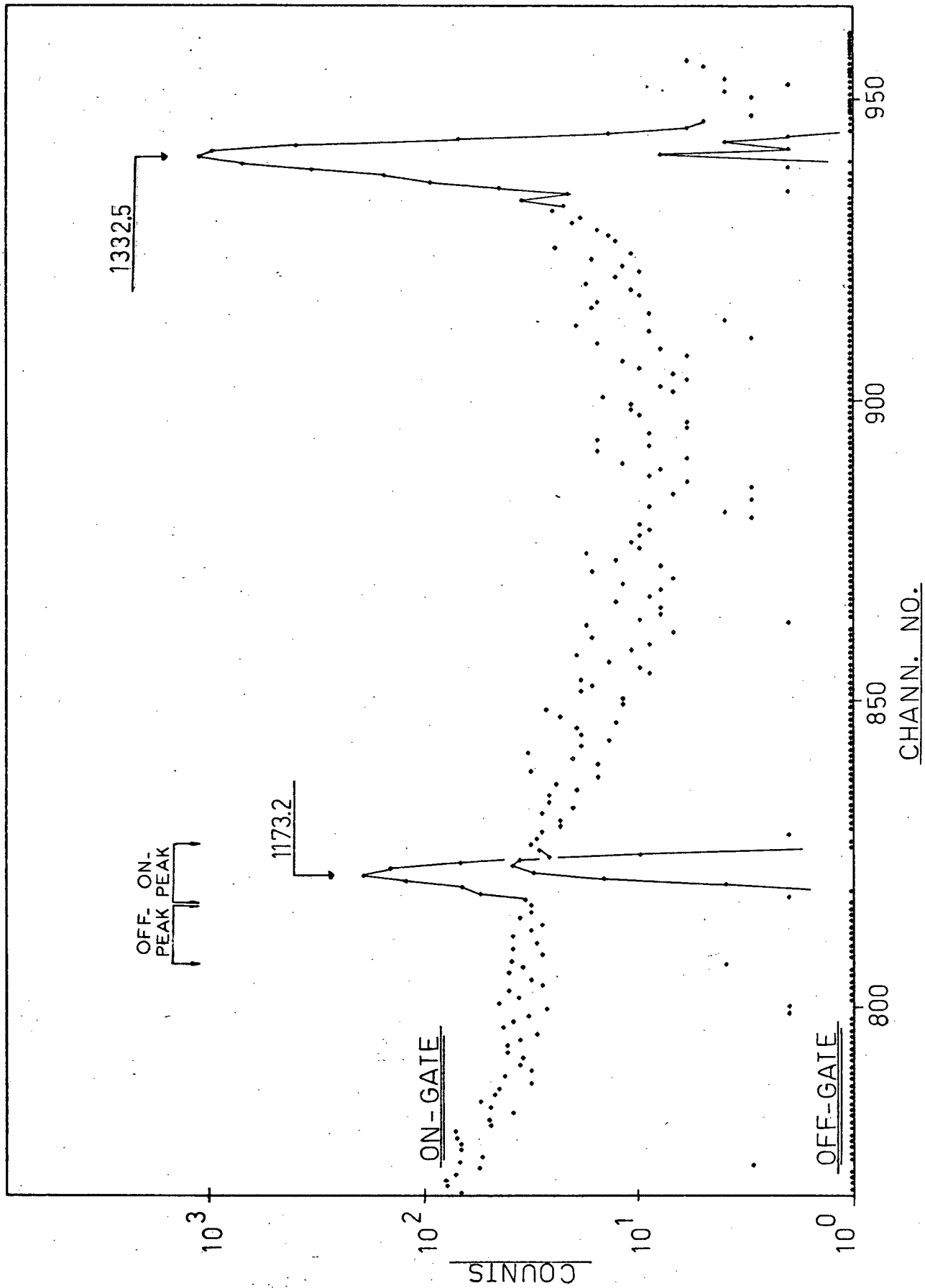

3. COINCIDENCE MEASUREMENTS FOR ^{160}Dy

Gamma spectra were taken in coincidence with the 197, the 215.5 and the 966 kev transitions, the 962-966 kev double peak and the approximate energy region 995-1015 kev. On-peak and off-peak spectra were taken for each of the five gates.

The gated region 995-1015 kev will contain in addition to the 1003 kev transition the 1005 kev transition, if it exists. Figure V-4(a,b) shows the on-peak and the off-peak spectra. The portions of both spectra above 500 kev are not shown since no peaks were observed in these regions.

Figure V-5 shows the spectrum in coincidence with the 962-966 kev double peak. The spectrum in coincidence with the 966 kev transition is shown in Figure V-6. The energy regions above 550 kev of both of these spectra are omitted, since no peaks were observed in these regions. The 962 and the 966 kev peaks were not separated by our gate detector. Thus to gate the 966 kev transition, the gate was reduced to half its former width (when set on the double peak) and moved to the high energy side of the double peak.

The spectrum in coincidence with the 215.5 kev transition is shown in Figure V-7(a,b). Because of low count rates, the portion of the spectrum above 1150 kev is omitted.

Figure V-8(a,b) shows the spectrum taken in coincidence with the 197 kev transition.

In the course of analysis of these spectra, certain peaks occurred which did not correspond to any of the known transitions. These peaks, which were 2 to 3 times as wide as the other peaks, occurred at energies of $E=E_\gamma-E_G$, where E_G is the average gate energy and E_γ is the energy of an intense transition. In the coincidence spectra these peaks are identified as E(S), where E is the peak energy.

Figure V-4 (a)

The 915-1015 kev Coincidence Spectra

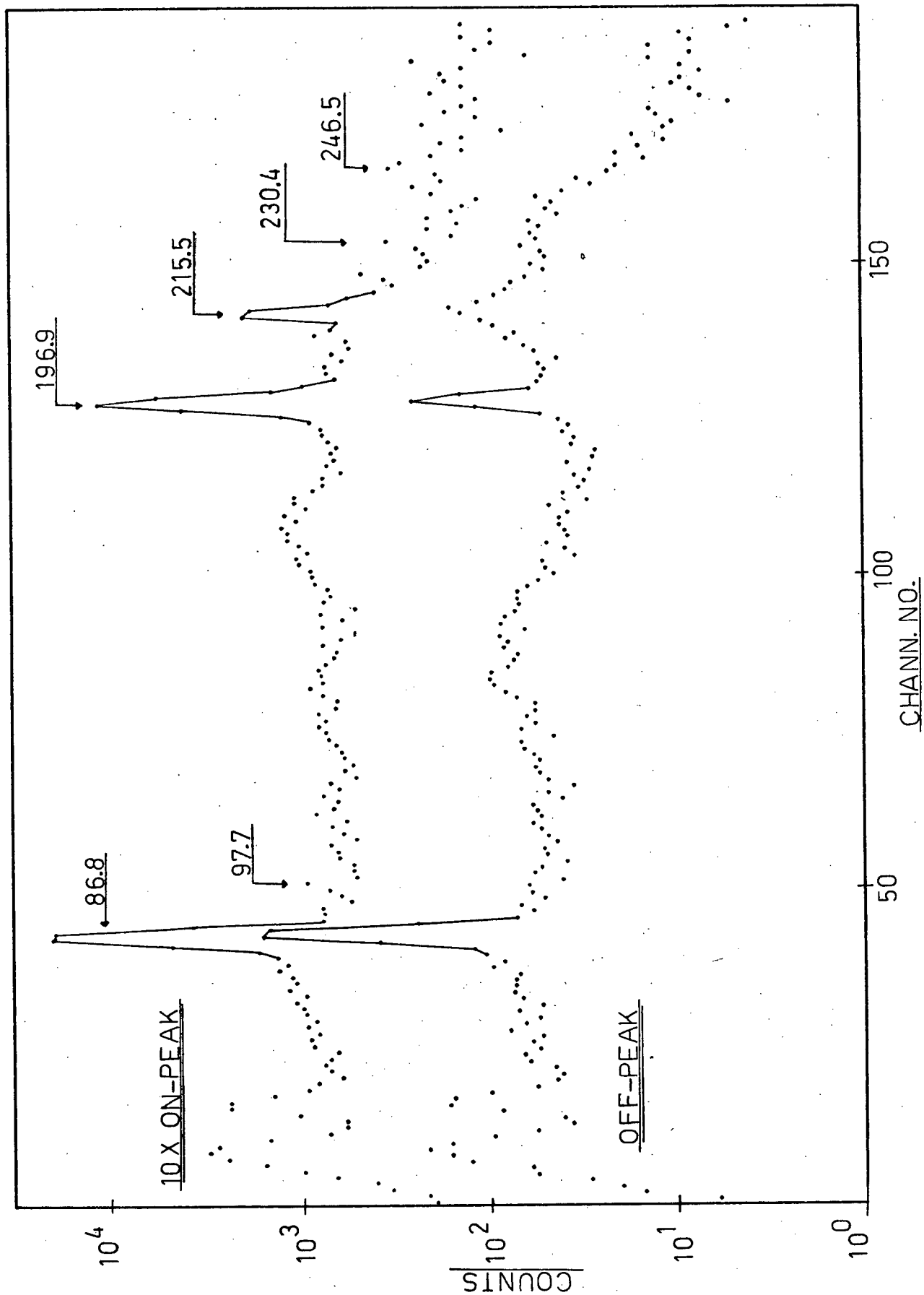

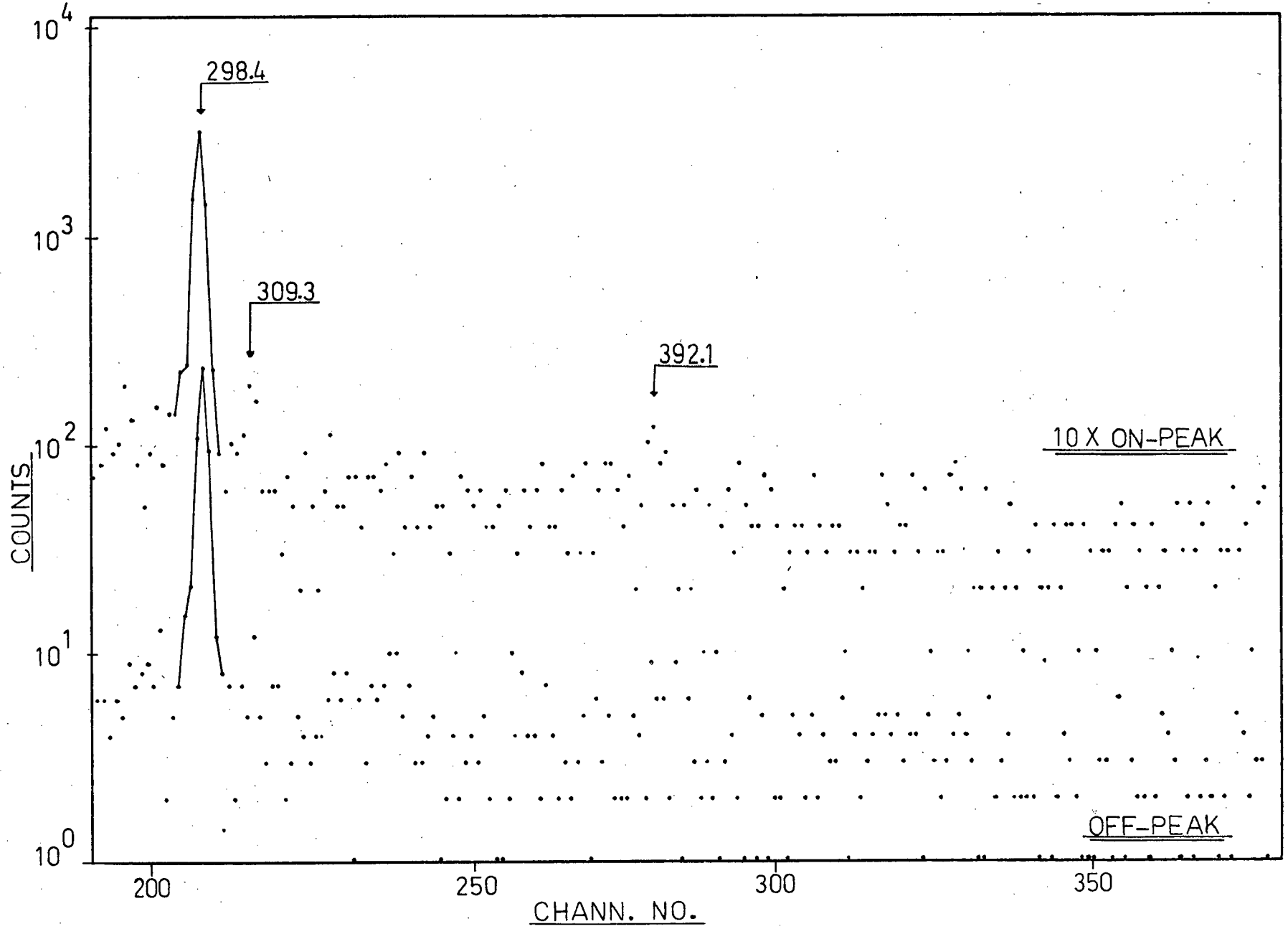
298.4
309.3
392.1
10 X ON-PEAK
OFF-PEAK
COUNTS
CHANN. NO.
10^4
10^3
10^2
10^1
10^0
200
250
300
350

Figure V-4 (b)

Figure V-5

The 962-966 kev On-Peak Spectrum

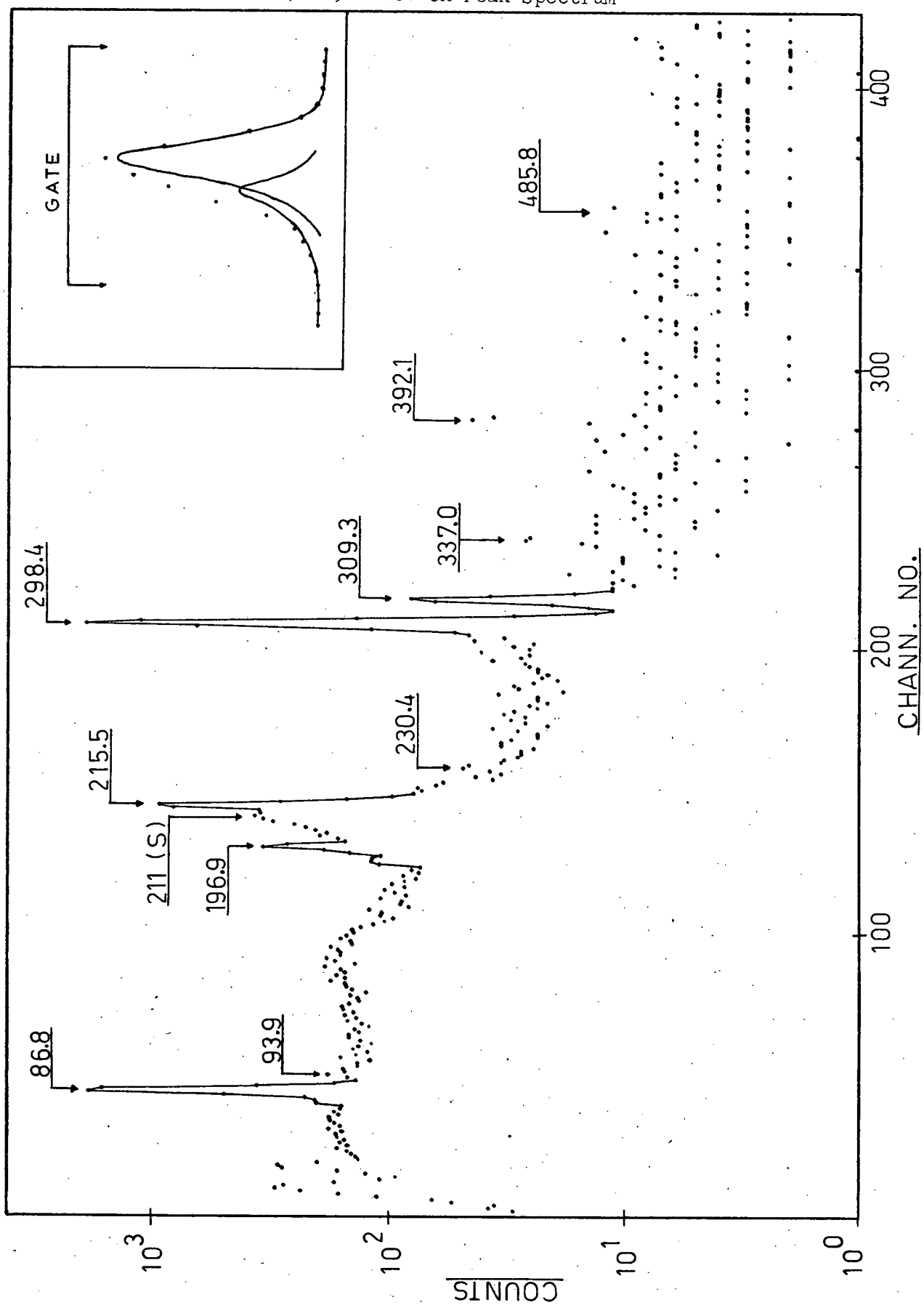

Figure V-6

The 966 kev On-Peak Spectrum

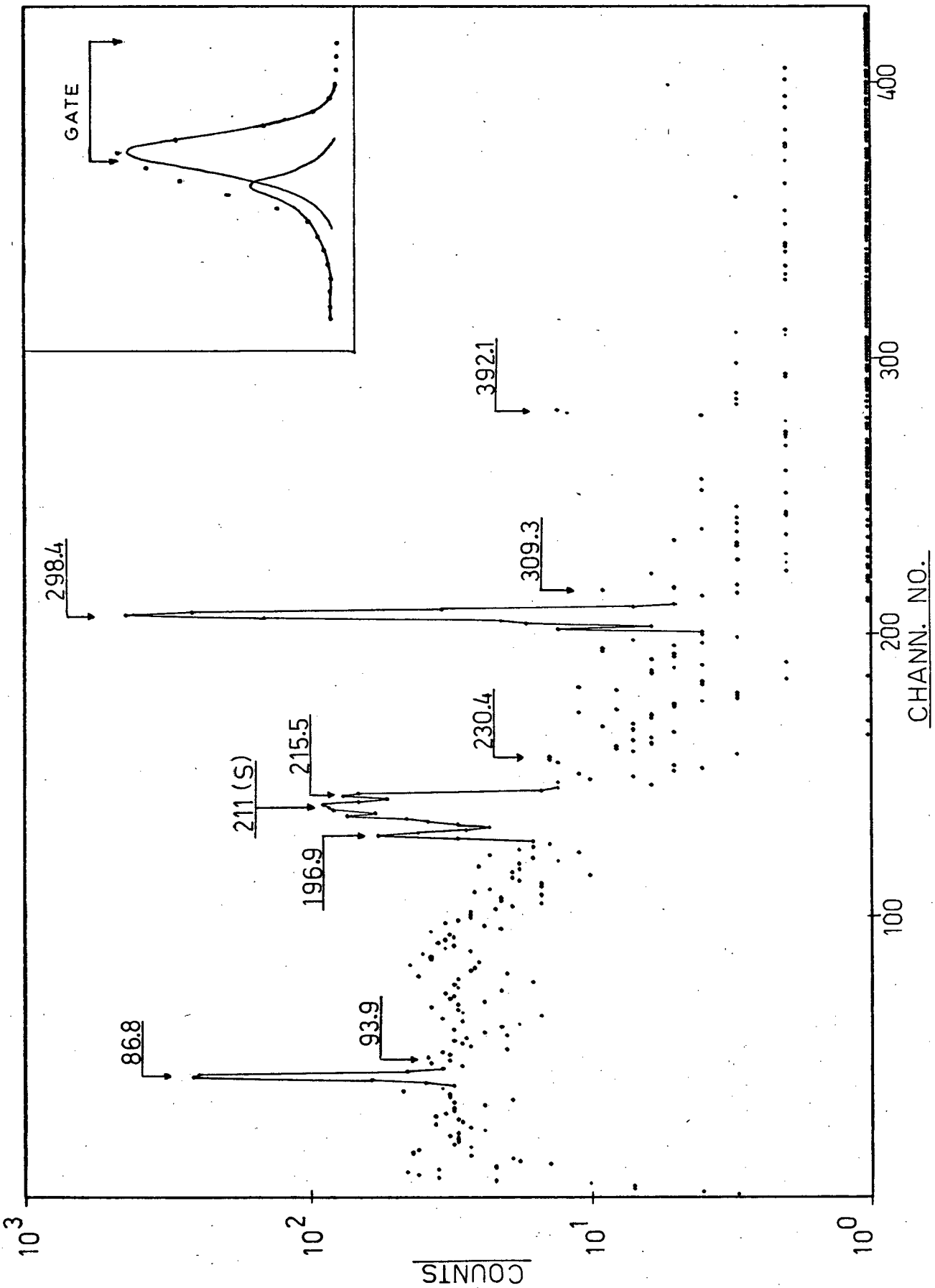

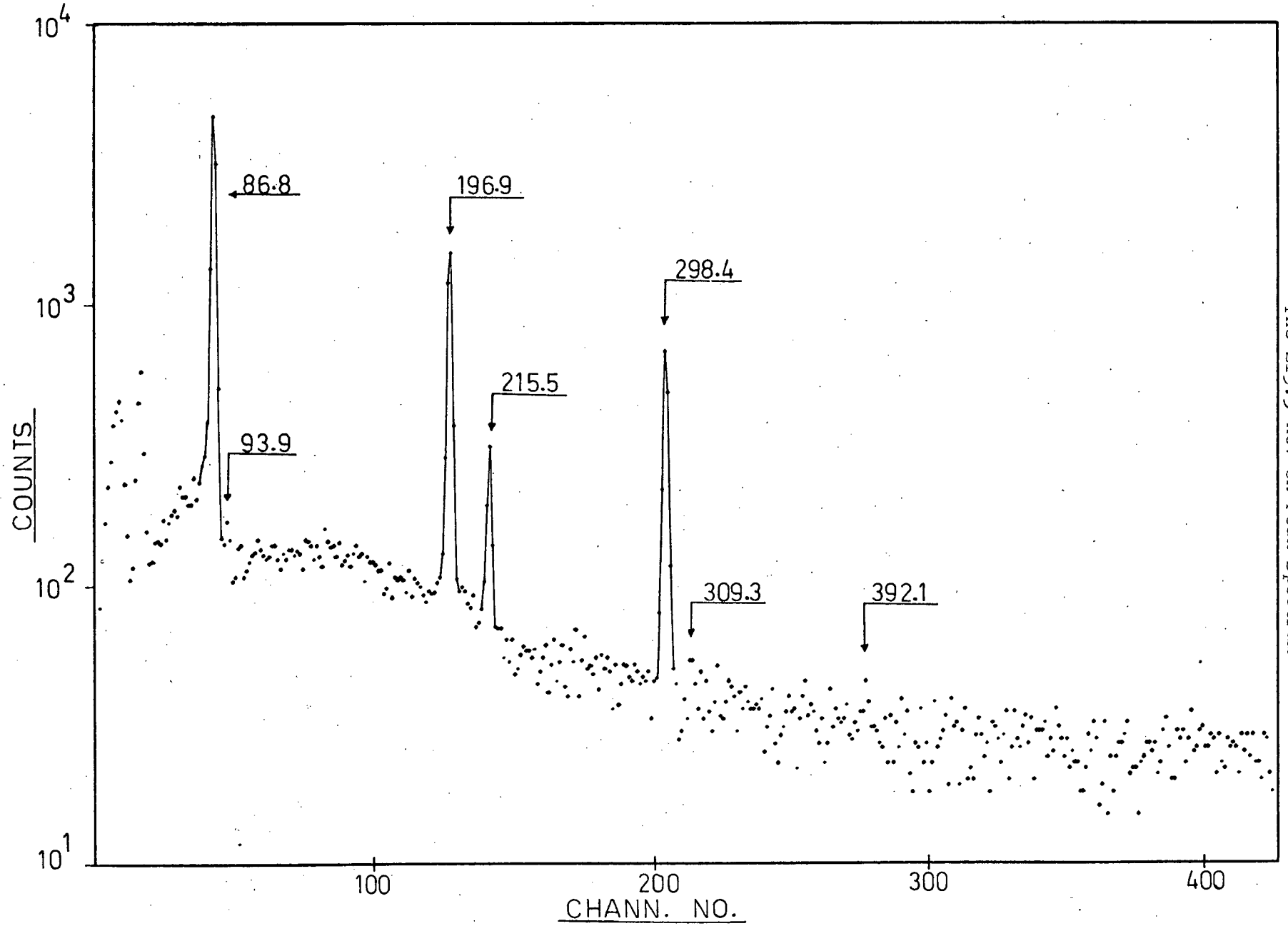

Figure V-7 (a)

The 215.5 kev On-Peak Spectrum

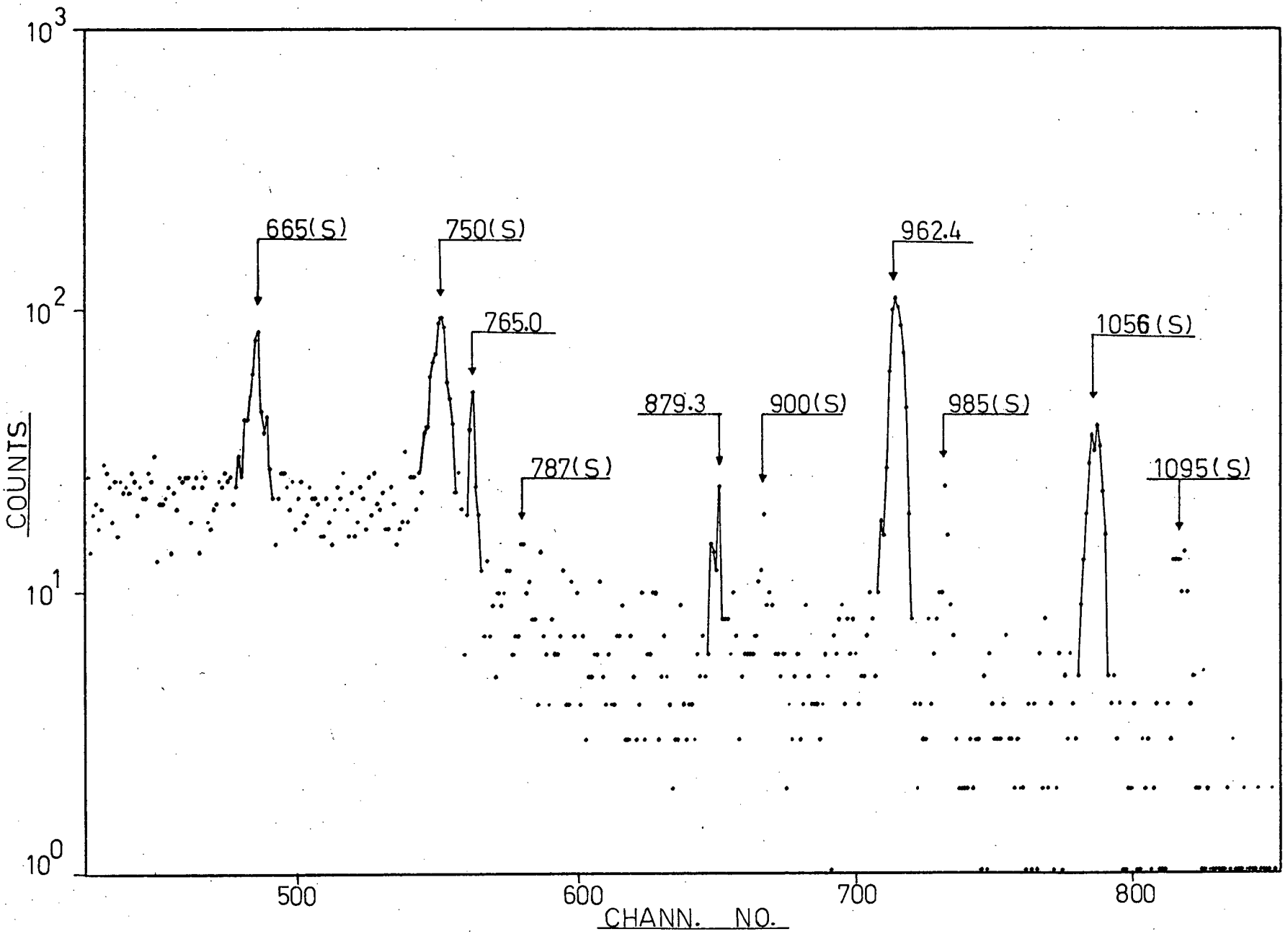
10^3
10^2
10^1
10^0
COUNTS
665(S)
750(S)
765.0
787(S)
879.3
900(S)
962.4
985(S)
1056(S)
1095(S)
500
600
700
800
CHANN. NO.

Figure V-7 (b)

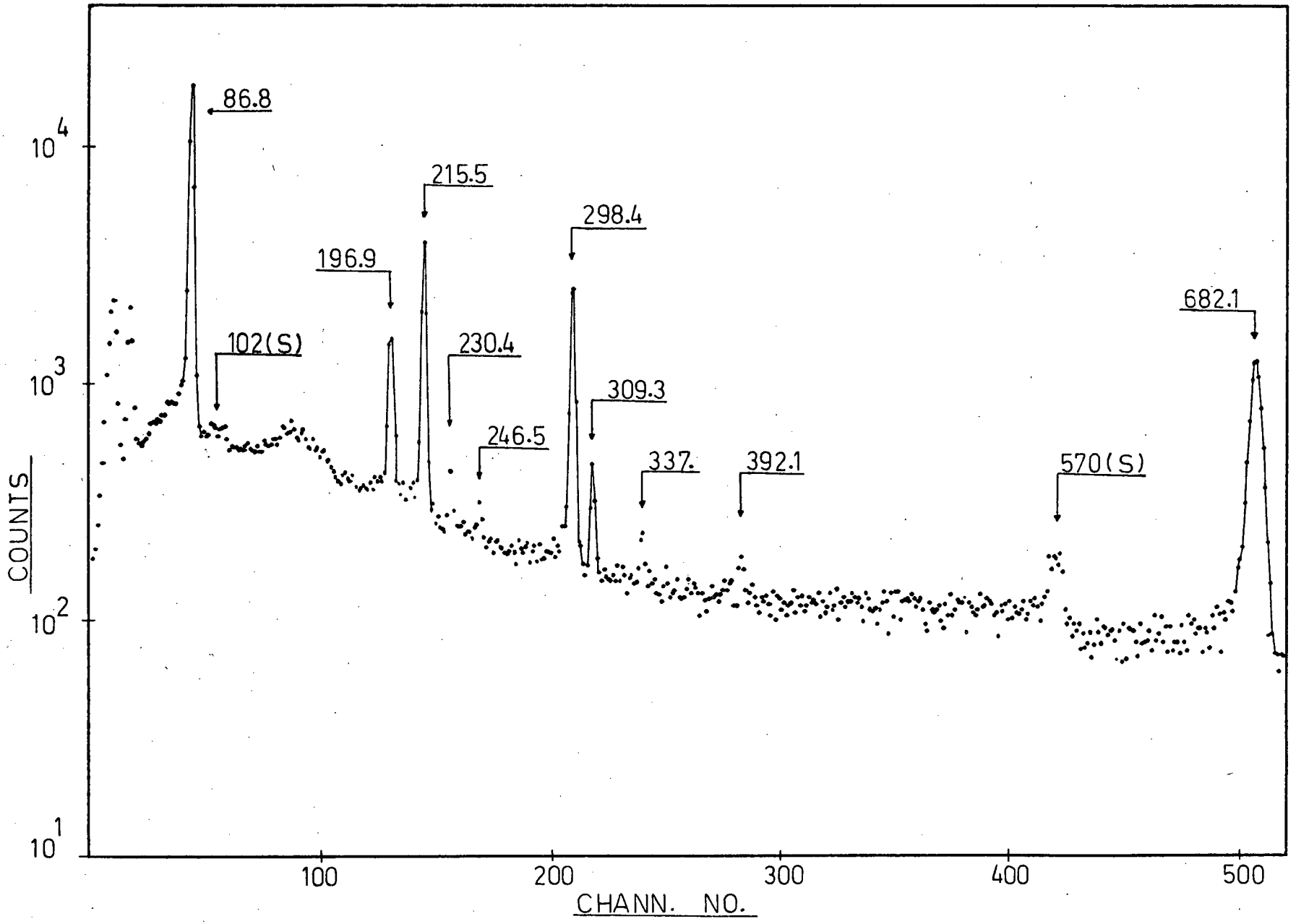

Figure V-8 (a)

The 197 kev On-Peak Spectrum

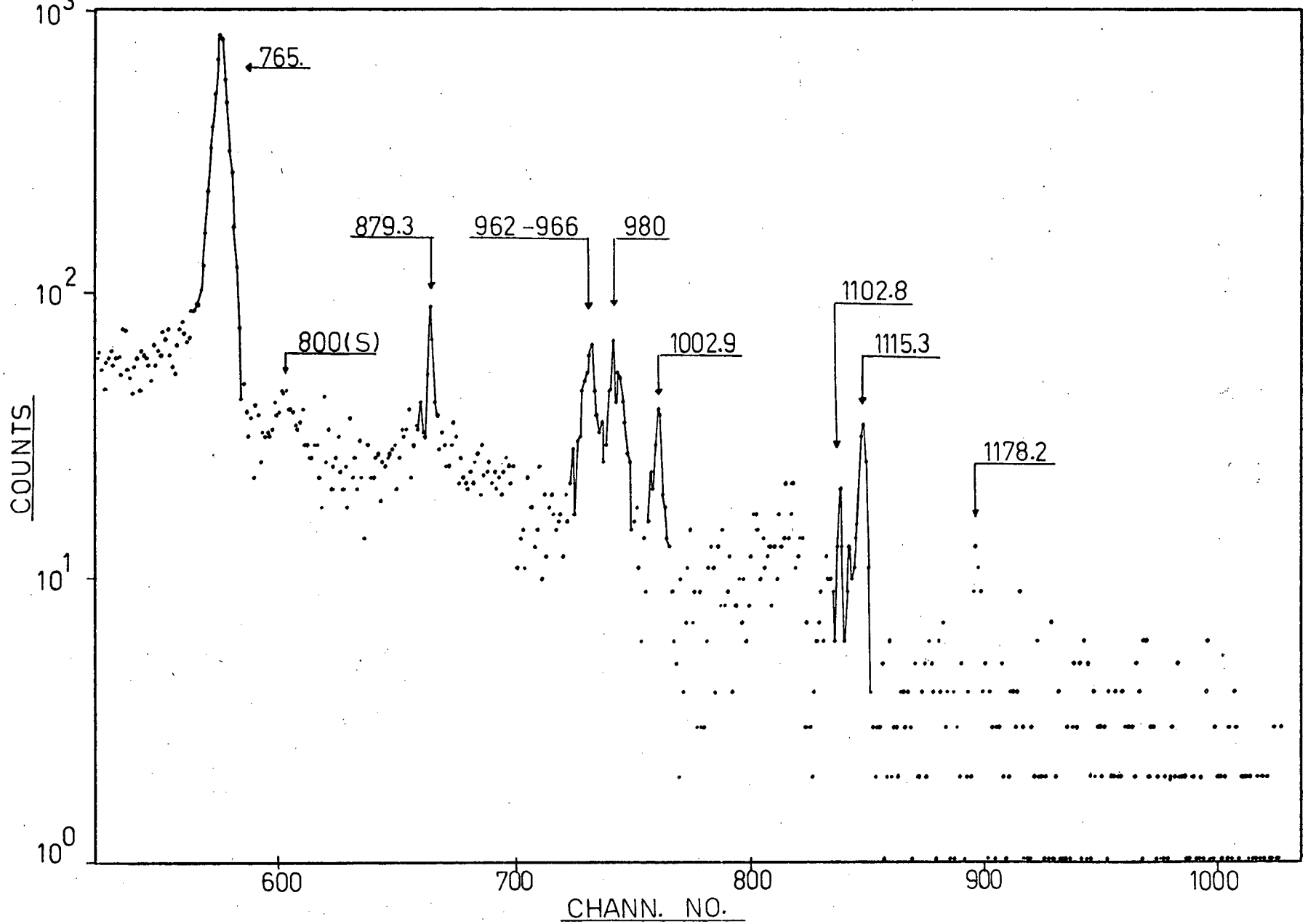
765.
879.3
962 -966
980
800(S)
1002.9
1102.8
1115.3
1178.2
COUNTS
CHANN. NO.
10^3
10^2
10^1
10^0
600
700
800
900
1000

Figure V-8 (b)

On the basis of the above observations, it was suspected that these peaks were caused by gamma-rays scattering from one detector into the other and depositing just enough energy to trigger the gate. The process should be Compton scattering, (almost backscattering). Calculations show that with the geometry used, each of the peaks marked with an (S) can be attributed to this process. To check this lead shields were placed between the detectors and a spectrum taken in coincidence with the 215.5 kev transition. This spectrum is shown in Figure V-9(a,b) along with a spectrum taken without the lead shields. Comparison of these two spectra confirms that these peaks are due to scattering from one detector into the other.

The intensity of each peak in the on-peak spectrum was corrected for background and random contributions. Tables V-3 through V-7 present the data and the corrected intensities for the five gates 197, 215.5, 966, 962-966 double peak and the energy region 995-1015 kev respectively. These intensities have all been normalized to counts in 5,000 seconds.

The existence of the transitions 97.7 and 246.5 kev in the spectrum taken in coincidence with the energy region 995-1015 kev, confirms the existence of the 1005 kev transition.

Figure V-9 (a)

The 215.5 kev On-Peak Spectrum With Lead Shield

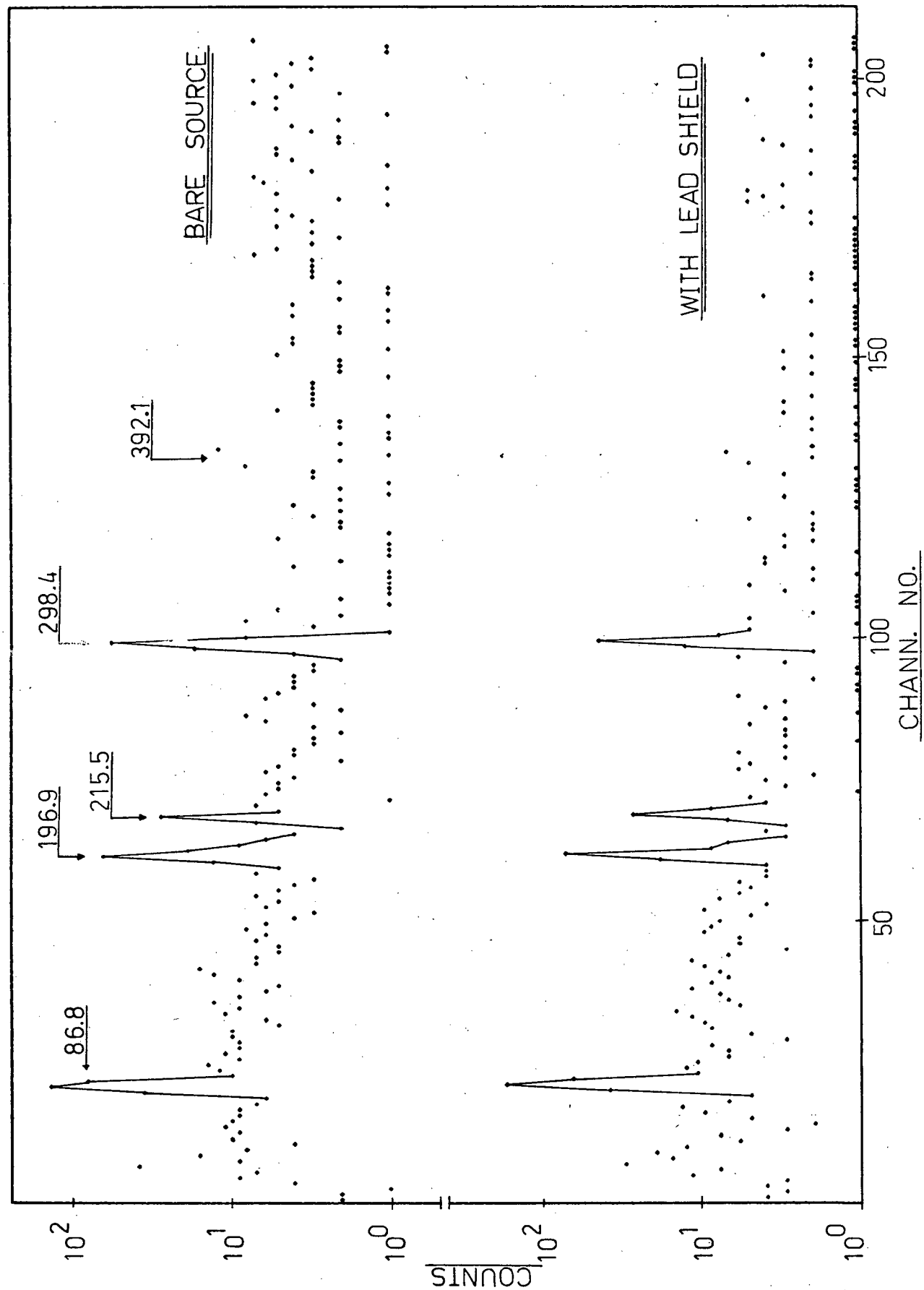

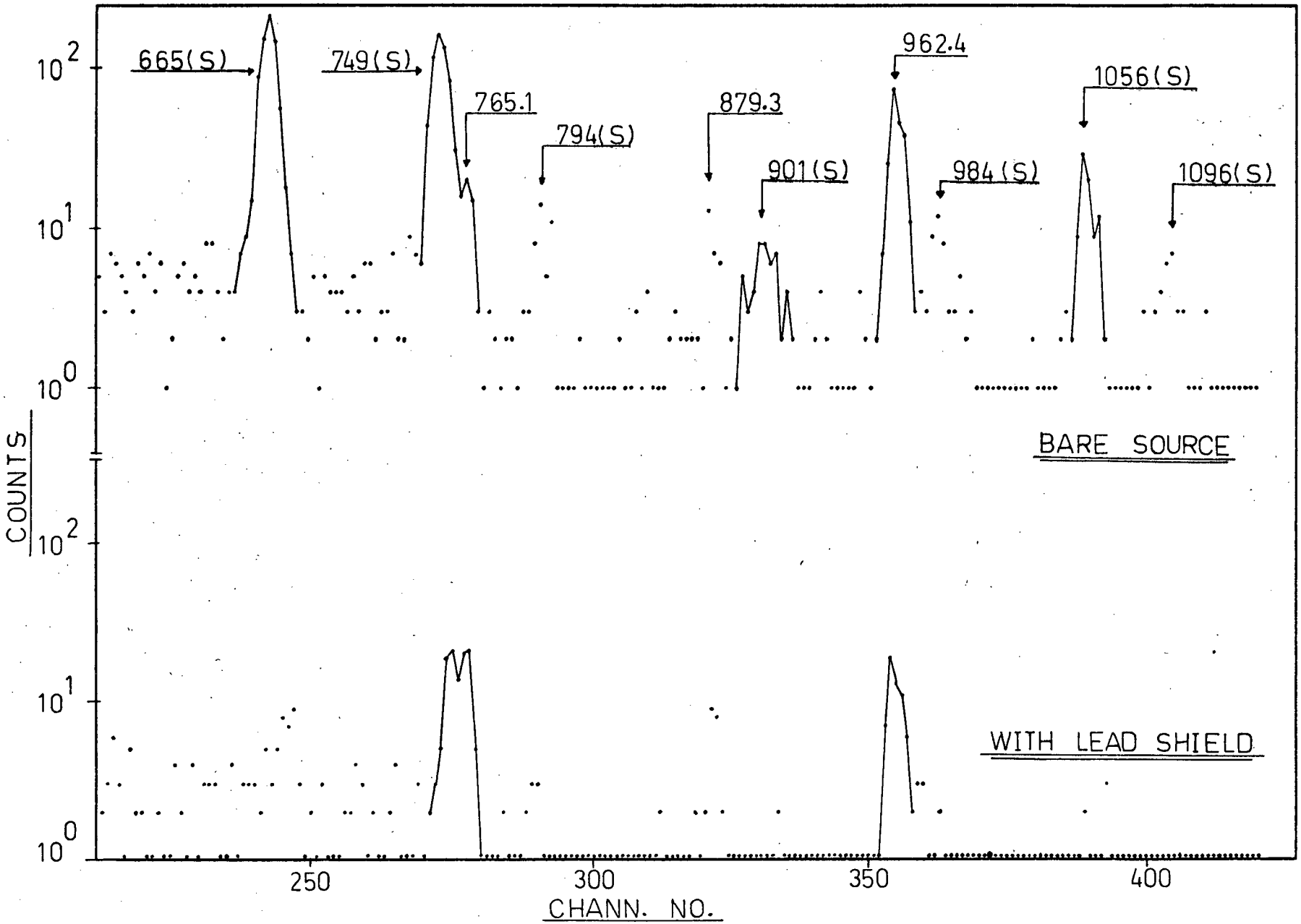
665(S)
749(S)
765.1
794(S)
879.3
901(S)
962.4
984(S)
1056(S)
1096(S)
BARE SOURCE
WITH LEAD SHIELD
COUNTS
CHANN. NO.
250
300
350
400

Figure V-9 (b)

TABLE V-3

SPECTRUM IN COINCIDENCE WITH THE 196.9 kev GATE

ENERGY	ON-PEAK INTENSITY		OFF-PEAK INTENSITY		CORRECTED FOR BACKGROUND	CORRECTED FOR CHANCE COINCID.
86.8	3730	(30)	1430	(25)	2300	2150
148.5	14	(5)	<4		>10	>10
196.9	300	(20)	260	(10)	40	
215.5	770	(20)	170	(10)	600	570
230.4	44	(6)	<2		>42	>37
246.5	19	(7)	<2		>17	>17
298.4	620	(15)	290	(15)	230	110
309.3	63	(9)	10	(2)	53	49
337.0	22	(7)	<2		>20	>18
349.3	8	(3)	<1		>7	> 7
392.1	14	(6)	15	(3)		
682.1	740	(20)	185	(15)	555	555
765.1	530	(20)	84	(15)	446	446
879.3	14	(3)	15	(2)		
962+966	24	(7)	21	(3)		
1002.9	16	4	<1		>15	>14
1102.8	6	(1)	2	(1)	4	4
1115.3	12	(1)	1		11	9
1178.2	4	(1)	3	(1)		

TABLE V-4

SPECTRUM IN COINCIDENCE WITH THE 215.5 kev GATE

ENERGY	ON-PEAK INTENSITY	OFF-PEAK INTENSITY	CORRECTED INTENSITY
86.8	2400 (35)	1220 (50)	1180
93.9	28 (7)	<10	>18
196.9	770 (17)	225 (20)	545
215.5	120 (10)	150 (20)	
298.4	350 (15)	340 (20)	
309.3	10 (2)	9 (2)	
392.1	11 (2)	13 (2)	
765.1	18 (5)	6 (2)	12
879.3	14 (4)	13 (2)	
962.4	150 (7)	7 (1)	143
966.2	11 (2)	12 (2)	

TABLE V-5

SPECTRUM IN COINCIDENCE WITH THE 966 kev GATE

ENERGY	ON-PEAK INTENSITY	OFF-PEAK INTENSITY	CORRECTED INTENSITY
86.8	1150 (50)	1120 (50)	
93.9	60 (30)	<10	50
196.9	175 (25)	160 (20)	
215.5	175 (25)	165 (30)	
230.4	28 (8)	24 (5)	
298.4	2280 (30)	270 (10)	∿2000
309.3	<20	15 (3)	
320.5	20 (6)	<5	>15
392.1	70 (8)	11 (4)	∿60

TABLE V-6

SPECTRUM IN COINCIDENCE WITH THE 962-966 kev GATE

ENERGY	ON-PEAK INTENSITY	OFF-PEAK INTENSITY	CORRECTED INTENSITY
86.8	1860 (30)	1120 (50)	740
93.9	38 (12)	<10	~30
196.9	180 (30)	160 (20)	
215.5	720 (50)	165 (30)	550
230.4	20 (5)	24 (5)	
246.5	12 (2)	11 (3)	
298.4	1940 (40)	270 (10)	1670
309.3	83 (5)	15 (3)	~70
337.0	35 (7)	<10	>25
392.1	40 (7)	11 (4)	~30
485.8	12 (4)	4 (2)	8

TABLE V-7

SPECTRUM IN COINCIDENCE WITH THE 995-1015 kev GATE

ENERGY	ON-PEAK INTENSITY	OFF-PEAK INTENSITY	CORRECTED INTENSITY
86.8	490 (8)	435 (8)	55
97.7	6 (1)	3 (1)	3
196.9	204 (5)	48 (3)	~160
215.5	46 (4)	58 (4)	
230.4	2 (1)	2 (1)	
246.5	6 (1)	<1	>5
298.4	58 (3)	55 (4)	
309.3	3 (1)	2 (1)	
392.1	2 (1)	2 (1)	

CHAPTER VI

RESULTS AND MODEL COMPARISONS

The decay scheme of ^{160}Dy, constructed on the basis of our gamma, K-conversion electron and gamma-gamma coincidence measurements, is presented in Figure VI-1. When assigning the spin values of some energy levels we have also used the results of the directional correlation measurements of references 18 and 19, and the coincidence results of reference 14 for guidance and confirmation of our results. The spin assignments are discussed in section VI-1.

The decay scheme of Figure VI-1 is essentially the same as those reported by other investigators, although it differs in some details. Specifically, transitions 237.6 and 242.5 kev reported by Ludington et al.[14] are found to belong respectively to the naturally occurring ^{228}Th and ^{226}Ra activities. The new 111.8 kev gamma-ray is placed in the decay scheme, on the basis of energy fit, as a transition between the 1398.8 and 1286.8 kev levels. The new 97.7, 148.5 and the 320.5 kev transitions were observed in the spectra taken in coincidence with the 995-1015, the 197 and the 966 kev gates respectively.

The placement of the transition 1285.8 kev by Ludington et al.[14] as populating the 0^+ ground state from the 3^- state at 1286.8 kev, is very improbable. We agree with the suggestion by McAdams and Otteson[17] that this transition takes place from an energy level at 1285.8 kev, established by Grigor'ev et al.[20] as a $J=1^-$ state at 1285.4 kev, to the ground state. Our results showed that the energy of this peak shifted from 1285.4 kev to 1286.5 kev when D, the "Source-Detector" distance, was decreased from 15 cm to 0 cm. Since this peak is not a pure sum peak (see Figure III-8), we conclude that there is a true cross-over transition of energy 1285.4 kev, having at close distances

Figure VI-1

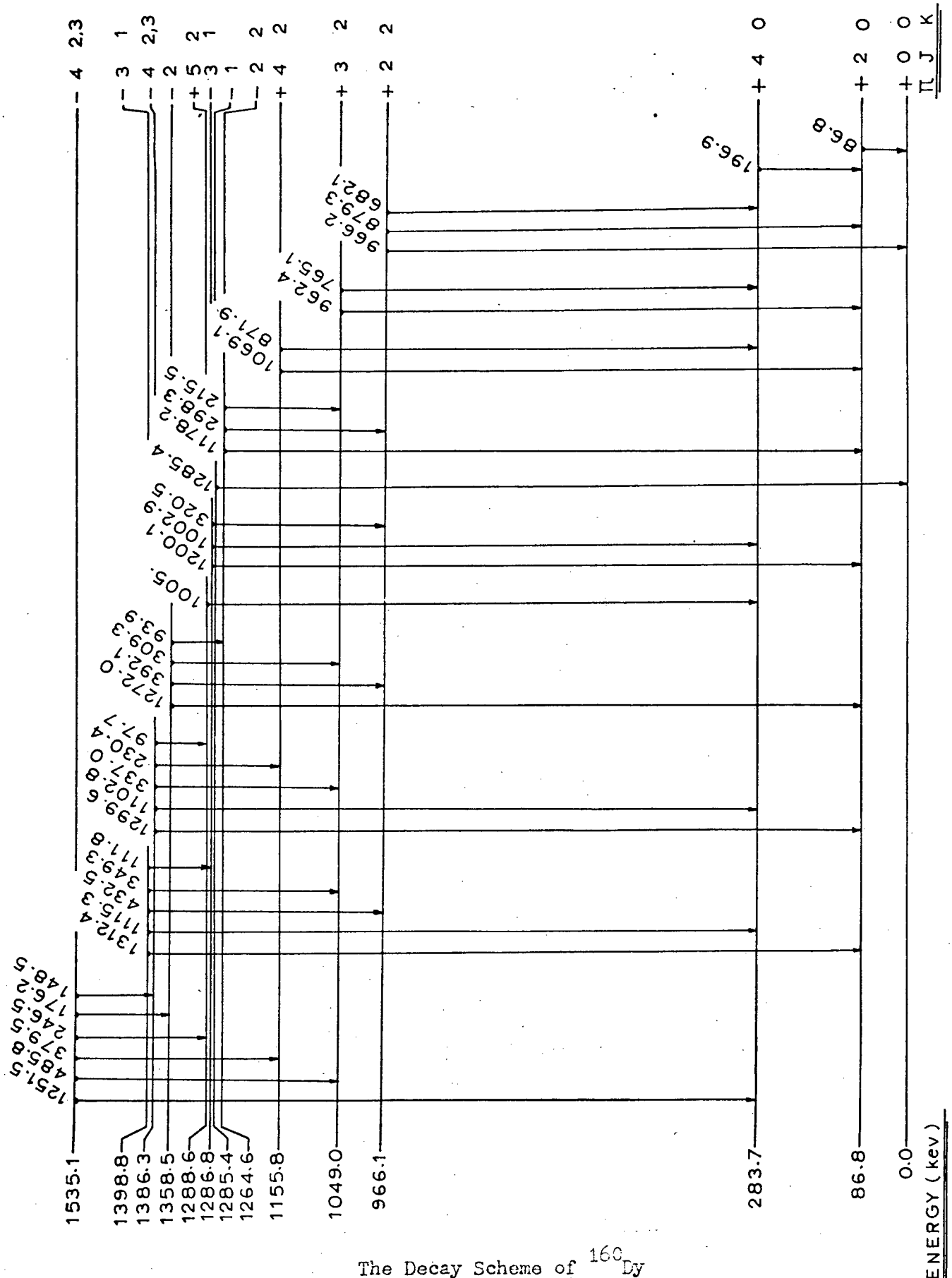

The Decay Scheme of ^{160}Dy

contributions from the coincidence summing of the 1200 kev and the 86.8 kev transitions.

1. SPIN ASSIGNMENTS AND BRANCHING RATIOS

The spin, J, of the positive parity levels of ^{160}Dy have been established unambiguously by earlier investigations on the basis of E2 branching ratios, directional correlation measurements and the predictions of the collective model. Transitions between these even parity levels are all of E2 multipolarity. The experimental branching ratios for two E2 transitions from the state J_iN_i to two final states J_fN_f and $J_f'N_f'$, all with positive parity, are presented in Table VI-1. N is an ordinal quantum number, labeling the states of the same J in order of increasing energy. It will be shown in section VI-2 that K is a reasonably good quantum number for the even parity states, so that these states may be identified with the two J and K quantum numbers instead of J and N.

The odd parity states of ^{160}Dy depopulate mostly by E1 transitions to the even parity levels. The experimental E1 branching ratios are presented in Table VI-2. The choice of E1 multipolarity is made for the gamma rays 379.5, 485.8 and 1251.5 kev, neglecting the E3 possibility for reasons previously stated (See chapter IV, page 56).

Since E1 transitions are prohibited by the collective model, these transitions must be of single particle origin[9]. The theoretical branching ratio for two E1 transitions from the odd parity state J_iK_i to two even parity states J_fK_f and $J_f'K_f'$, is given by

$$\frac{B(E1;J_iK_i \rightarrow J_fK_f)}{B(E1;J_iK_i \rightarrow J_f'K_f')} = \left| \frac{(J_i 1 K_i K_f - K_i \mid J_i 1 J_f K_f)}{(J_i 1 K_i K_f' - K_i \mid J_i 1 J_f' K_f')} \right|^2 \qquad (6.1)$$

TABLE VI-1

EXPERIMENTAL E2 BRANCHING RATIOS

Initial level (kev)	$\frac{\gamma_1}{\gamma_2}$	$\frac{J_iN_i \to J_fN_f}{J_iN_i \to J'_fN'_f}$	$\frac{B(E2;J_iN_i \to J_fN_f)}{B(E2;J_iN_i \to J'_FN'_f)}$
966.1	$\frac{966.2}{879.3}$	$\frac{22 \to 01}{22 \to 21}$	.52±.03
966.1	$\frac{682.1}{879.3}$	$\frac{22 \to 41}{22 \to 21}$	.068±.006
1049.0	$\frac{765.1}{962.4}$	$\frac{31 \to 41}{31 \to 21}$	.64±.05
1155.8	$\frac{871.9}{1069.1}$	$\frac{42 \to 41}{42 \to 21}$	5.6±1.3

TABLE VI-2

EXPERIMENTAL E1 BRANCHING RATIOS

Initial level (kev)	$\frac{\gamma_1}{\gamma_2}$	Branching Ratio
1264.6	$\frac{215.5}{298.3}$	.44±.05
1286.8	$\frac{1002.9}{1200.1}$	.76±.05
1358.4	$\frac{309.3}{392.1}$	1.3±.2
1386.3	$\frac{230.4}{337.0}$	.74±.12
1398.8	$\frac{1115.3}{1312.4}$	.89±.06
1535.1	$\frac{485.8}{379.5}$	1.3±.4

where $(J_i 1 K_i K_f - K_i | J_i 1 J_f K_f)$ are the Clebsch-Gordon coefficients. For K-forbidden E1 transitions, i.e. for $|K_f - K_i| > 1$, the branching ratios are calculated from the expression given in reference 23.

The J and the K values of the odd parity levels were assigned by comparing the experimental E1 branching ratios of Table VI-2 to the predictions of equation (6.1) for all possible values of J_i and K_i. These comparisons are provided in the following pages.

Information on the K values of these levels were obtained by comparing the observed intensities of the transitions to the even parity levels, to the single particle transition rates as given in reference 24. Those transitions whose multipolarities were not determined by conversion electron measurements, were assigned the lowest possible electric multipolarity, which was E1 in all cases. The intensities of the transitions from each level were normalized so that the ratio of the observed intensity to the single particle estimate for the transition to the K=0 band, i.e. to the 86.8 or 283.7 kev levels, was unity. The ratio of these normalized intensities to the single particle estimates are presented in Table VI-3 and shown schematically in Figure VI-2. The broad lines and the semi-broad lines represent the transitions, whose intensities are enhanced over the normalized single particle estimates by factors of greater than 50 and between 10 and 50 respectively. The narrow lines represent the transitions which are enhanced or slowed by factors of less than 10, attributable to the statistical factors which we have neglected.

K-forbidden transitions are slowed by factors which depend on the degree of forbiddenness $\nu = \Delta K - 1$; the larger the ν the more inhibited the transition[9]. The enhancement or the inhibition of the transitions to the K=2 band, as compared to those to the K=0 band, provide information on the K assignment of

TABLE VI-3

COMPARISON WITH SINGLE PARTICLE TRANSITION RATES

Initial Level (kev)	Final Level (kev)	K_f	Ratio	K_i
1264.6	86.8	0	1	
	966.1	2	120	≥ 2
	1049.0	2	53.3	
1286.8	86.8	0	1	
	283.7	0	.77	1
	966.1	2	.20	
1358.4	86.8	0	1	
	966.1	2	6.7	1,2
	1049.0	2	9.0	
1386.3	283.8	0	1	
	1049.0	2	24	
	1155.8	2	17.6	≥ 2
	1288.6	2	20	
1398.9	86.8	0	1	
	283.7	0	.90	
	966.1	2	.22	1
	1049.0	2	.27	
1535.1	283.7	0	1	
	1049.0	2	13.3	
	1155.8	2	11	≥ 2
	1288.6	2	18.8	

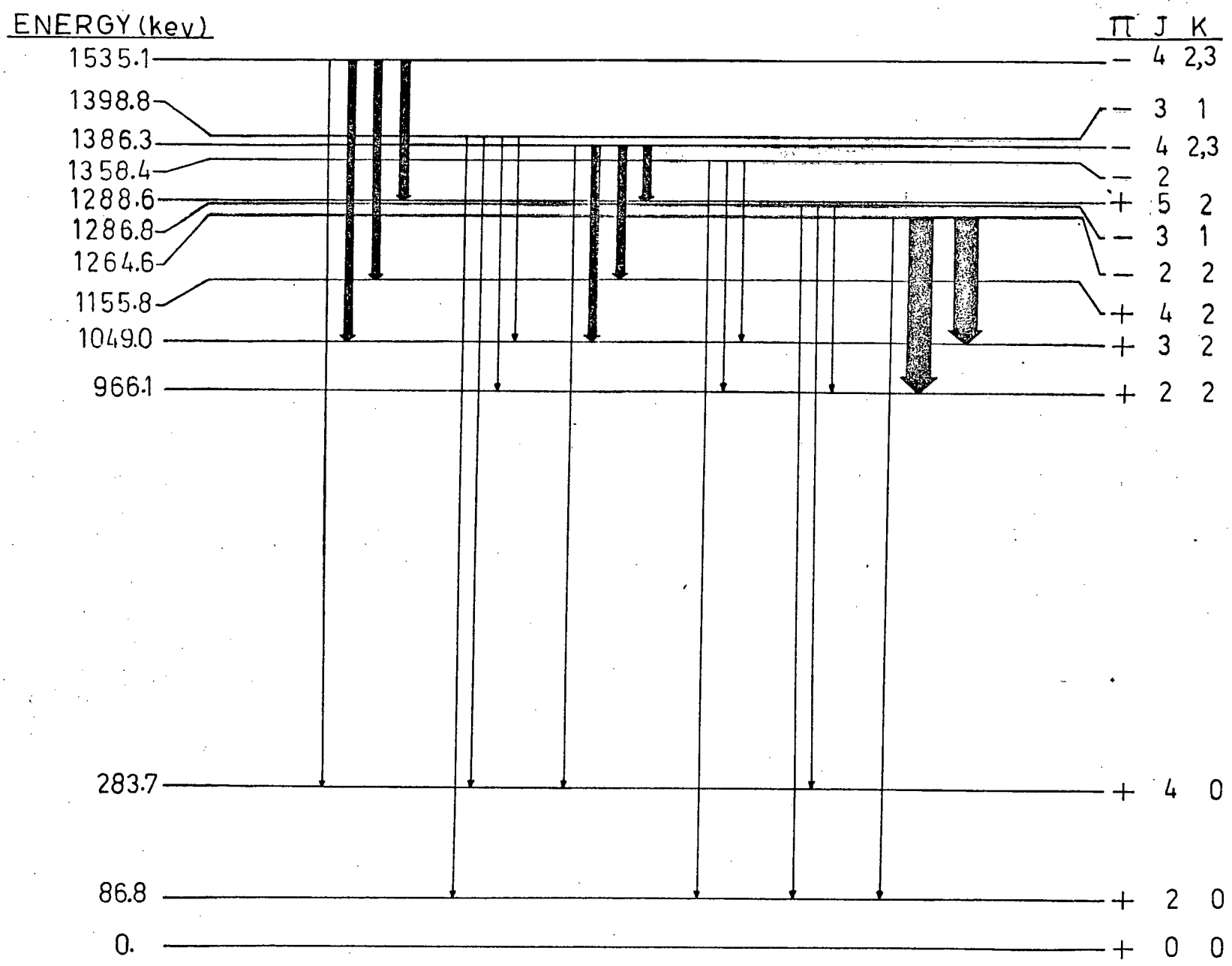

Figure VI-2

Comparison With Single Particle Transition Rates

the initial odd parity level. For example for the 1264.6 kev level, the enhancement of the transitions to the K=2 band by factors of 120 and 50 over those to the K=0 band favors an assignment of $K_i \geq 2$. If K_i was equal to 0 or 1, the transitions to the K=2 band would have been retarded or unchanged respectively, relative to those to the K=0 band.

The justifications for the J and the K assignments are stated below for each of the seven odd parity levels.

Level 1264.6 kev J=2, K=2

The three E1 transitions from this level to the final even parity levels $J_f K_f$ = 32, 22 and 20 restrict the spin of this level to J = 2 or 3. The theoretical branching ratios for the transitions 215.5 and 298.3 kev, i.e. $\frac{B(E1, J_i K_i \to 32)}{B(E1, J_i K_i \to 22)}$, for possible values of $J_i K_i$ are

J_i = \ K_i =	0	1	2	3
2	2.0	2.0	.50	
3	8.75	8.75	1.40	.35

Comparison to single particle estimates and the experimentally observed branching ratio of .44±.05 are consistent with the assignment J_i=2, K_i=2. The J=2 assignment is in agreement with the results of directional correlation measurements of references 18 and 19.

Level 1285.4 kev J=1

The only transition observed from this level is the 1285.4 kev transition to the ground state. Grigor'ev et al.[20] have identified this transition, on the basis of conversion electron measurements, to be of multipolarity E1. This restricts the spin assignment of this level to J=1.

Level 1286.8 kev J=3, K=1

Since this level depopulates by E1 transitions 1002.9 and 1200.1 kev to the levels J_fK_f = 40 and 20 respectively, the spin of this level is restricted to J=3. The branching ratio for these two transitions, i.e. $\frac{B(E1;3K_i \to 40)}{B(E1;3K_i \to 20)}$, for possible values of K_i are

J_i = \ K_i =	0	1	2	3
3	1.33	.75	.75	.75

The observed value of .76±.05 is consistent with any of the K assignments 1, 2 or 3. The assignment K=1 is more plausible since transitions from this level to the K=2 band are not enhanced over those to the K=0 band.

Level 1358.4 kev J=2

The two E1 transitions from this level, i.e. the 309.3 and 392.1 kev transitions, populate states of JK = 32 and 22. This restricts the J assignment of this level to 2 or 3. The branching ratios for these two transitions for the possible values of J_iK_i are

J_i = \ K_i =	0	1	2	3
2	2.0	2.0	.50	
3	8.75	8.75	1.40	.35

Although the observed value of 1.4±.2 suggests an assignment J_iK_i = 32, this level has been identified by directional correlation measurements as a J=2 state[18,19]. Also the comparison with single particle estimates do not support a K=2 assignment. This level, with a J=2 assignment, will not

correspond to any definite value of K, and could therefore correspond to the mixing of various K values, as suggested by Gunther et al.[13].

Level 1386.3 kev J=4, K=2 or 3

The depopulation of this state by two E1 transitions 230.4 and 337.0 kev to the states with JK = 42 and 32, restricts the spin of this state to J=3 or 4. The branching ratio of these two transitions for possible values of J_iK_i are

J_i= \ K_i=	0	1	2	3	4
3	1.29	1.29	1.29	.143	
4	5.42	5.42	.60	.60	5.42

Comparison with single particle estimates and the observed value of .74±.12 support the assignment J=4 and K=2 or 3.

Level 1398.8 kev J=3, K=1

Since this state depopulates by the two E1 transitions 1115.3 and 1312.4 kev to the final states JK= 40 and 20, the spin of this level is restructed to J=3. The branching ratio for these two transitions for possible values of K_i are

J_i= \ K_i	0	1	2	3
3	1.33	.75	.75	.75

The observed value of .89±.06 is consistant with any of the three assignments K_i=1, 2 or 3. The K=1 assignment is more plausible, since the transitions to the K=2 band are neither enhanced nor retarded as compared to those to the K=0 band.

Level 1535.1 kev J=4, K=2 or 3

Since the E1 transitions 379.5 and 485.8 kev join this level with the final states JK = 42 and 32, the spin of this level has to be J=3 or 4. The branching ratios for the possible values of J_iK_i are

J_i= \ K_i=	0	1	2	3	4
3	.775	.775	.775	7.0	
4	.185	.185	1.65	1.65	.185

The observed value of 1.3±.4, and the evidence from the single particle comparison that $K_1 \geq 2$, support the assignment J=4 and K=2 or 3.

2. MODEL FITTING FOR THE POSITIVE PARITY LEVELS

The theory of a rigid asymmetric rotor was presented in section 2 of chapter II. The two parameters of this theory, i.e. the asymmetry parameter γ and the energy scale factor $\frac{\hbar^2}{4B\beta^2}$, are best obtained using the two states of J=2. Equating the expressions for the energies of these states, given in Table II-1, with the observed values of 86.8 and 966.1 kev we obtain

$$\gamma = 11.9^\circ \qquad \text{and} \qquad \frac{\hbar^2}{4B\beta^2} = 19.91 \text{ kev.}$$

Since γ is less than 15°, K is essentially a good quantum number. This leads to the energy levels forming into bands of K=0 with J=0,2,4..., and K=2 with J=2,3,4... . This value of γ is in excellent agreement with the $\gamma = 11.9^\circ$ of reference 12 and $\gamma = 12.2^\circ$ of reference 5.

The energies of all other positive parity levels are calculated using these two parameters. These theoretical predictions are presented in Table VI-4, along with the observed values. With a maximum deviation of 1.8%, the agreement

TABLE VI-4

EVEN PARITY ENERGY LEVELS

STATE J	K	OBSERVED ENERGY (kev)	ASSYM. ROTOR PREDICTIONS	% DEVIATIONS
2	0	86.8	≡86.8	-
4	0	283.7	287.3	%1.3
2	2	966.1	≡966.1	-
3	2	1049.0	1052.7	%.35
4	2	1155.8	1171.0	%1.3
5	2	1288.8	1313.1	%1.8

between theory and experiment is excellent.

Another test of the theory is the comparison of the predicted E2 branching ratios with the observed values. Using the value of $\gamma = 11.9°$ in equation (4.6) of chapter II, these theoretical predictions are calculated. These predicted branching ratios are presented in Table IV-5 along with the experimentally observed values.

3. MODEL FITTING FOR THE ODD PARITY STATES

The theory of the odd parity states was presented in section 3 of chapter II. The application of the theory is facilitated by noting that the moments of inertia of equation (3.3) of chapter II satisfy the condition

$$I_{11}+I_{22}+I_{33} = 12\, B\zeta^2 \qquad (6.2)$$

Equating the energies of the two J=2 states, i.e. 1264.6 kev and 1358.4 kev, with ϵ_2^1 and ϵ_2^2 of equation (3.5) of chapter II, and using the above condition, we obtain

$$\begin{aligned} I_{11} &= 5.999 \pm (35.564 - I_{13}^2) \\ I_{33} &= 5.999 \mp (35.564 - I_{13}^2) \\ I_{22} &= .0008 \end{aligned} \qquad (6.3)$$

where I_{11} and I_{33} must have opposite signs appearing in front of the square root. It was found that the energy eigenvalues were the same for the sign combinations +- and -+ for $I_{11}I_{33}$. Also since I_{11} and I_{33} are real, $|I_{13}| \leq 5.96$.

The energies of the two J=1 states are calculated, and they are

$$\epsilon_1^1 = 1247.3 \text{ kev} \qquad \epsilon_1^2 = 1275.1 \text{ kev}.$$

Using the expressions of equation (6.3), the matrix equations of the J=3

TABLE VI-5

THEORETICAL E2 BRANCHING RATIOS

INITIAL STATE	$\frac{J_i K_i \to J_f K_f}{J_i K_i \to J'_f K'_f}$	OBSERVED VALUE	ASSYM. ROTOR PREDICTIONS
966.1	$\frac{22 \to 00}{22 \to 20}$	.52±.03	.48
966.1	$\frac{22 \to 40}{22 \to 20}$	.068±.006	.057
1049.0	$\frac{32 \to 40}{32 \to 20}$	.64±.05	.70
1155.8	$\frac{42 \to 40}{42 \to 20}$	5.6±1.3	7.8

and J=4 states are expressed in terms of the one variable I_{13}. The eigenvalues of these states are obtained by diagonalizing their determinants, for various values of I_{13} varied between the limits -5.96 and +5.96.

It was observed that the eigenvalues of the J=4 state were insensitive to variations of I_{13}, remaining constant to within .1 kev. The eigenvalues of the J=3 state, because of the asymmetry of its determinant, did not converge for all values of I_{13}. But whenever these eigen values converged, they converged to the same value to within .1 kev.

The theoretical predictions of the energies of the J=1,2,3 and 4 states are presented in Table VI-6, along with the observed values.

Since variations of I_{13} are found to be insignificant, I_{13} can be assigned any value consistent with equations (6.3) and (3.3) of chapter II.

4. CONCLUSIONS

The information deduced from the present experimental data, and those of the other investigations, lead to a fairly complete decay scheme of ^{160}Dy, populated by the β^- decay of ^{160}Tb. The four new transitions found in this investigation have very low intensities. Should there be any other transitions, as yet undetected, they must be extremely weak.

Comparison of the energies of the even parity levels and the branching ratios for transitions from these levels, to the predictions of the asymmetric rotor model demonstrate the validity of this model for the ^{160}Dy nucleus. Although the symmetric rotor model with band mixing enjoys the same degree of success in predicting these observed values, the asymmetric model is more appealing because of its simplicity in having only two parameters.

A unique interpretation of the odd parity states in ^{160}Dy, like that of the even parity states, does not seem possible at present. There is fair

TABLE VI-6

THEORETICAL ENERGIES OF THE ODD PARITY LEVELS

STATE J	STATE N	OBSERVED ENERGIES	THEORETICAL e_J^N	% DEVIATION
1	1		1247.3	
2	1	1264.6	≡1264.6	
1	2	1285.4	1275.1	% .8
3	1	1286.8	1317.2	%2.3
2	2	1358.4	≡1358.4	
4	1	1386.3	1372.1	%.10
3	2	1398.8	1483.5	%5.7
4	2	1535.1	1648.4	%6.2

agreement between the observed energies of these levels and the predictions of the theory of odd parity states as proposed by M.G. Davidson[10]. However, many difficulties are encountered in applying this model even with the assumption of rigidity of the nucleus, as in solving for the eigenvalues of an asymmetric matrix. Unlike the model proposed by J.P. Davidson[8], which requires K to be an even integer, this model is consistent with the experimental evidence that K can have odd values. An alternative explanation would be the mixing of rotational bands of K=0, 1 and 2 as proposed by Gunther et al.[13].

It is hoped that further development of the theory of odd parity states will include predictions of E1 transition probabilities from these levels to the even parity states.

References

1. A. Bohr, Dan. Mat. Fys. Medd 26 No. 14 (1952)
2. A. Faessler and W. Greiner, Z. Physik 168 (1962) 425
3. A. Faessler and W. Greiner, Z. Physik 177 (1964) 177
4. P.O. Lipas, Nucl. Phys. A119 (1968) 398
5. A.S. Davydov and G.P. Fillipov, Nucl. Phys. 8 (1958) 237
6. A.S. Davydov and V.S. Rostovsky, Nucl. Phys. 12 (1959) 58
7. A.S. Davydov and A.A. Chaban, Nucl. Phys. 20 (1960) 499
8. J.P. Davidson, Nucl. Phys. 33 (1962) 664
9. J.P. Davidson, Collective Models of the Nucleus. Academic Press, (1968)
10. M.G. Davidson, Nucl. Phys. 69 (1965) 455
11. O. Nathan, Nucl. Phys. 4 (1957) 125
12. G.T. Ewan et al, Nucl.Phys. 22 (1961) 610
13. C. Gunther et al, Nucl. Phys. A122 (1968) 401
14. M.A. Ludington et al, Nucl. Phys. A119 (1968) 398
15. M. Finger et al, Czech. J. Phys. B19 (1969) 1017
16. G.E. Keller and E.F. Zganjan, Nucl. Phys. A147 (1970) 527
17. R.E. McAdams and O.H. Otteson, Z. Physik 250 (1972) 359
18. J.M. Jaklevic et al, Nucl. Phys. A99 (1967) 83
19. K.S. Krane and R.M. Steffen, Nucl. Phys. A164 (1971) 439
20. E.P. Grigor'ev et al, English Translation in Acad. of Sci. USSR Bull. (Phys. Ser.) 33 (1969) 585
21. K.T. Hecht, in Selected Topics in Nuclear Spectroscopy, Edited by P.J. Verhaar, North-Holland Pub. Co. (1964) p. 54
22. R.D. Evans, The Atomic Nucleus, McGraw-Hill Book Co. (1955) p. 221
23. A. Bohr and B.R. Mottelson, Sov. J. Atom. Energy 14 (1963) 41

References (cont.)

24. S.A. Moszkowski, in Alpha-, Beta- and Gamma-Ray Spectroscopy, Edited by K. Siegbahn, North-Holland Pub. Co. (1968) p. 881

25. L.A. Sliv and I.M. Band, Coefficients of Internal Conversion of Gamma Radiation, Leningrad Physics-Technical Institute (1956)

26. J.R. Johnson, Ph.D. Thesis, University of British Columbia

27. L.K. Ng, Ph.D. Thesis, University of British Columbia

28. G.T. Ewan, in Progress in Nuclear Techniques and Instrumentation, Edited by F.J.M. Farley, North-Holland Pub. Co. vol.3 (1963) p. 123